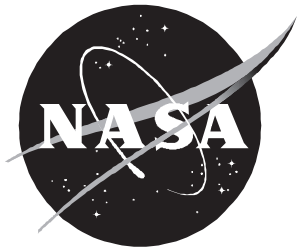

NASA Technical Memorandum 4697

Control Effectiveness and Tip-Fin Dihedral Effects for the HL-20 Lifting-Body Configuration at Mach Numbers From 1.6 to 4.5

Christopher I. Cruz and George M. Ware
Langley Research Center • Hampton, Virginia

National Aeronautics and Space Administration
Langley Research Center • Hampton, Virginia 23681-0001

December 1995

Available electronically at the following URL address: http://techreports.larc.nasa.gov/ltrs/ltrs.html

Printed copies available from the following:

NASA Center for AeroSpace Information
800 Elkridge Landing Road
Linthicum Heights, MD 21090-2934
(301) 621-0390

National Technical Information Service (NTIS)
5285 Port Royal Road
Springfield, VA 22161-2171
(703) 487-4650

Summary

A wind tunnel investigation has been made in the Langley Unitary Plan Wind Tunnel at Mach numbers (M) from 1.6 to 4.5 to define the control effectiveness of a lifting-body configuration (HL-20) in the supersonic speed range. The lifting body is being considered as a possible future crewed spacecraft. The configuration has a low aspect ratio body with a flat undersurface. Three fins, a small centerline fin and two outboard tip fins set at dihedral angles (Γ) of 50°, are mounted on the aft body. The control surfaces consist of elevons on the outboard fins and four body flaps, two on the upper and two on the lower aft body. An all movable center fin was used for yaw control. Tests were made with elevons and body flaps deflected to ±30° and the center fin deflected to 5°.

Almost full negative body flap deflection was required to trim the HL-20 (moment reference center at 0.54-percent body length from nose) to positive values of lift in the M range from approximately 1.6 to 2.5. Elevons were about twice as effective as body flaps. The elevons were effective as a roll control, but because of Γ, they produced about as much adverse yawing moment as favorable rolling moment. The body flaps produced less rolling moment and much less adverse yawing moment than the elevons. The yaw effectiveness of the all movable center fin was essentially constant over the angle of attack range at each M. The value of yawing moment, however, was small. Center-fin deflection produced almost no rolling moments.

A limited investigation of the effect of Γ was made. Data indicated that at $\Gamma < 50°$, the model was directionally unstable over most of the M range. Decreasing Γ from 90°, increased the trimmed lift-drag ratio (L/D) at $M < 3.0$ but decreased the L/D at $M > 3.0$. The baseline $\Gamma = 50°$ appears to be a reasonable compromise for stability and performance.

Introduction

The National Aeronautics and Space Administration is investigating a number of configurations for possible crewed spacecraft. Two studies are the Assured Crew Return Capability (ACRC) Program (refs. 1 and 2) and the Personnel Launch System (PLS) Program (refs. 3 through 7). The ACRC Program provides for the safe return to Earth of crew members of the Space Station in case of emergency. For this purpose, one or more return vehicles would be docked at the station ready for immediate use. The vehicles are to be carried to the Space Station in the 15 ft by 60 ft cargo bay of the Space Shuttle. The PLS, however, will be used to augment Space Shuttle capabilities in the transportation of crew members to and from the space station. The PLS vehicle will be independently launched with an expendable booster and will return to Earth after exchanging crew members.

One of the candidate configurations under study for both the ACRC and PLS programs is a lifting-body vehicle that is designed to be volumetrically efficient and yet to have aerodynamic performance parameters that allow a low g atmospheric entry and a runway landing. This configuration was designed to have moderate L/D over the speed range. Moderate hypersonic L/D (1.0 to 1.4) give the vehicle a cross range capability to reach a suitable landing site or recovery area. At subsonic speeds, the L/D should be sufficient for the vehicle to complete a conventional horizontal shuttle-like landing. The lifting-body configuration of the investigation presented herein, designated HL-20, consists of a low aspect ratio body with a flat undersurface and blunt base. Center and outboard fins are mounted on the upper aft body. The outboard fins are rolled outward from the vertical 40° (50° from the horizontal). Control surfaces are mounted on the outboard fins and the aft body.

A series of wind tunnel investigations has been undertaken to define the aerodynamic and the aerothermodynamic characteristics of the HL-20 from low-subsonic to hypersonic speeds (refs. 8 through 15). The test discussed herein was initiated to obtain additional aerodynamic information on the control characteristics of the HL-20 for computer simulation of the flight behavior of the vehicle. In addition, the tip-fin dihedral angle (Γ) of the outboard fins was varied from 0° to 90° to gain insight on how this angle might affect configuration stability and performance. The test was conducted in the

Unitary Plan Wind Tunnel (UPWT) at the Langley Research Center by using a 0.07-scale model of a proposed 24.6-ft-long ACRC vehicle. The Mach number (M) range was from 1.6 to 4.5 at a test Reynolds number of 3.4×10^6 based on body length. (The estimated flight Reynolds number varies from 27×10^6 at $M = 1.6$ to a Reynolds number of 7×10^6 at $M = 4.5$.) The model was tested over a nominal angle-of-attack (α) range of −2° to 30° at sideslip angles (β) of 0° and 2°. Control effectiveness of elevons and body flaps with deflections of 0°, ±10°, ±20°, and ±30° were studied. The all movable center fin was tested at 0° and 5°.

Symbols

The longitudinal data are referred to the stability-axis system and the lateral-directional data are referred to the body-axis system (fig. 1). All coefficients are based on the dimensions of the body without fins. The data are normalized by the planform area, the length, and the span of the body. The moment reference center was located at the vehicle center of gravity which is at 54 percent of the body length from the nose and 0.08 percent of the body length above the flat lower surface.

ACRC Assured Crew Return Capability

b body span, in.

C_D drag coefficient, $\frac{\text{Drag}}{qS_{\text{ref}}}$

C_L lift coefficient, $\frac{\text{Lift}}{qS_{\text{ref}}}$

C_l rolling-moment coefficient, $\frac{\text{Rolling moment}}{qS_{\text{ref}}}$

C_{l_β} $\frac{\Delta C_l}{\Delta\beta}$ taken at $\beta = 0°$ and 2°, per deg

C_m pitching-moment coefficient, $\frac{\text{Pitching moment}}{qS_{\text{ref}}}$

C_n yawing-moment coefficient, $\frac{\text{Yawing moment}}{qS_{\text{ref}}b}$

C_{n_β} $\frac{\Delta C_n}{\Delta\beta}$ taken at $\beta = 0°$ and 2°, per deg

C_p pressure coefficient, $\frac{(p_{\text{local}} - p_{\text{free stream}})}{q}$

C_Y side-force coefficient, $\frac{\text{Side force}}{qS_{\text{ref}}}$

C_{Y_β} $\frac{\Delta C_Y}{\Delta\beta}$ taken at 0° and 2°, per deg

FS fuselage station

g acceleration of gravity, ft/sec^2

L/D lift-drag ratio

l body length, in.

M	Mach number
PLS	Personnel Launch System
p	static pressure, lb/in^2
q	free-stream dynamic pressure, lb/in^2
S_{ref}	basic body planform area (excluding fins), in^2
UPWT	Unitary Plan Wind Tunnel
X	longitudinal body axis
Y	lateral body axis
Z	vertical body axis
α	angle of attack, deg
β	angle of sideslip, deg
Γ	tip-fin dihedral angle (measured from horizontal), deg
Δ	an increment
δ_a	aileron (differential pitch) control deflection angle, $\frac{(\delta_{e_L} - \delta_{e_R})}{2}$ or $\frac{(\delta_{BF_L} - \delta_{BF_R})}{2}$, deg
δ_{BF}	body flap deflection angle (positive when deflected downward), deg
δ_e	elevon deflection angle (positive when deflected downward), deg
δ_r	rudder deflection angle (positive when trailing edge deflected left), deg

Subscripts:

basic	baseline configuration (no control deflections)
L	left
max	maximum value
R	right
trim	trimmed condition (zero moment)

Description of Model

Sketches of the model are presented in figure 2 and a photograph of the model installed in the UPWT is shown in figure 3. Model dimensional information is given in table I. The aluminum model was a 0.07-scale representation of a proposed 24.6-ft-long vehicle. The configuration consisted of a low aspect ratio body with a flat undersurface and a blunt base. Three fins were mounted on the upper aft portion of the model. The center fin was relatively small, and the larger outboard fins were set at $\Gamma = 50°$, a toe-in angle of 1.25°, and an incidence angle at the body intersection of 6.6°. (See fig. 2(d).) The fins had a thick, flat plate cross section with a cylindrical leading edge and blunt trailing edge.

Control surfaces, referred to as elevons, made up the trailing edges of the outboard fins. In addition, the model had four body flap control surfaces, two on the upper body and two on the lower. The body flap outer surfaces were flush with the body contour and could only be deflected outward. For positive body flap deflection, the lower body flap was deflected downward while the upper body flap remained undeflected. For negative body deflection, the upper body flap was deflected upward and the lower body flap remained undeflected. During the test reported herein, only the left elevon or left upper or lower body flap was deflected. Body flap and elevon deflections of 0°, ±10°, ±20°, and ±30° were tested. The center vertical fin was pivoted 5° about its midchord for yaw control. The Γ of the outboard fins (in the plane of the hinge line) was varied by replacing the original fins ($\Gamma = 50°$) with those having $\Gamma = 0°$, 25°, and 90°.

Apparatus, Test, and Corrections

Tests were conducted in the Langley Unitary Plan Wind Tunnel. The tunnel has a supersonic, closed-circuit design with two test sections. The flow in the low-speed test section can be varied from $M = 1.5$ to 2.86. The high-speed test section operates at $M = 2.36$ to 4.63. Additional information about the facility may be found in reference 16. The investigation reported herein was conducted in the low-speed test section at $M = 1.6$, 2.0, and 2.5 and in the high-speed test section at $M = 3.0$, 3.5, 4.0, and 4.5. All tests were made at a constant Reynolds number of 2.0×10^6 per ft (3.4×10^6 per ft based on body length). The model was mounted on a sting through its base. Forces and moments were measured with an internally mounted strain-gage balance.

Model α and β were corrected for the sting and balance deflection under load and tunnel flow angularity. In an attempt to ensure turbulent flow over the model, transition grit was applied in accordance with reference 17 and is shown in figure 4. Two techniques to apply grit were used. In the low-speed test section, no. 50 grit sand grains were thinly sprinkled in 0.0625-in. bands that were 1.2 in. aft of the nose and 0.3 in. perpendicular to the leading edges of the fins. In addition, 0.0625-in. bands of grit were added along the lower body radius. The grit was located in the same positions on the model for tests in the high-speed test section. In this case, however, individual grains of no. 35 grit were applied at regular spacing of 4 grain diameters.

The model pitch range was limited to $\alpha \approx 18°$ at $M = 1.6$ and in some cases at $M = 2.0$ because of model unsteadiness at the higher α. At $M \geq 2.5$, full sweeps to $\alpha = 30°$ were made. The model was tested at $\beta = 0°$ and 2° over the α and M ranges. Data were taken as the model was moved from negative to positive α. Model base and cavity pressures were measured and are presented in figure 5 for the baseline configuration in the event that base corrections are desired.

Results and Discussion

Because the aerodynamic data generated in this investigation were to be used in a computer driven flight simulation program, the data were taken in a form that would readily adapt to that program. The simulator information is derived from the basic aerodynamic parameters for a configuration with controls undeflected and adds increments due to control deflection. Increments for aerodynamic damping, ground effects, and aeroelastic effects may also be added. From this information, the vehicle control matrix for the flight envelope is described. During the test, only a single control surface was deflected during a run. In this case, the left elevon or body flap was deflected. The resulting incremental change in the aerodynamic parameters was used with the baseline aerodynamics to make up the characteristics of the vehicle with multiple control surfaces deflected. For example, pitch control for −20° elevon deflection is made up of the baseline aerodynamic characteristics plus two times the aerodynamic increments produced by −20° deflection of the left elevon alone. The direct addition of increments may introduce errors. The aerodynamic interference effects of one control on the other must be considered. Fortunately, the elevons and the body flaps of the lifting-body model are physically separated by a distance that tends to minimize interference. Data presented in figure 6 compare the pitching moment determined from a test with both elevons deflected −10° (ref. 9) and the pitching moment from a single elevon deflected with its effect doubled. The data show good agreement.

The aerodynamic characteristics of the lifting-body model with controls deflected, which are presented in figures 6 through 12, were determined by adding increments as previously described. The equations are

$$C_L = C_{L_{\text{basic}}} + \Delta C_{L_{\delta_e}} + \Delta C_{L_{\delta_{\text{BF}}}}$$

$$C_D = C_{D_{\text{basic}}} + \Delta C_{D_{\delta_e}} + \Delta C_{D_{\delta_{\text{BF}}}}$$

$$C_m = C_{m_{\text{basic}}} + \Delta C_{m_{\delta_e}} + \Delta C_{m_{\delta_{\text{BF}}}}$$

$$L/D = C_L / C_D$$

Longitudinal Characteristics

Pitch control. The longitudinal aerodynamic characteristics of the lifting-body model with elevons deflected from –30° to 30° as a pitch control are presented in figures 7 and 8. Examining the trim characteristics of the model with controls undeflected indicates that the HL-20 trims at very low α ($\alpha < 5°$) to about $M = 3.0$. Positive elevon deflection (fig. 7) trims the model at even lower α and negative lift values. At $M = 3.5$ to 4.5, the model is less stable and trim occurs at a higher α. Positive control at these M trims the model to lower α, but lift remains positive. Increasing the elevon deflection angle from 20° to 30° has little effect on the longitudinal characteristics at $M = 3.5$ and 4.5.

With an elevon deflection of –30° (fig. 8), the model was trimmed at $\alpha = 4°$ for $M = 1.6$ and 2.0. As M is increased, the stability level decreased and the elevons trimmed the HL-20 to as high as $\alpha = 20°$ at $M = 4.5$. Unlike positive elevon deflection, negative elevon deflection continued to be effective at $\delta_e = -30°$.

The effects of pitch control that uses body flaps alone are shown in figures 9 and 10. The trends exhibited by body flap deflection are the same as those of elevon deflection. That is, low trim effectiveness is due in part to high longitudinal stability at low M and increasing trim effectiveness as the stability level decreases with increasing M. Overall, the body flaps are about half as effective a pitch control device as the elevons in this M range.

Tip-fin dihedral effects. The effect on the longitudinal characteristics of the HL-20 of varying Γ from 90° to 0° is presented in figure 11. At all M and $\alpha > 4°$ or 5°, there is an increase in lift coefficient, lift curve slope, L/D, and longitudinal stability as the fins are rotated to the horizontal position. At $\alpha < 4°$, the negative incidence of the tip fins, 6.6° (fig. 2(d)), produces a negative increment of lift. As a result, longitudinal trim shifts from small negative α to small positive α at $M = 1.6$ to 3.0. Overall, fin rotation has little effect on trim angle at $M = 1.6$ to 3.0. At the higher M, where the stability level is less, the HL-20 is trimmed at increasingly higher α. The trim range due to fin rotation at $M = 4.5$ is 8° to 23°. Conversely, the effect of fin rotation on $(L/D)_{\max}$ becomes less with increasing M. The difference in $(L/D)_{\max}$ at $M = 1.6$ for $\Gamma = 90°$ and $\Gamma = 0°$ is about 0.4, whereas for $M = 4.5$, the difference is about half that value.

Lateral Characteristics

Tip-fin dihedral effects. The lateral-directional characteristics of the HL-20 are presented in figure 12 in the form of the stability parameters C_{Y_β}, C_{n_β}, and C_{l_β} plotted with α at each test M. Data are shown for the baseline $\Gamma = 50°$ and for 90°, 25°, and 0°. The baseline HL-20 was directionally stable, with positive values of C_{n_β}, over the α range at $M = 1.6$ and 2.0. At higher M, directional stability fell to zero or negative values at $\alpha < 10°$. The baseline HL-20 had positive effective dihedral and negative values of C_{l_β} over most of the test α and M range.

Varying Γ had an effect on the directional stability of the HL-20. At lower α, decreasing Γ (decreasing aft lateral plane area) decreased directional stability, as expected. At higher α, however, the model with fins vertical lost stabilizing effectiveness, perhaps due to the shielding of the body. As a result, the configurations with lesser Γ were more directionally stable. This effect became more pronounced with increasing M.

Roll control effects. All lateral control tests were made with the baseline configuration, that is, the model with $\Gamma = 50°$. Roll control was accomplished through differentially deflecting the elevons on the outboard fins or the body flaps on the upper aft body. These data are presented in figures 13 and 14, respectively. Because the longitudinal data suggested a need to trim the configuration to more positive α (at least at the low-supersonic M), only negative control deflections are shown. The effectiveness values are for conditions with left elevon or left upper body flap set at −10°, −20°, and −30° while the right control remained at 0°. These deflections represent −5°, −10°, and −15° aileron deflections and about −5°, −10°, and −15° elevon settings. The elevons, with their longer transverse moment arm, were more effective than the body flaps. The effectiveness of both sets of controls decreased with increasing M. The effectiveness of the body flaps was near zero at $M \geq 3.0$. Simultaneous deflection of elevons and body flaps was not tested and whether their effectiveness values are directly additive is unknown.

Differential deflection of the elevons as a roll control produced as much adverse yawing moment ΔC_n as rolling moment ΔC_l because of the rolled out fin configuration. Differential deflection of the elevons acted as much like a rudder as it did like ailerons. The yawing moment associated with body flap deflection, however, was near zero (at M where the body flap had any effectiveness). Therefore, if the elevons are used for roll control, a control device such as a rudder may be needed to offset the yawing moments produced.

Yaw control effects. Yaw control was accomplished by pivoting the small center fin about its midchord. Yaw effectiveness data are given in figure 15. These data were derived by taking the difference between data taken at center-fin deflection angles of 0° and 5° and were reported in reference 9. The yaw effectiveness of the all movable center fin was essentially constant over the α range at each M. Unlike differential elevon deflection, center-fin deflection produced almost no cross-coupled moment, that is, no rolling moment. The effectiveness of the center fin as a yaw control, however, was low at these test M.

Summary Aerodynamic Characteristics

Longitudinal trim characteristics. The aerodynamic characteristics of the baseline HL-20 are summarized as the variation of the trimmed values of α, lift coefficient, and L/D plotted with M in figure 16. Data are shown for the HL-20 with controls undeflected and with elevons and body flaps deflected −30°. With controls neutral, the HL-20 trims near zero lift values at M from 1.6 to 3.0. With −30° pitch control (elevon or body flap), the vehicle has positive lift and L/D over the M range, but in the range $M < 3.0$, the values remain low. The effectiveness of the elevons is about twice that of the body flaps.

Directional stability and tip-fin dihedral effects. The effects of varying Γ from 90° to 0° with controls undeflected are summarized in figure 17. Trimmed values of α, L/D, and directional stability parameter for various Γ are plotted over the test M range. Only with tip fins horizontal does the HL-20 (with controls undeflected) trim at positive lift over the test M. At $M < 3.0$, decreasing Γ increases trimmed L/D; whereas at $M > 3.0$ decreasing Γ decreases L/D.

The baseline model ($\Gamma = 50°$) has positive directional stability at M from 1.6 to 2.5 and $M > 3.5$. In the intermediate M range, the directional stability is neutral or slightly negative. With $\Gamma = 25°$ and 0°, the model is directionally unstable across the test M range. When the Γ was set to 90°, the directional stability was positive, although the stability level dropped to small values at $M = 4.0$ and 4.5. The baseline $\Gamma = 50°$ appears to be a reasonable compromise for stability and performance.

Concluding Remarks

A wind tunnel investigation has been made in the Langley Unitary Plan Wind Tunnel to define the control effectiveness of a lifting-body configuration (HL-20) in the supersonic speed range. The

lifting body is being considered as a possible future crewed spacecraft. Tests were made with elevon controls on the outboard fins or body flaps on the fuselage deflected to ±30°. Yaw control tests were made with the all movable center fin deflected 5°. Almost full negative body flap deflection was required to trim the HL-20 (moment reference center at 0.54-percent body length from nose) to positive values of lift in the Mach number range from approximately 1.6 to 2.5. Elevons were about twice as effective as body flaps as a longitudinal trim device. The elevons were effective as a roll control, but because of tip-fin dihedral angle, produced about as much adverse yawing moment as rolling moment. The body flaps were less effective in producing rolling moment, but produced little adverse yawing moment. The yaw effectiveness of the all movable center fin was essentially constant over the angle-of-attack range at each Mach number. The value of yawing moment, however, was small. Center-fin deflection produced almost no rolling moments.

A limited investigation of the effect of tip-fin dihedral angle on aerodynamic characteristics of the HL-20 was made. Data indicated that at tip-fin dihedral angles less than 50°, the model was directionally unstable over most of the Mach number range. Decreasing tip-fin dihedral angle from 90°, increased the trimmed lift-drag ratio at Mach numbers up to 3.0, but decreased the lift-drag ratio above a Mach number of 3.0. The baseline tip-fin dihedral angle of 50° appears to be a reasonable compromise for stability and performance.

NASA Langley Research Center
Hampton, VA 23681-0001
September 19, 1995

References

1. Ware, George M.; Spencer, Bernard, Jr.; and Micol, John R.: Aerodynamic Characteristics of Proposed Assured Crew Return Capability (ACRC) Configuration. AIAA-89-2172, July/Aug. 1989.

2. Hook, W. Ray; and Freeman, Delma C., Jr.: Lifting-Body Option for a Space Station Rescue Vehicle. IAF-89-246, Oct. 1989.

3. Naftel, J. Chris; Powell, Richard W.; and Talay, Theodore A.: Performance Assessment of a Space Station Rescue and Personnel/Logistics Vehicle. *J. Spacecr. & Rockets*, vol. 27, no. 1, Jan.–Feb. 1990, pp. 76–81.

4. Piland, William M.; Talay, Theodore A.; and Stone, Howard W.: Personnel Launch System Definition. IAF-90-160, Oct. 1990.

5. Talay, Theodore A.; and Stone, Howard W.: The Personnel Launch System—A Lifting Body Approach. IAF-91-202, Oct. 1991.

6. Talay, Theodore A.: The HL-20 Personnel Launch System. AIAA-92-1416, Mar. 1992.

7. Stone, Howard W.; and Piland, William M.: The 21st Century Space Transportation System Design Approach: HL-20 Personnel Launch System. *J. Spacecr. & Rockets*, vol. 30, no. 5, Sept.–Oct. 1993, pp. 521–528.

8. Ware, George M.: *Transonic Aerodynamic Characteristics of a Proposed Assured Crew Return Capability (ACRC) Lifting-Body Configuration*. NASA TM-4117, 1989.

9. Ware, George M.: *Supersonic Aerodynamic Characteristics of a Proposed Assured Crew Return Capability (ACRC) Lifting-Body Configuration*. NASA TM-4136, 1989.

10. Cruz, Christopher I.; Ware, George M.; Grafton, Sue B.; Woods, William C.; and Young, James C.: *Aerodynamic Characteristics of a Proposed Personnel Launch System (PLS) Lifting-Body Configuration at Mach Numbers From 0.05 to 20.3*. NASA TM-101641, 1989.

11. Ware, George M.; and Cruz, Christopher I.: *Subsonic Aerodynamic Characteristics of the HL-20 Lifting-Body Configuration*. NASA TM-4515, 1993.

12. Cruz, Christopher I.; and Ware, George M.: Predicted Aerodynamic Characteristics for HL-20 Lifting-Body Using the Aerodynamic Preliminary Analysis System (APAS). AIAA-92-3941, July 1992.

13. Ware, G. M.; and Cruz, C. I.: Aerodynamic Characteristics of the HL-20. *J. Spacecr. & Rockets*, vol. 30, no. 5, Sept.–Oct. 1993, pp. 529–536.

14. Micol, John R.: Experimental and Predicted Aerodynamic Characteristics of a Proposed Assured Crew Return Vehicle (ACRV) Lifting-Body Configuration at Mach 6 and 10. AIAA-90-1403, June 1990.

15. Horvath, Thomas J.; Rhode, Matthew N.; and Buck, Gregory M.: Aerothermodynamic Measurements on a Proposed Assured Crew Return Vehicle (ACRV) Lifting-Body Configuration at Mach 6 and 10 in Air. AIAA-90-1744, June 1990.

16. Jackson, Charlie M., Jr.; Corlett, William A.; and Monta, William J.: *Description and Calibration of the Langley Unitary Plan Wind Tunnel*. NASA TP-1905, 1981.

17. Braslow, Albert L.; Hicks, Raymond M.; and Harris, Roy V., Jr.: Use of Grit-Type Boundary-Layer-Transition Trips. *Conference on Aircraft Aerodynamics.* NASA SP-124, 1966, pp. 19–36.

Table I. Geometric Characteristics of the Model

Body alone:	
Aspect ratio	0.6
Length (reference length), in.	20.6
Span (reference span), in.	9.7
Planform area (reference area), in^2	152.2
Base area (excluding cavity area), in^2	23.2
Cavity area, in^2	4.9
Height (maximum), in.	4.7
Body with fins **(**$\Gamma = 50°$):	
Aspect ratio	1.5
Length (body), in.	20.6
Span (outboard fins tip to tip), in.	16.3
Planform area, in^2	178.6
Base area (no cavity and fin base area), in^2	23.2
Cavity area, in^2	4.9
Height (to tip of outboard fin), in.	5.9
Elevons:	
Chord, in.	1.1
Span, in.	4.1
Thickness, in.	0.4
Area (each), in^2	3.5
Body flaps:	
Chord, in.	1.5
Span, in.	2.3
Area (each), in^2	3.5

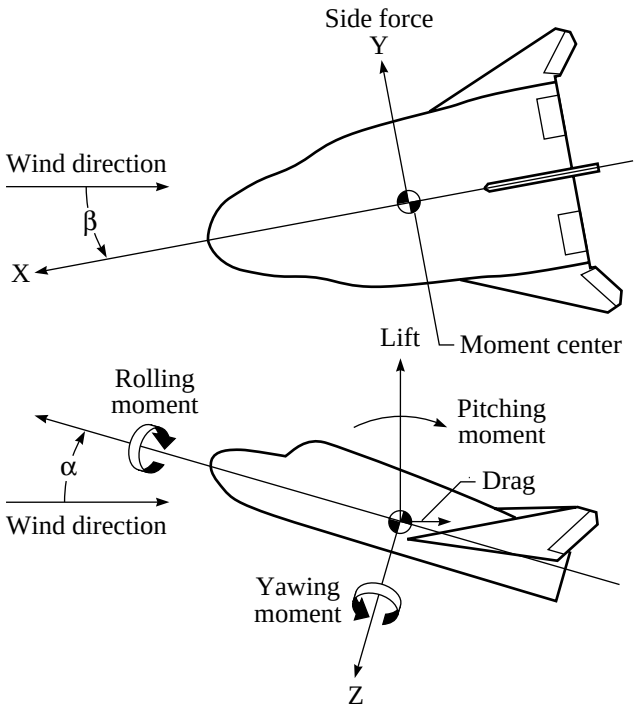

Figure 1. Sketch of axes system used in investigation.

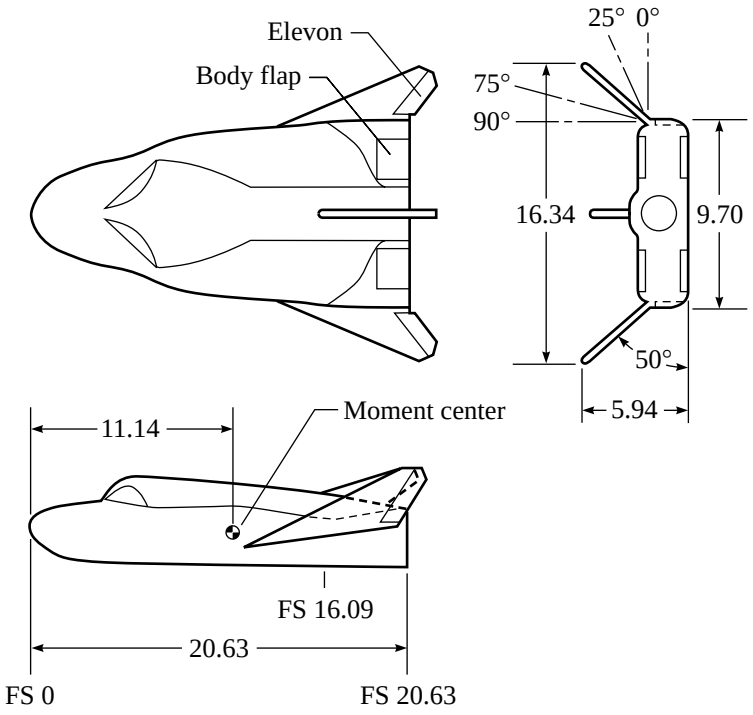

(a) General arrangement.

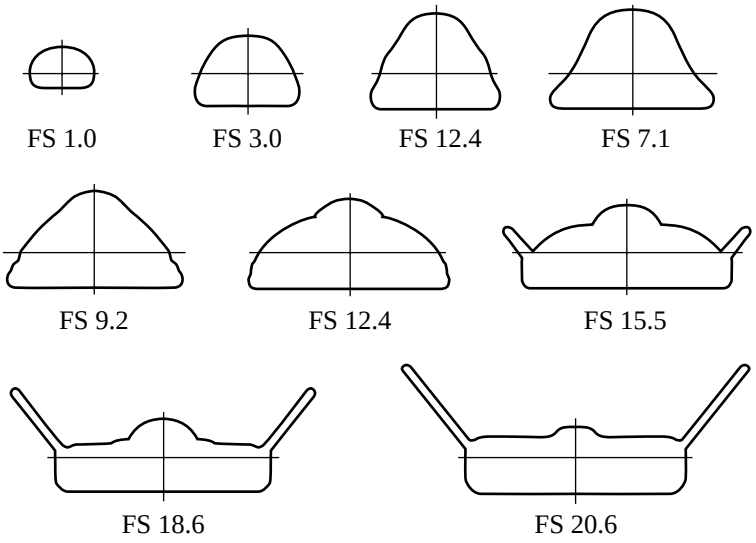

(b) Body cross sections.

Figure 2. Sketches of model used in investigation. All linear dimensions are in inches.

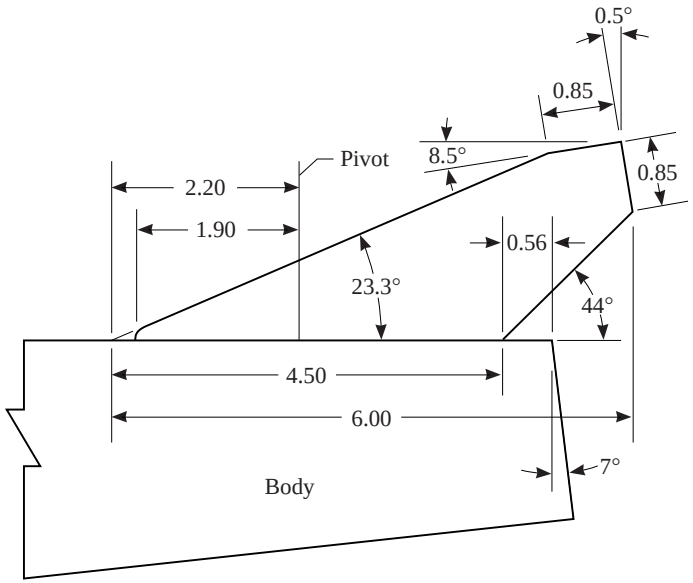

(c) Center-fin details.

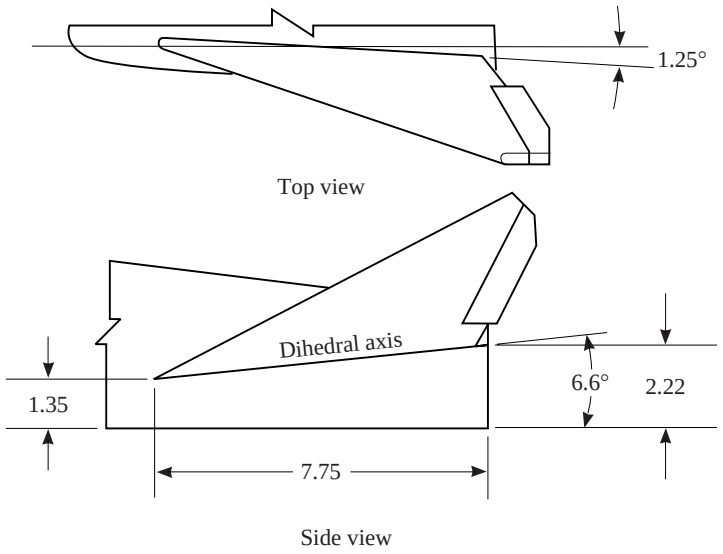

(d) Tip incidence and toe in.

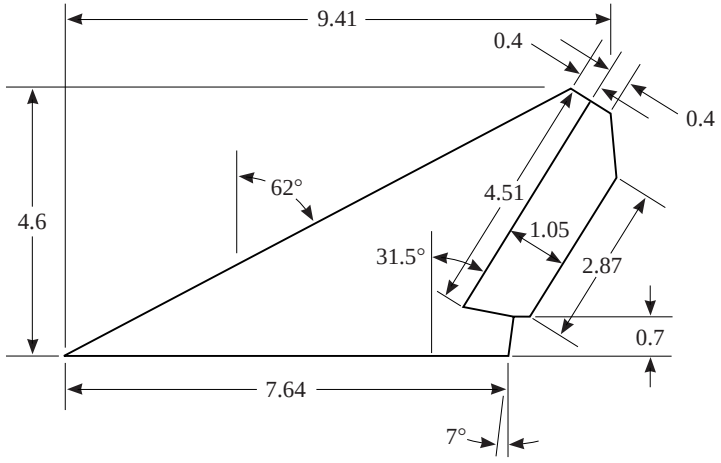

(e) Tip-fin details. (Measurements are in plane of fin.)

Figure 2. Concluded.

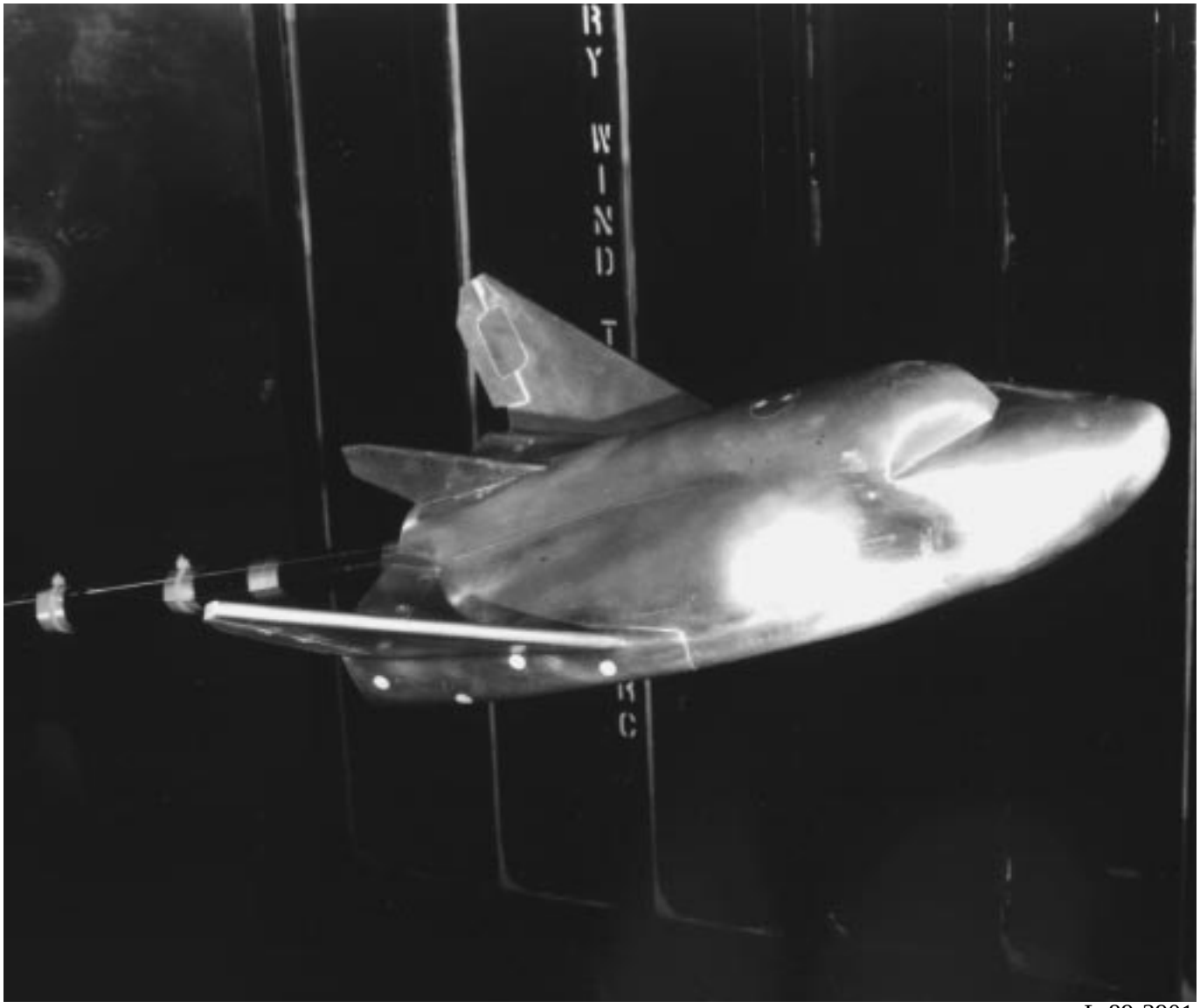

L-89-3901

Figure 3. The HL-20 model installed in tunnel.

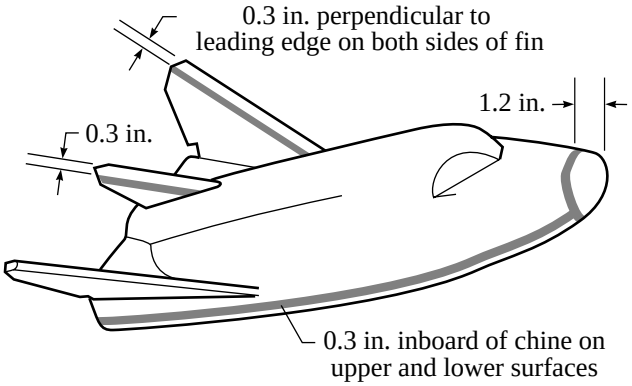

Test section	Mach number	Grit number	Grit diameter, in.	Band width, in.	Spacing, in.
1	1.6 to 2.5	50	0.013	0.0625	Sprinkled
2	3.0 to 4.5	35	0.022	0.022	0.09

Figure 4. Transition grit locations on model.

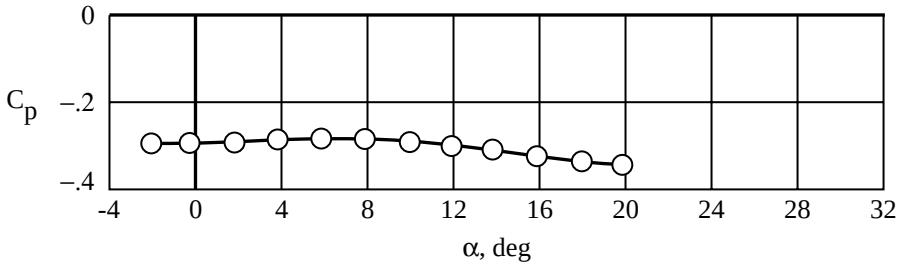

(a) M = 1.6.

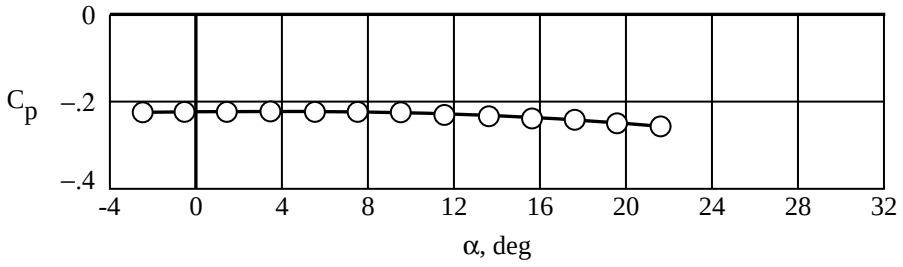

(b) M = 2.0.

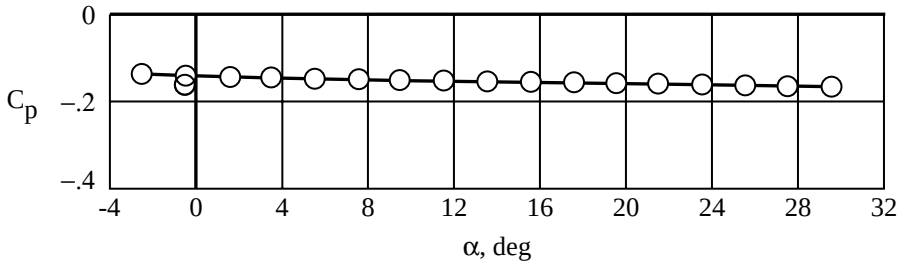

(c) M = 2.5.

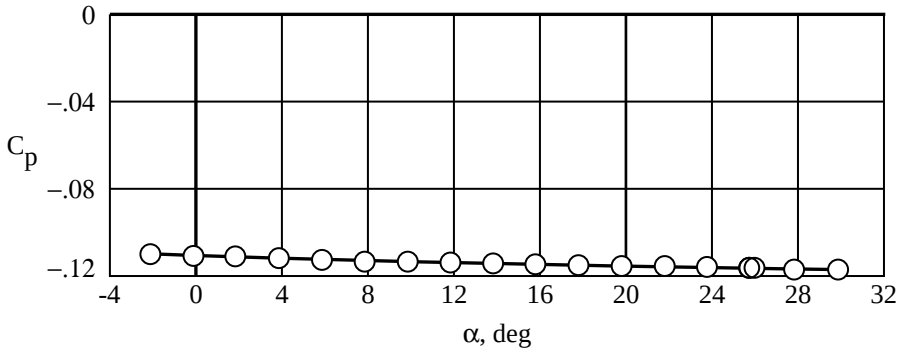

(d) M = 3.0.

Figure 5. Model base pressures measured in investigation.

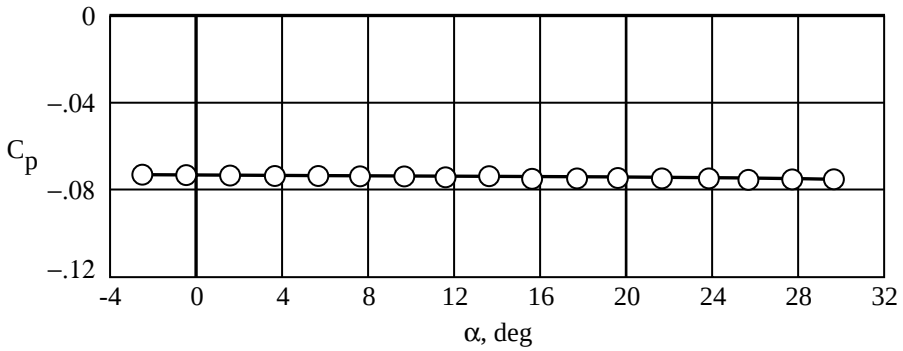

(e) $M = 3.5$.

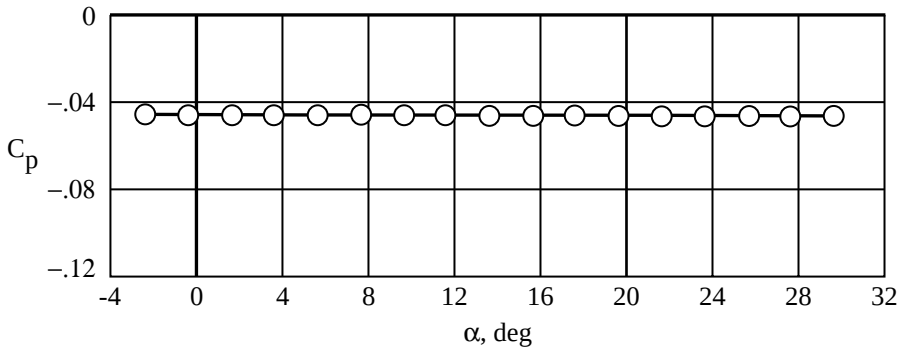

(f) $M = 4.0$.

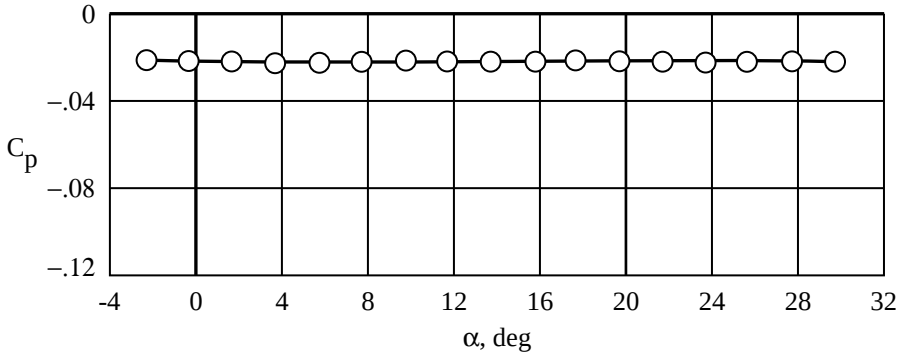

(g) $M = 4.5$.

Figure 5. Concluded.

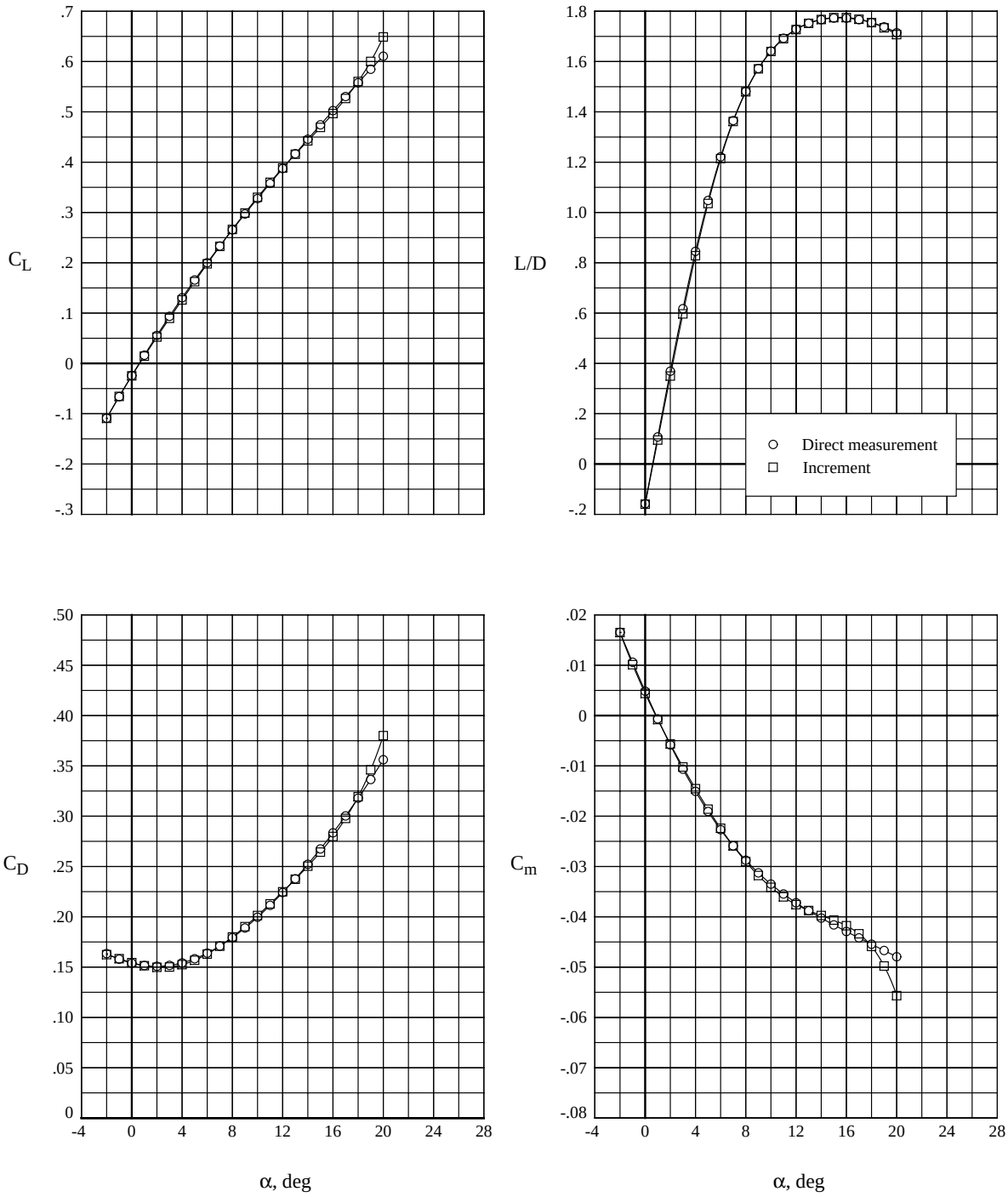

(a) $M = 1.6$.

Figure 6. Comparison of pitch control from direct measurement and increments. $\delta_e = -10°$.

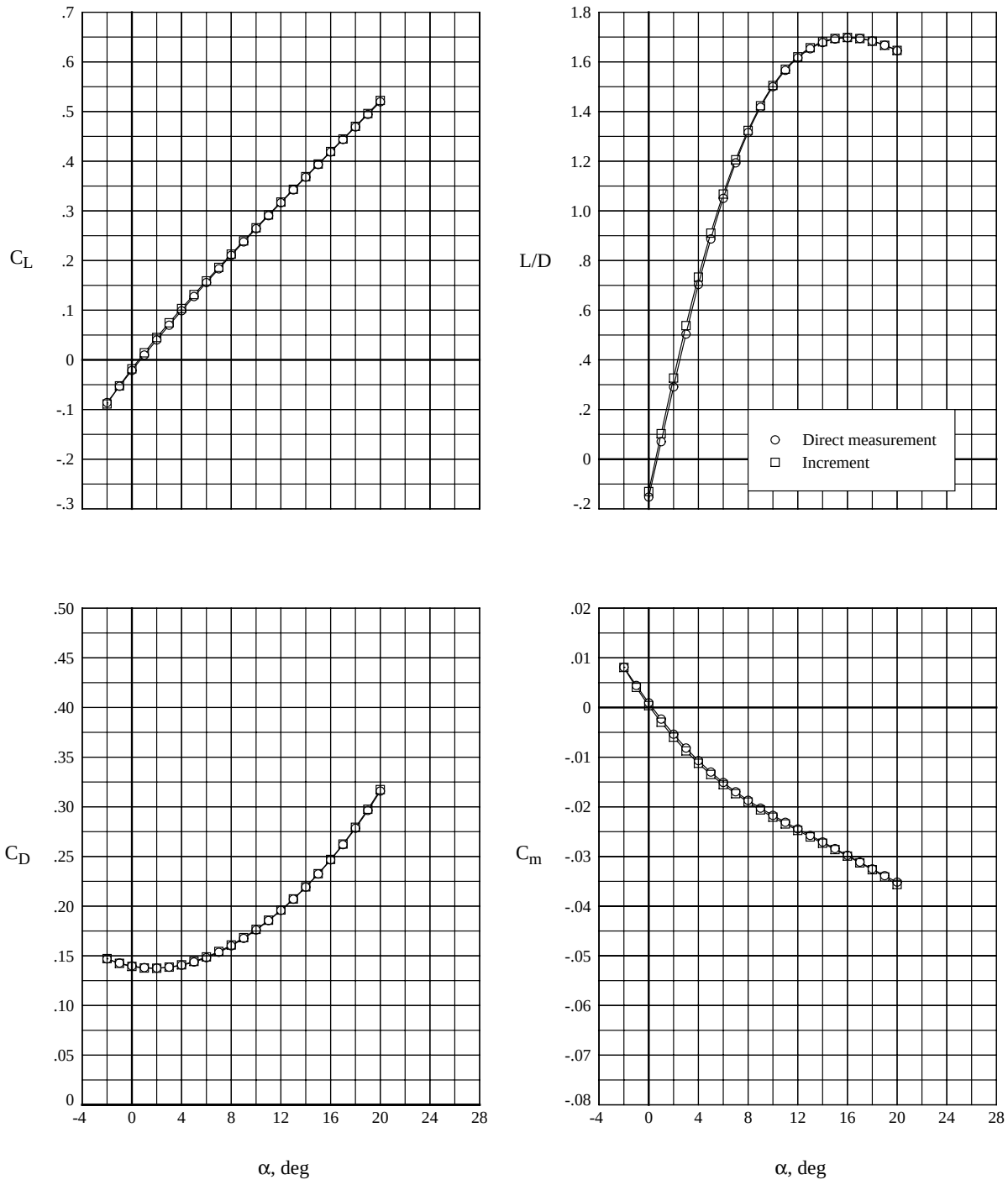

(b) $M = 2.0$.

Figure 6. Continued.

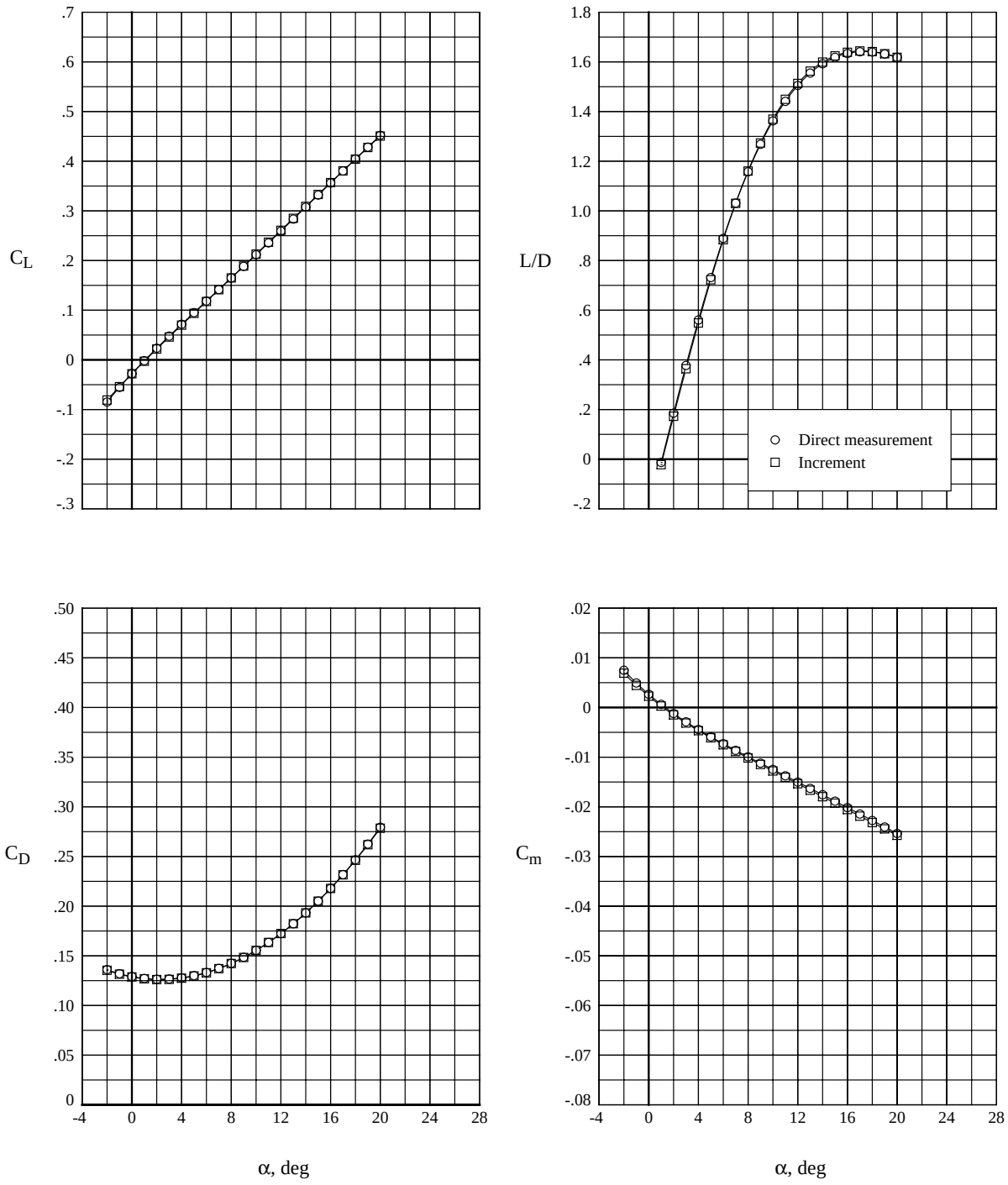

(c) $M = 2.5$.

Figure 6. Continued.

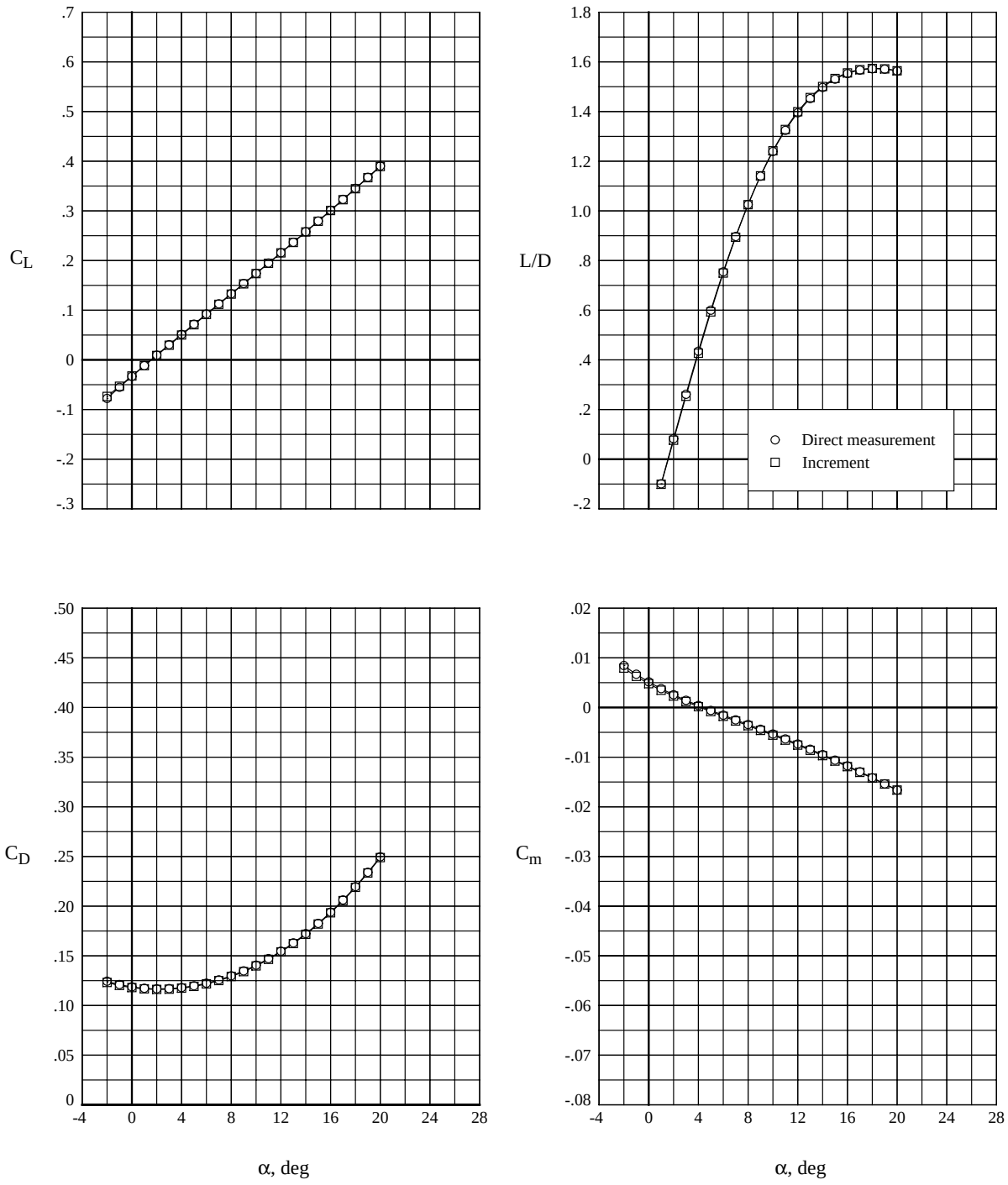

(d) $M = 3.0$.

Figure 6. Continued.

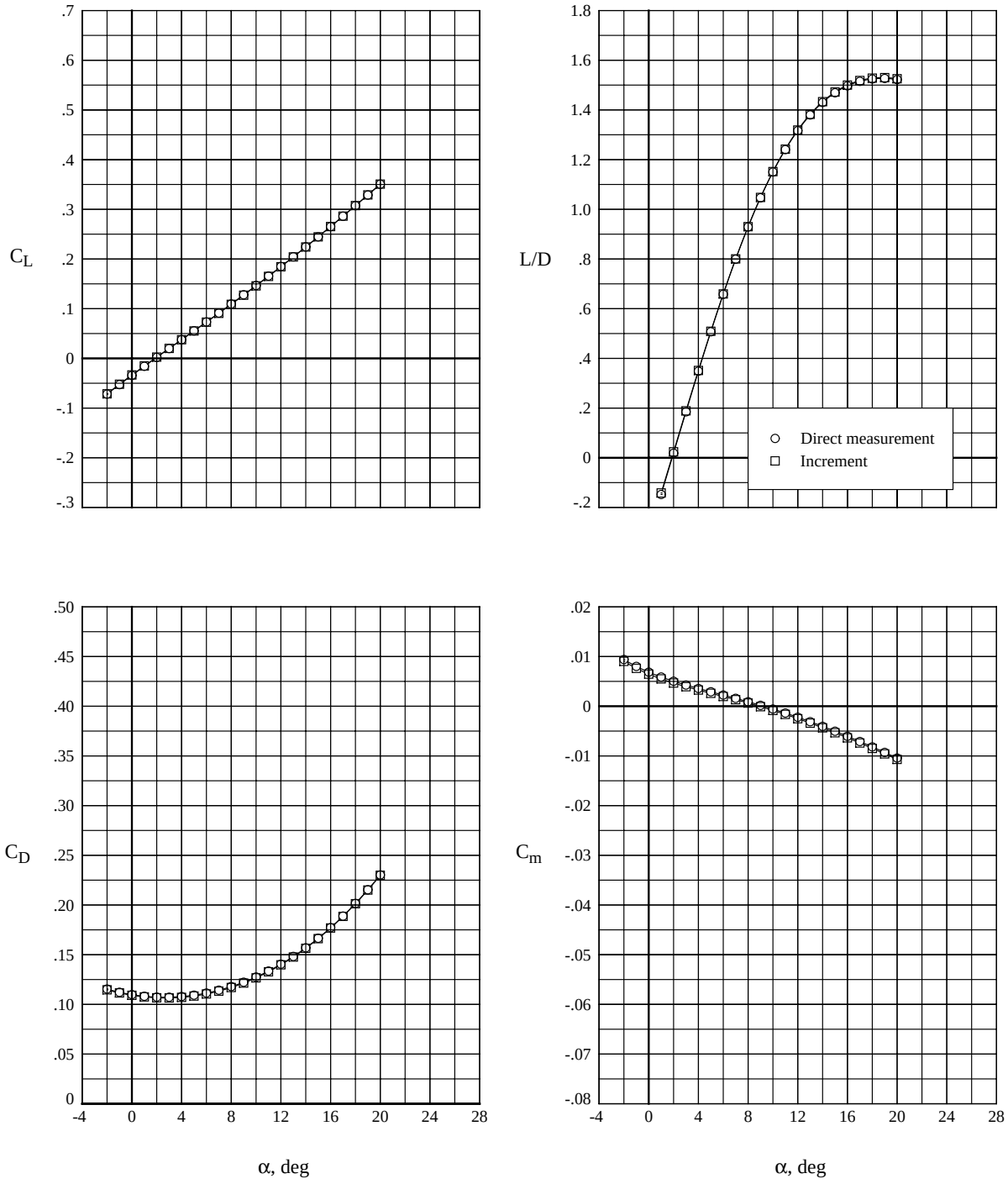

(e) $M = 3.5$.

Figure 6. Continued.

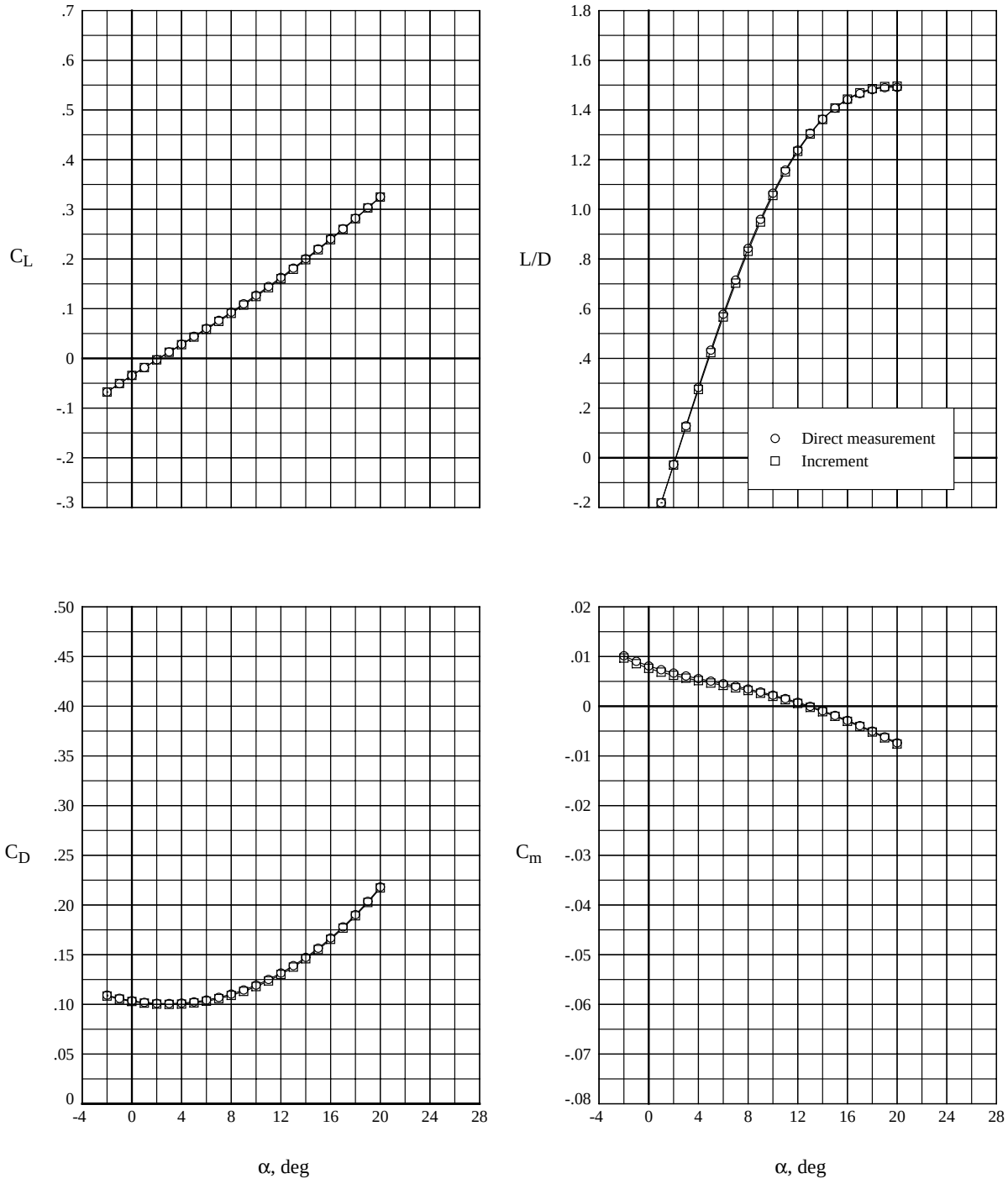

(f) $M = 4.0$.

Figure 6. Continued.

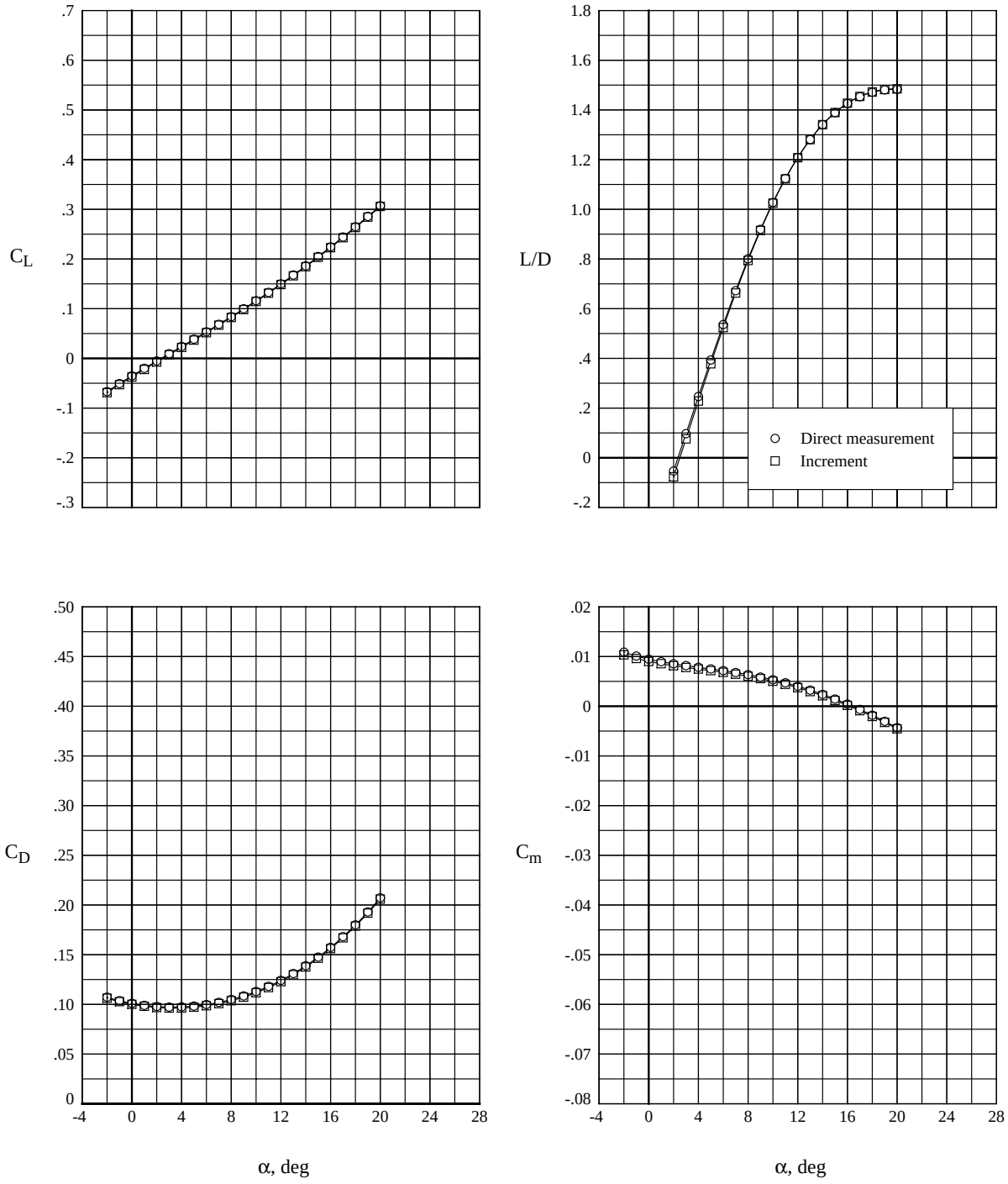

(g) $M = 4.5$.

Figure 6. Concluded.

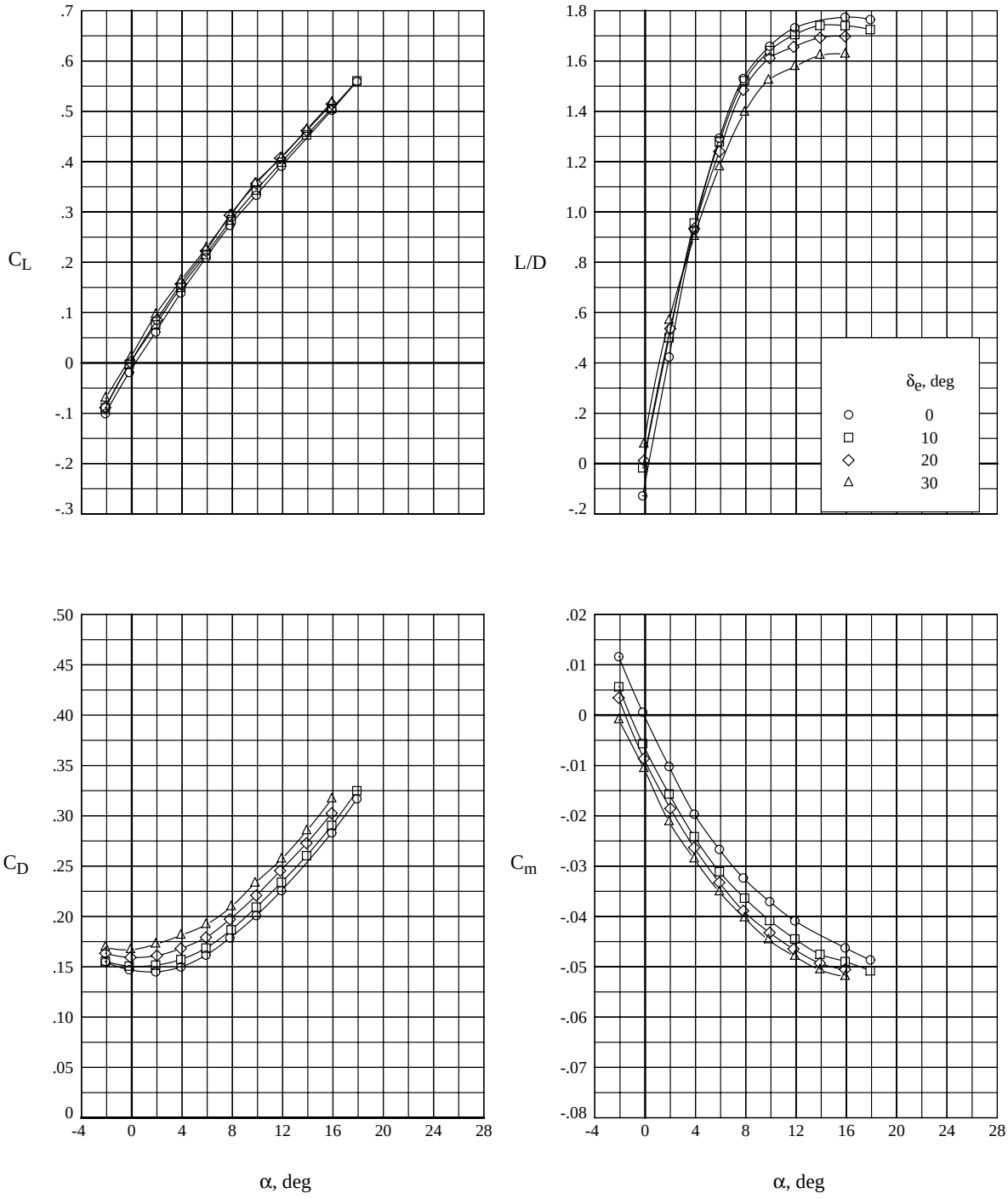

(a) M = 1.6.

Figure 7. Effect of positive elevon deflection on longitudinal aerodynamic characteristics.

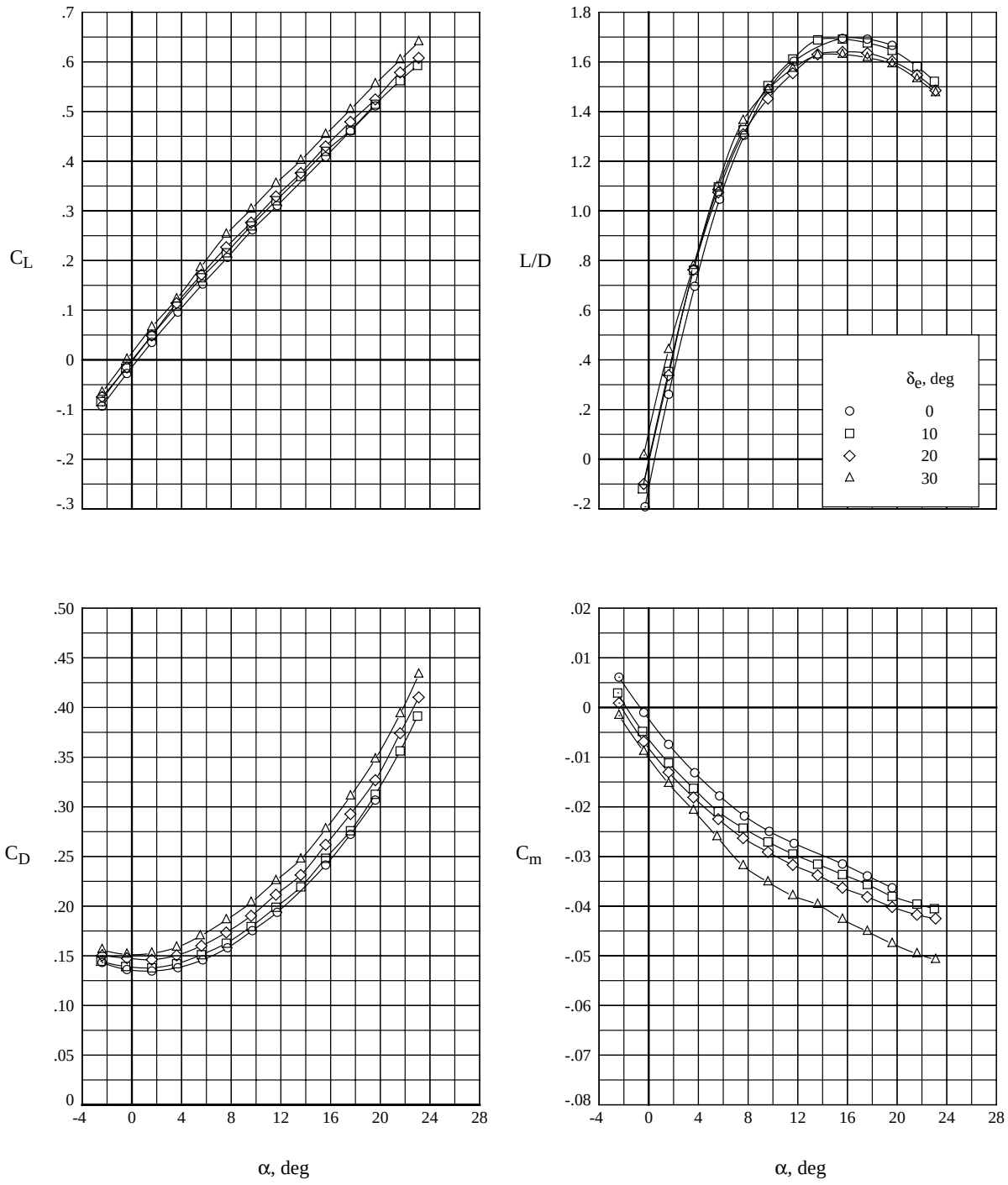

(b) $M = 2.0$.

Figure 7. Continued.

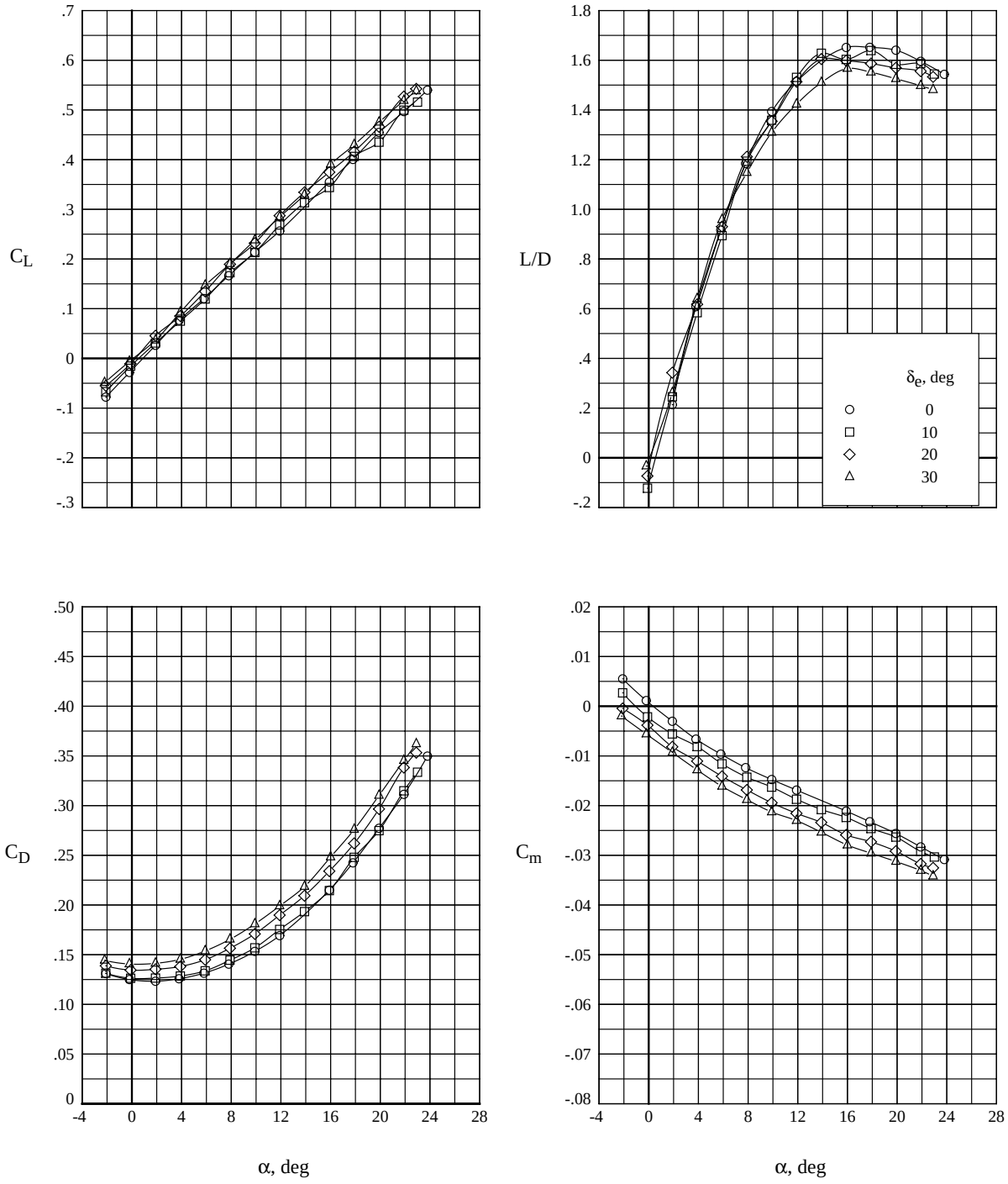

(c) $M = 2.5$.

Figure 7. Continued.

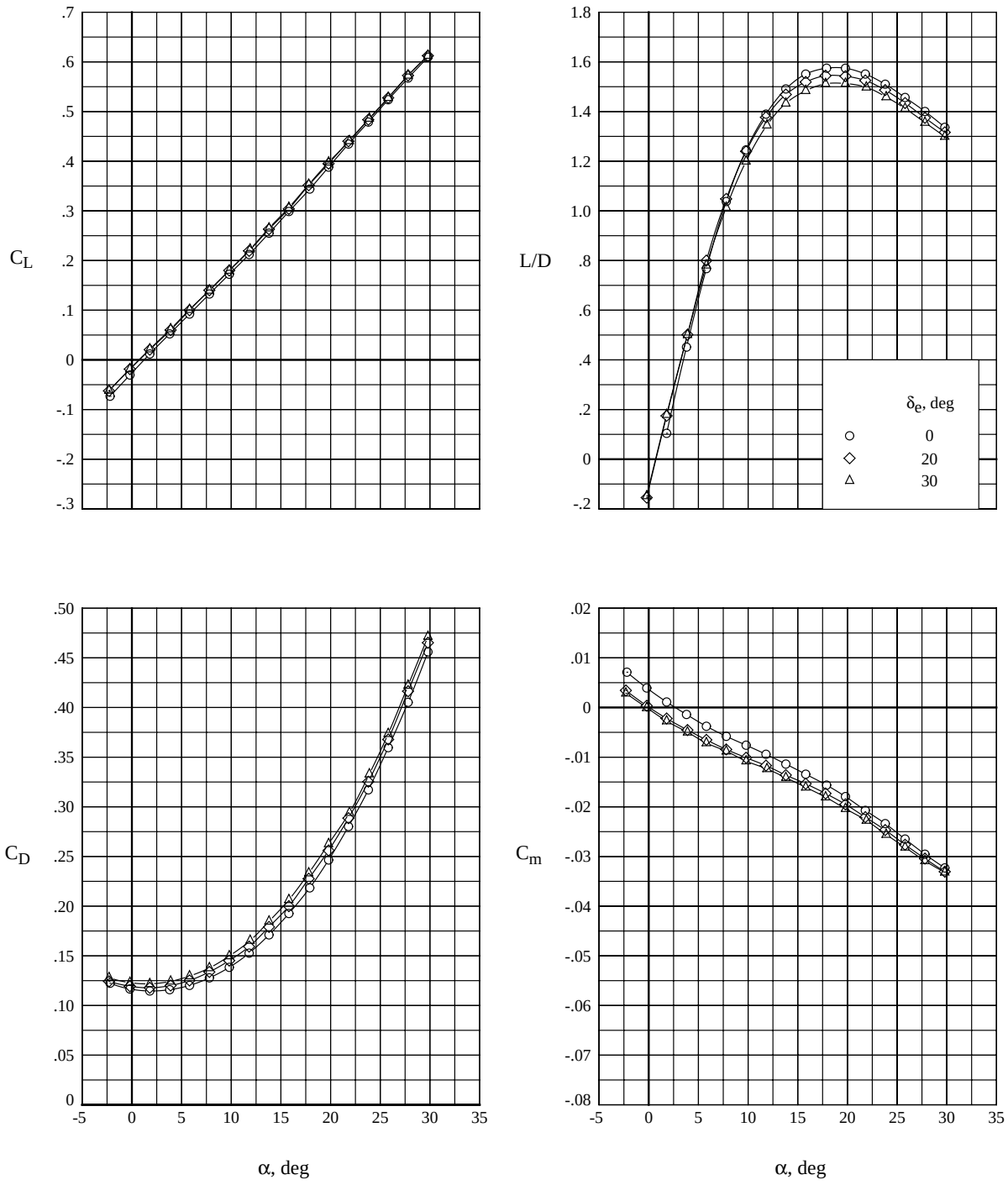

(d) $M = 3.0$.

Figure 7. Continued.

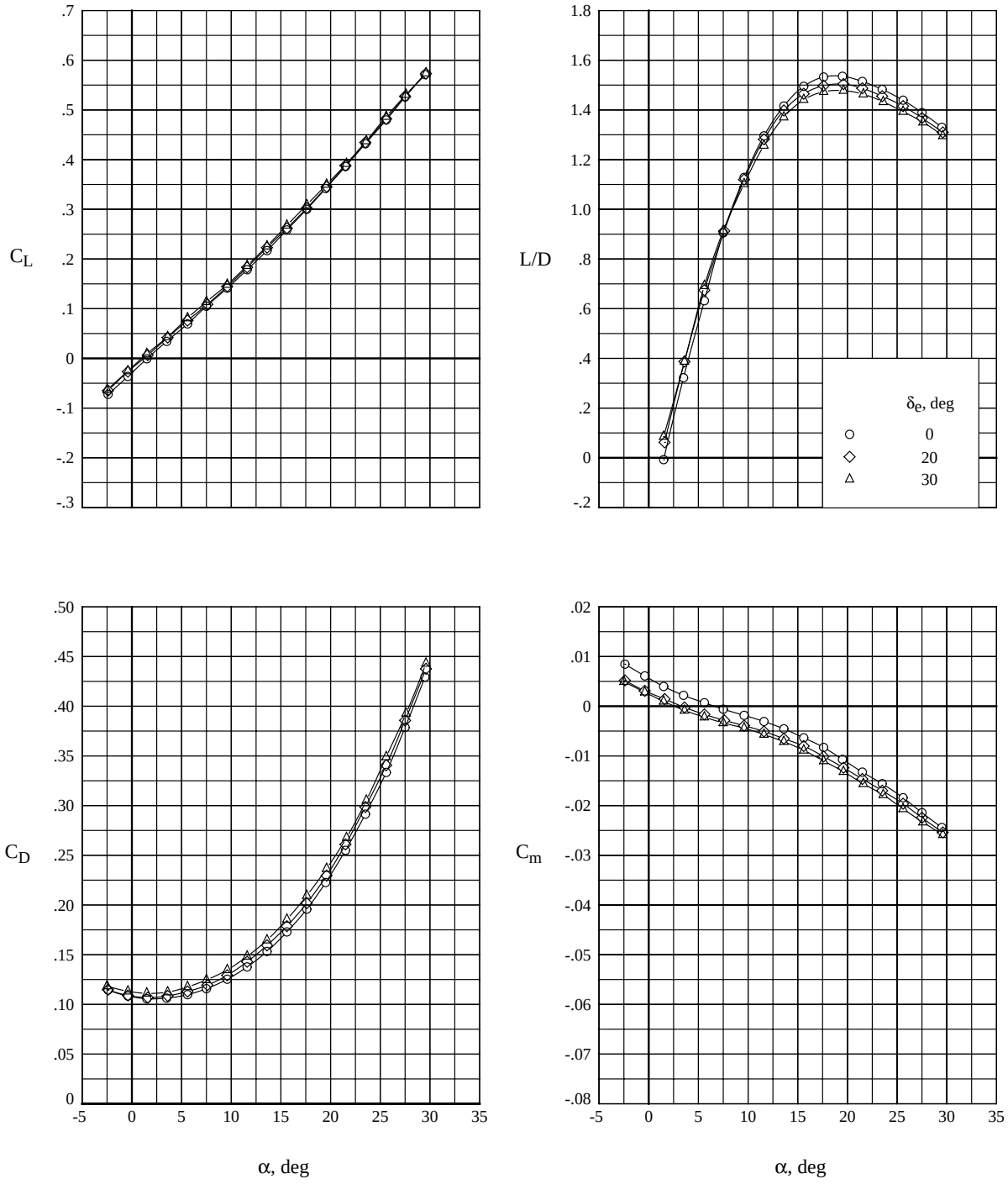

(e) $M = 3.5$.

Figure 7. Continued.

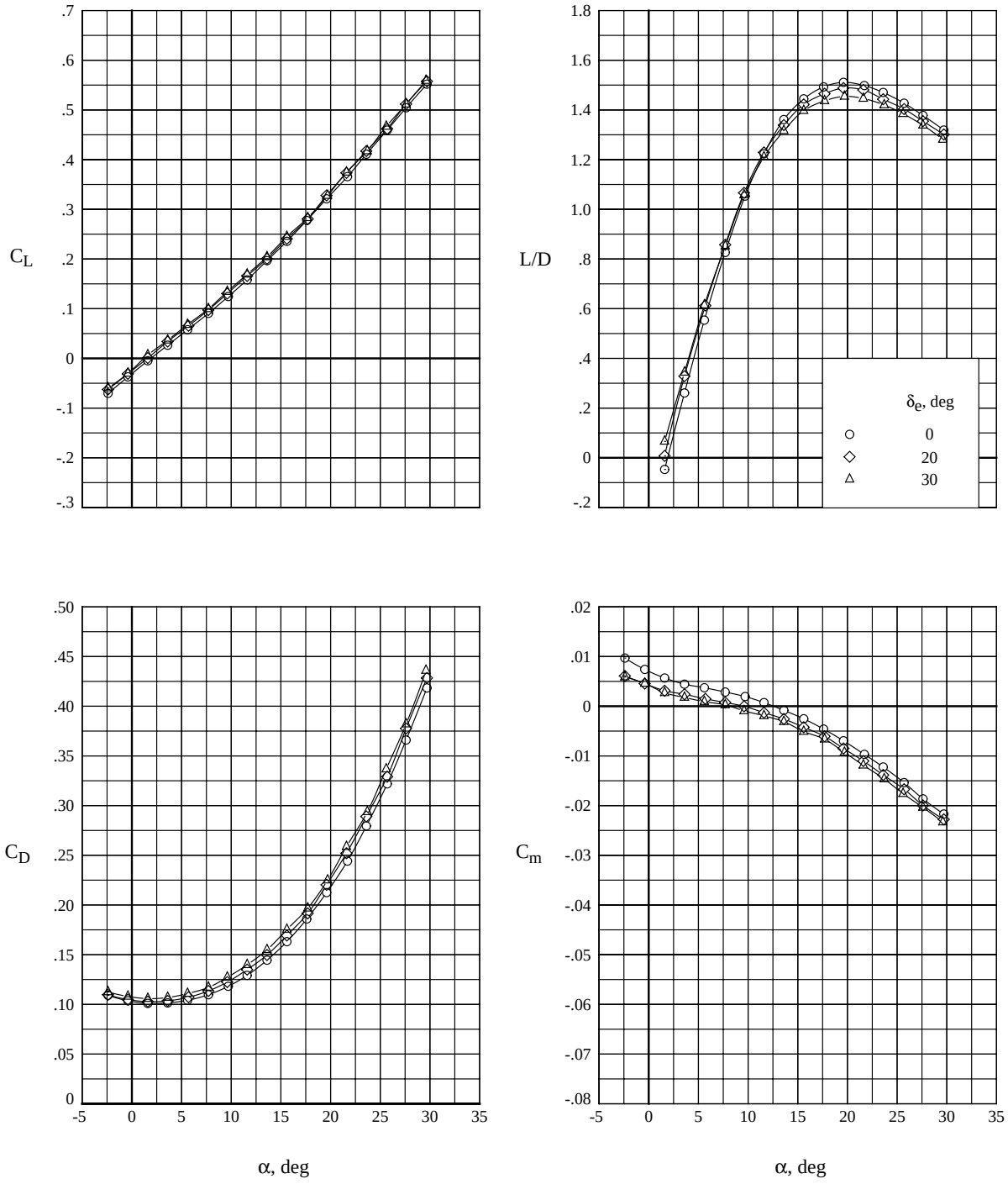

(f) M = 4.0.

Figure 7. Continued.

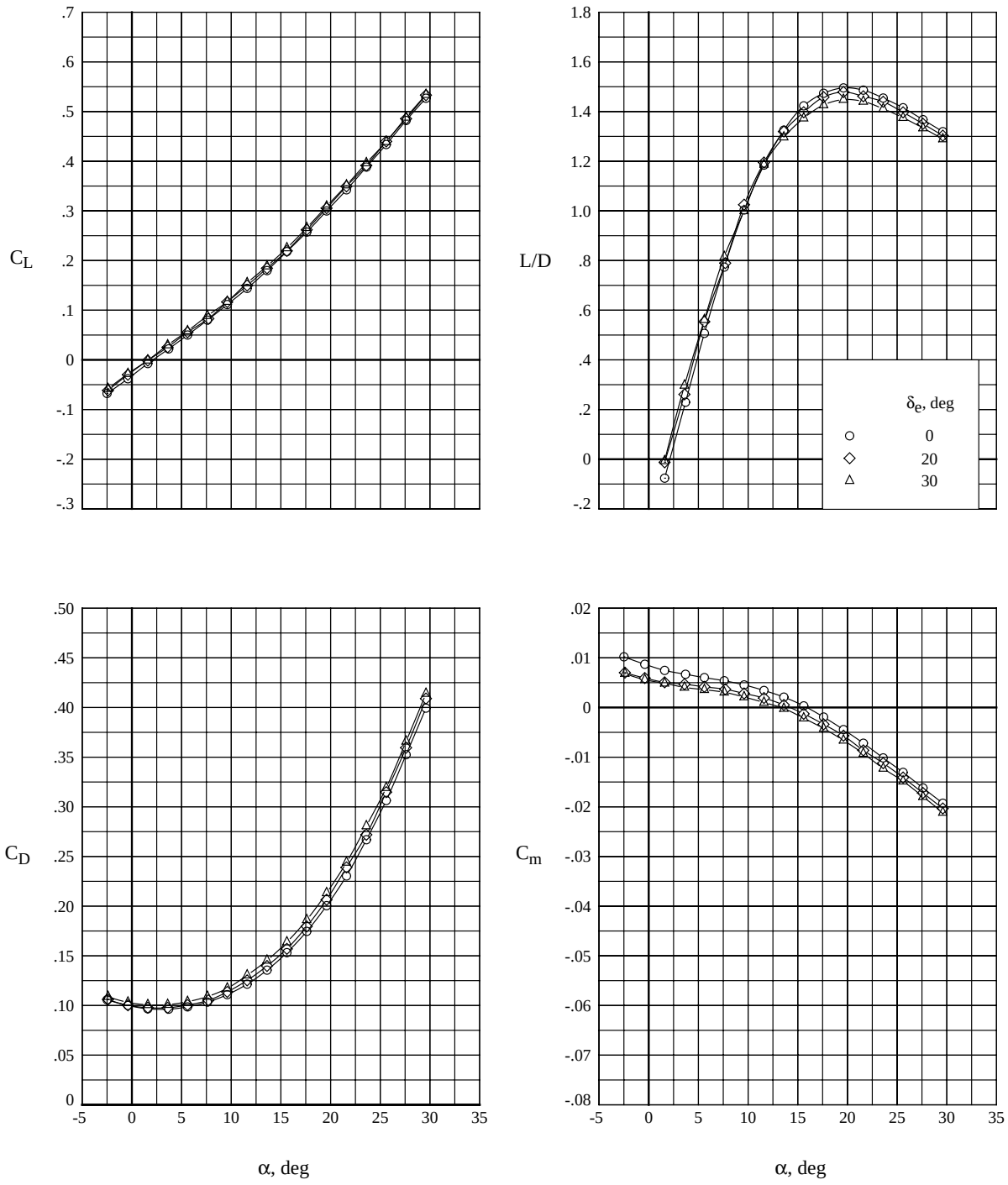

(g) $M = 4.5$.

Figure 7. Concluded.

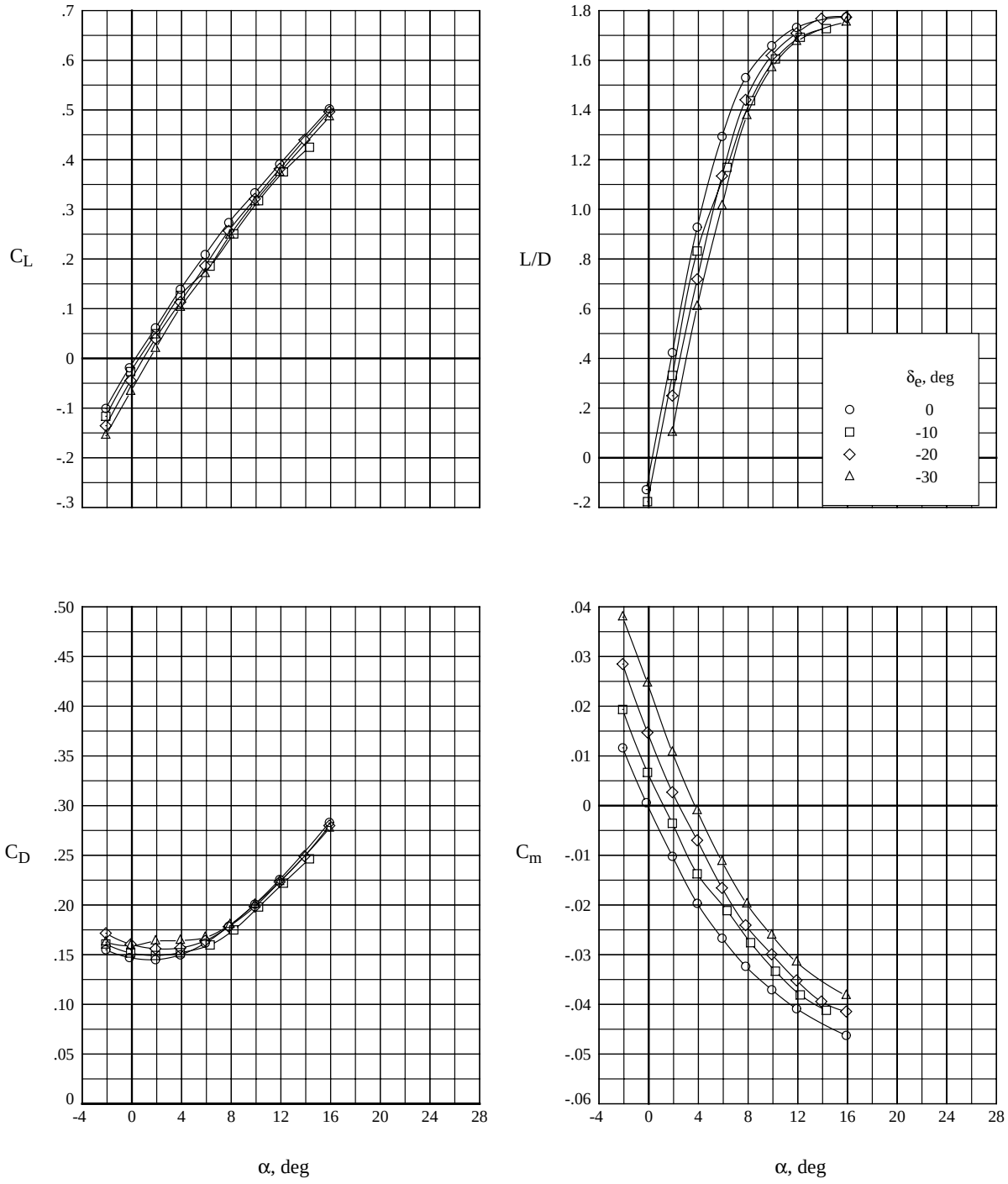

(a) $M = 1.6$.

Figure 8. Effect of negative elevon deflection on longitudinal aerodynamic characteristics.

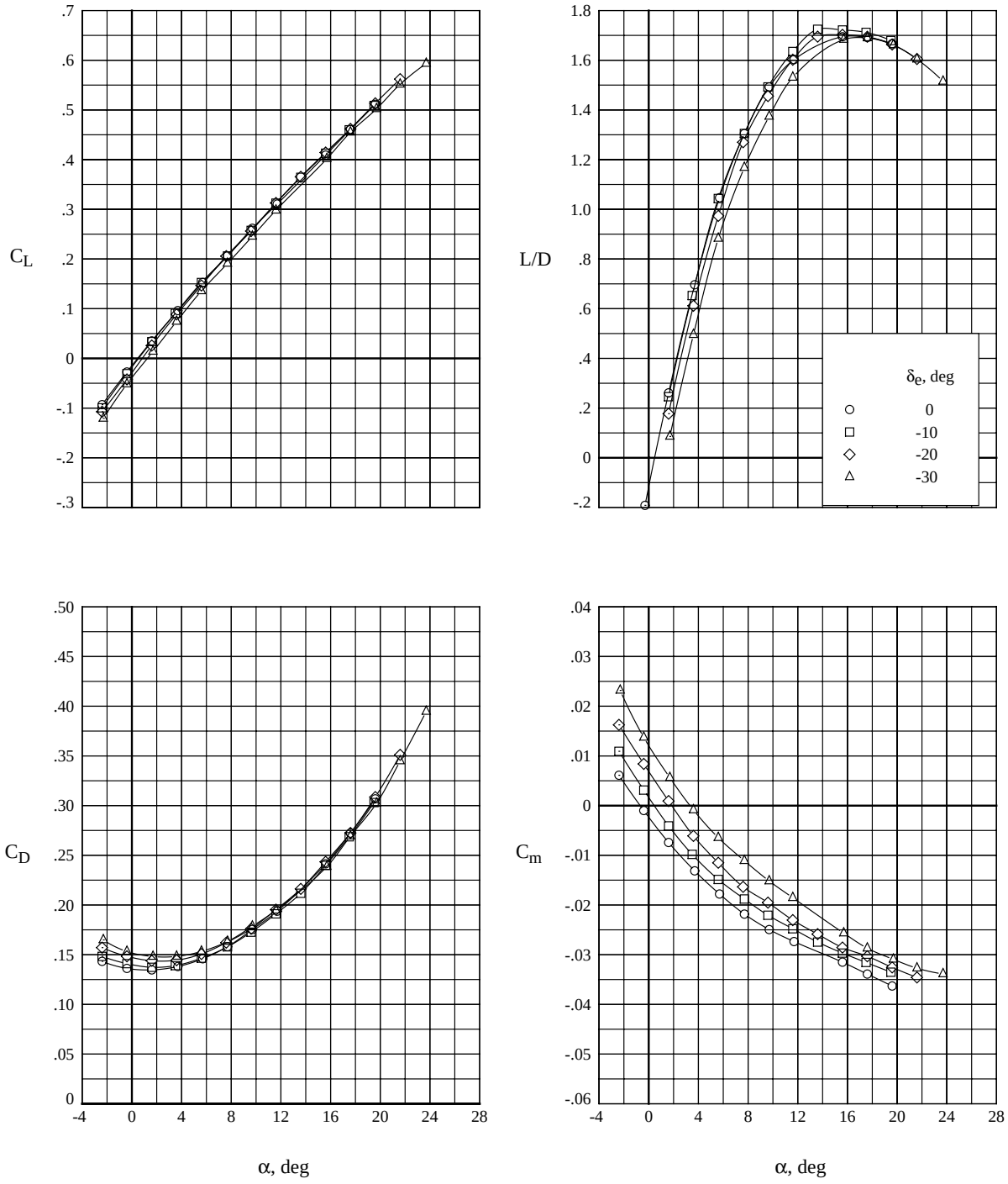

(b) M = 2.0.

Figure 8. Continued.

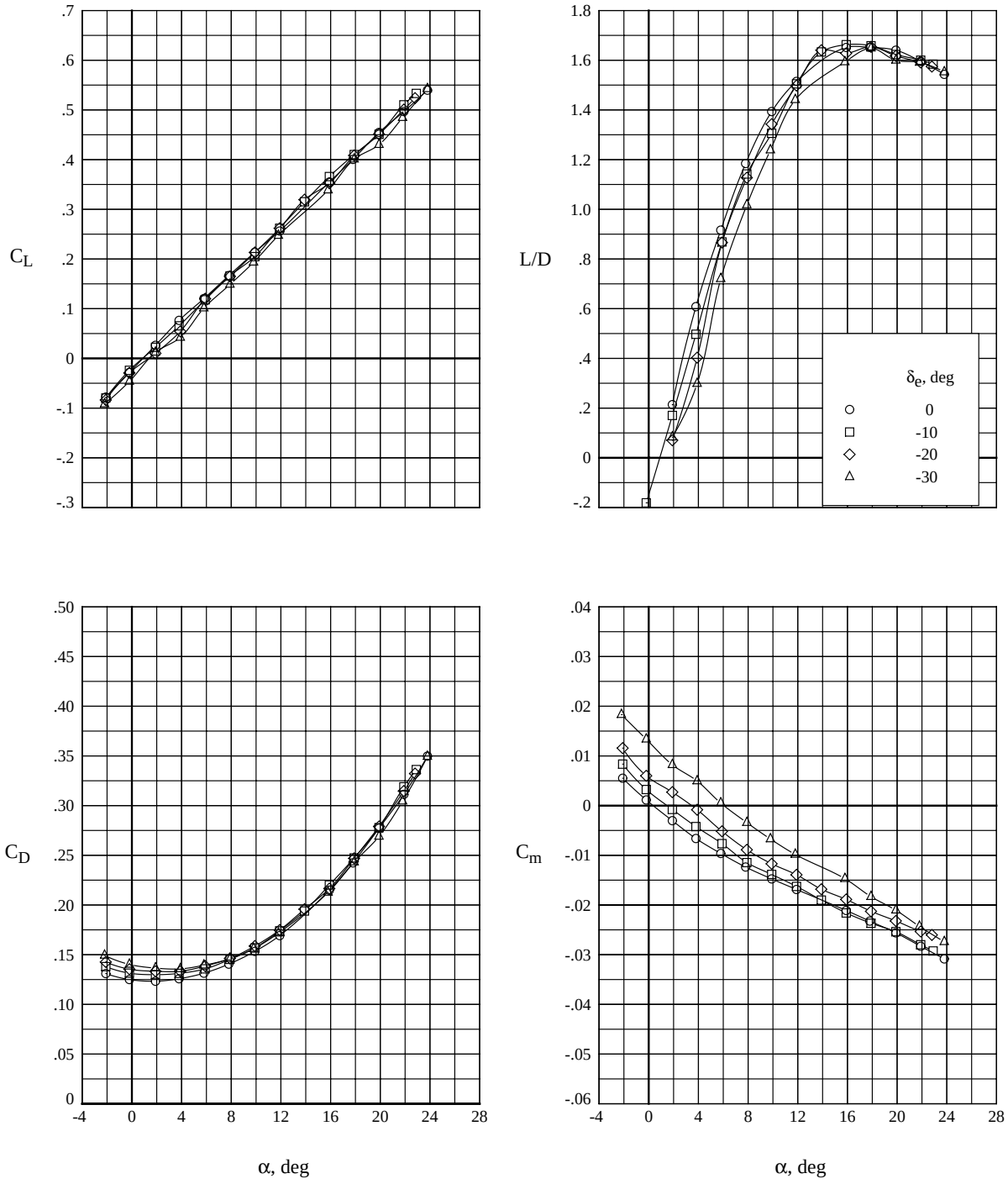

(c) M = 2.5.

Figure 8. Continued.

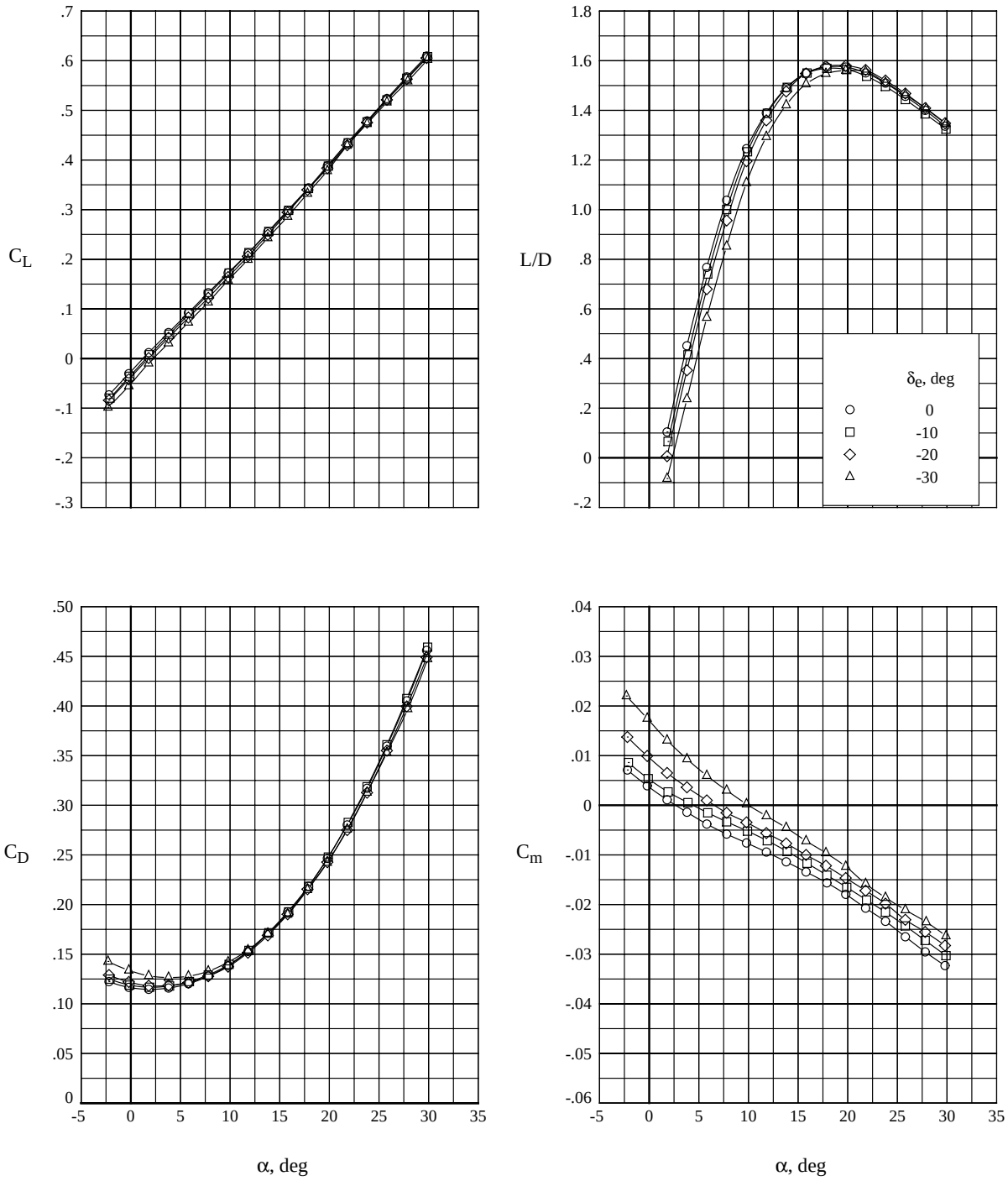

(d) M = 3.0.

Figure 8. Continued.

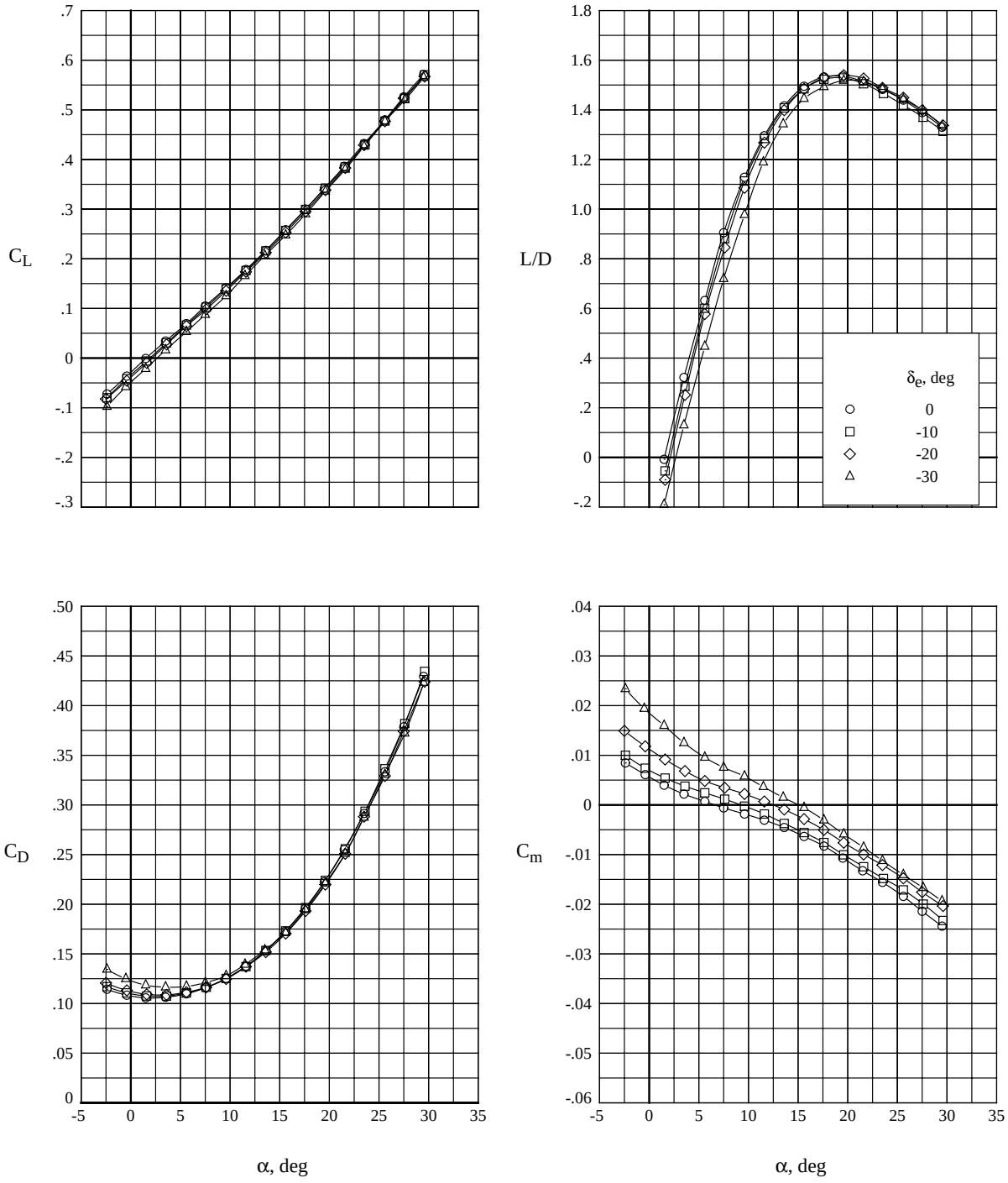

(e) $M = 3.5$.

Figure 8. Continued.

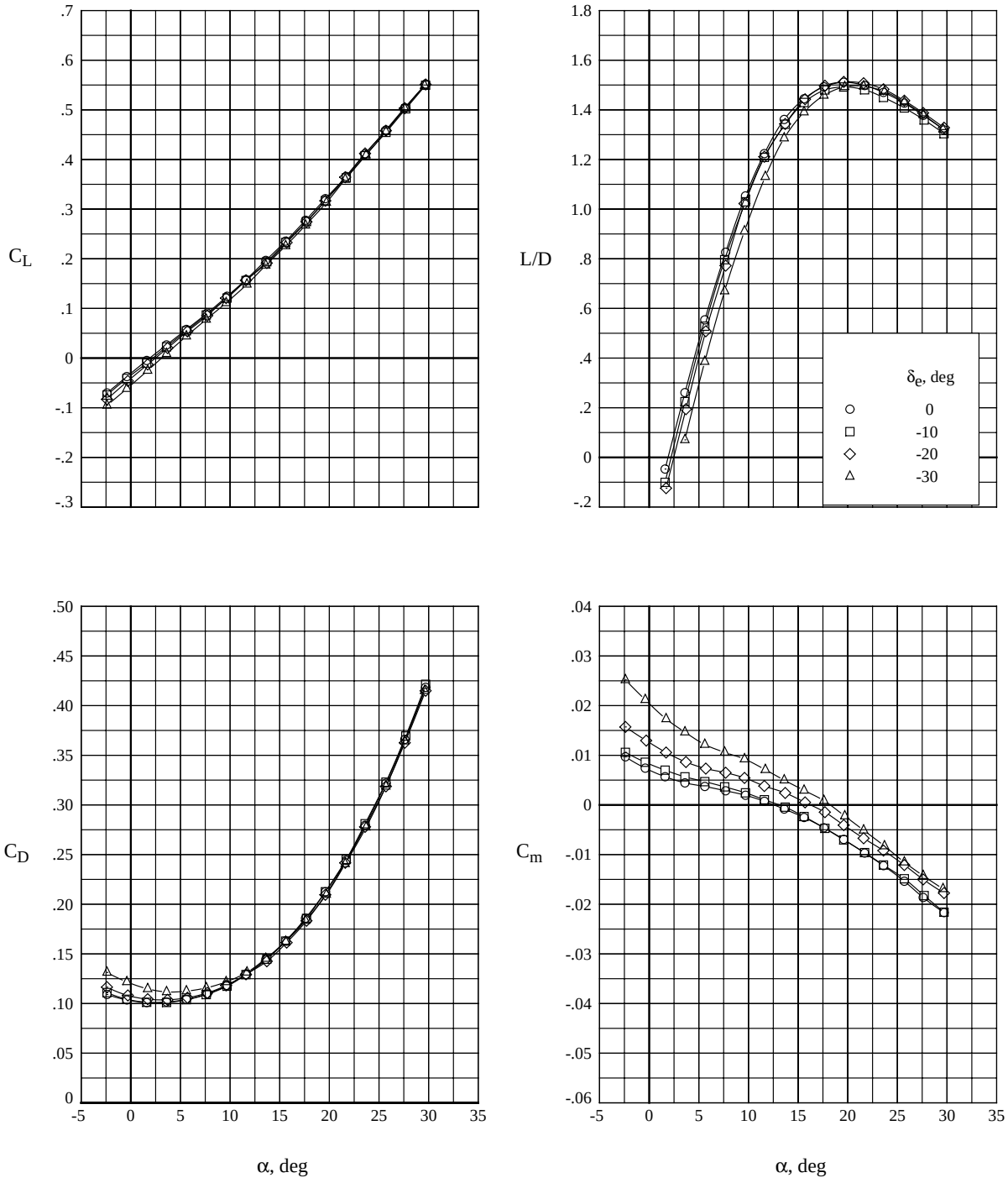

(f) $M = 4.0$.

Figure 8. Continued.

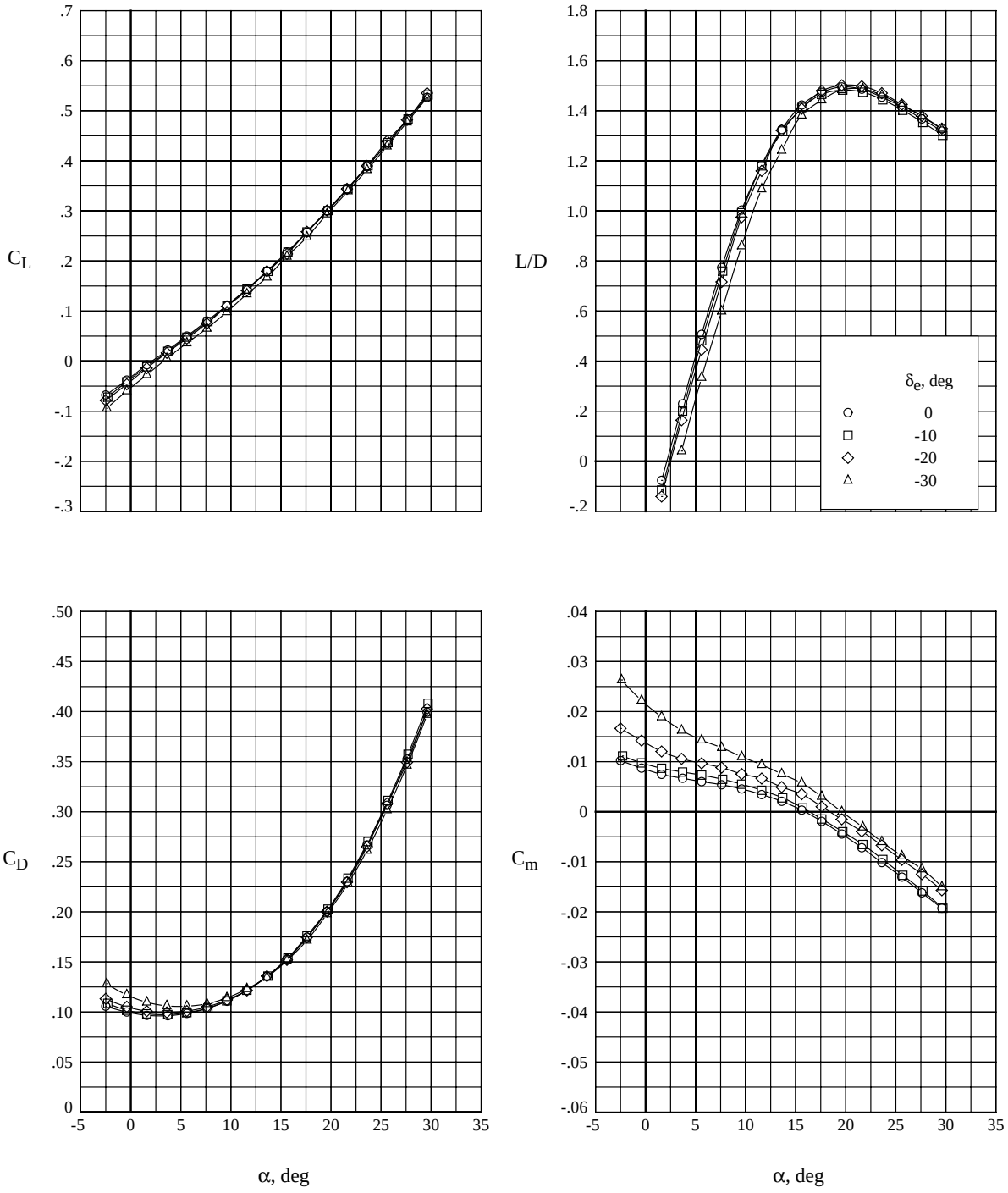

(g) $M = 4.5$.

Figure 8. Concluded.

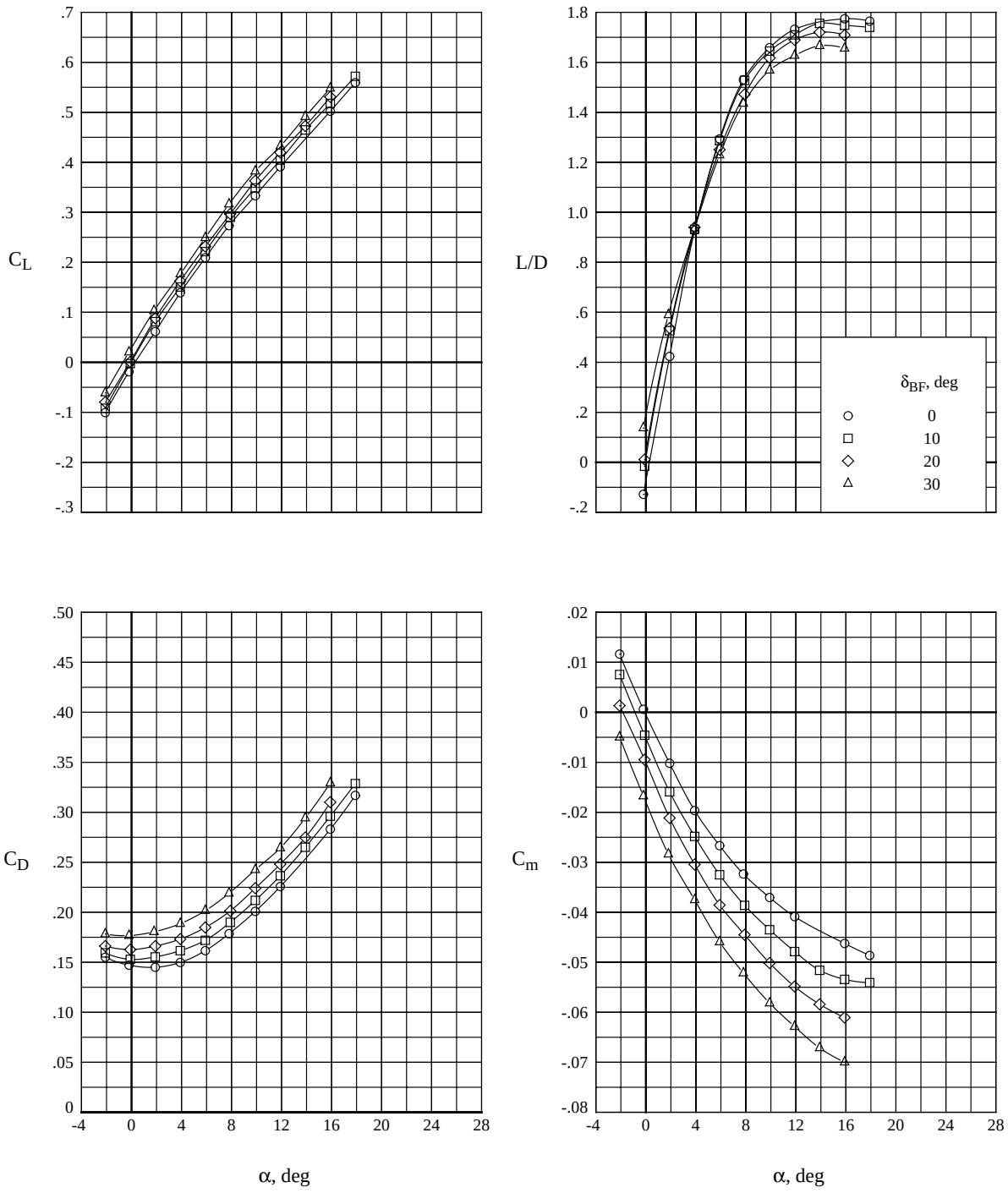

(a) M = 1.6.

Figure 9. Effect of positive body flap deflection on longitudinal aerodynamic characteristics.

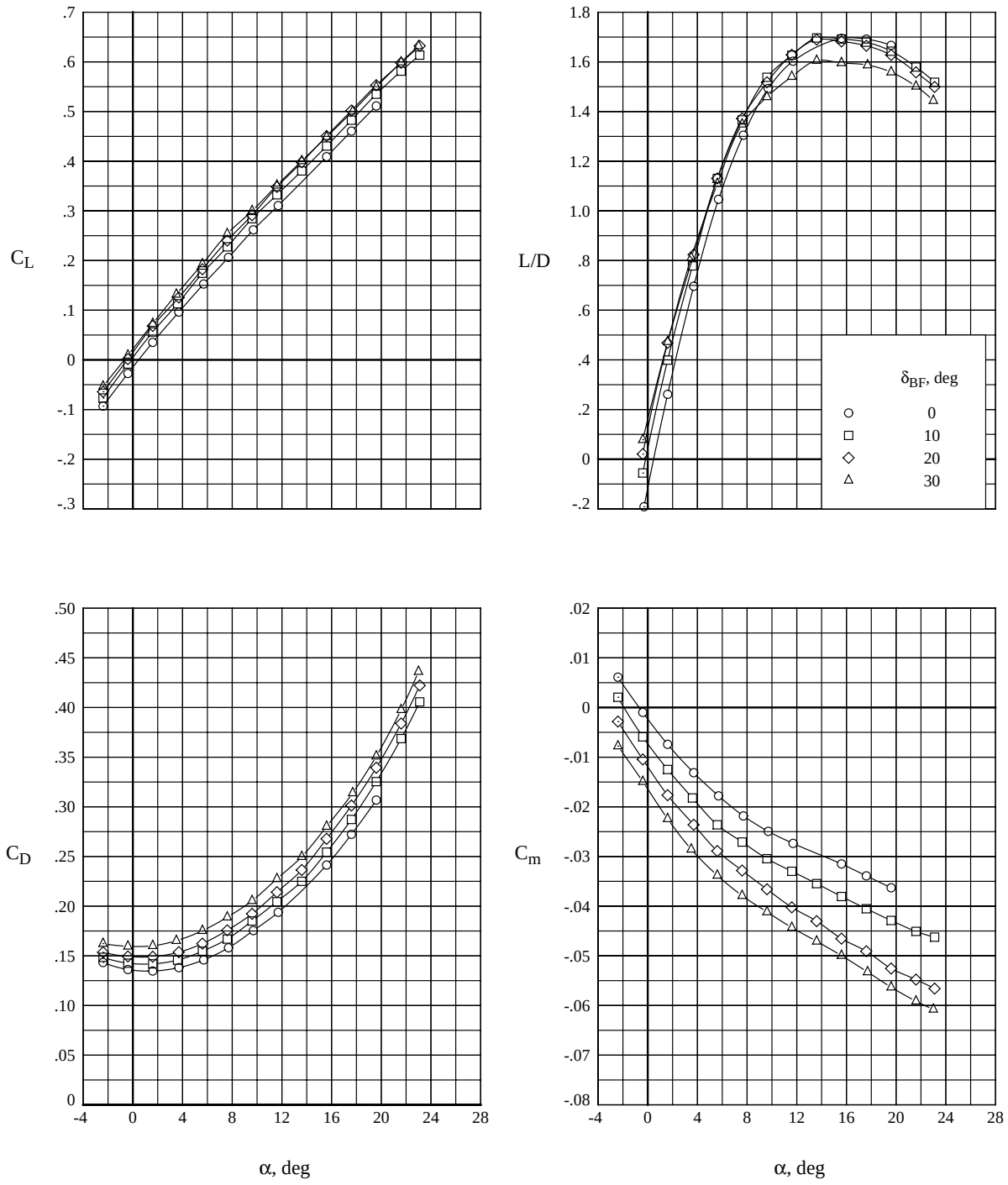

(b) $M = 2.0$.

Figure 9. Continued.

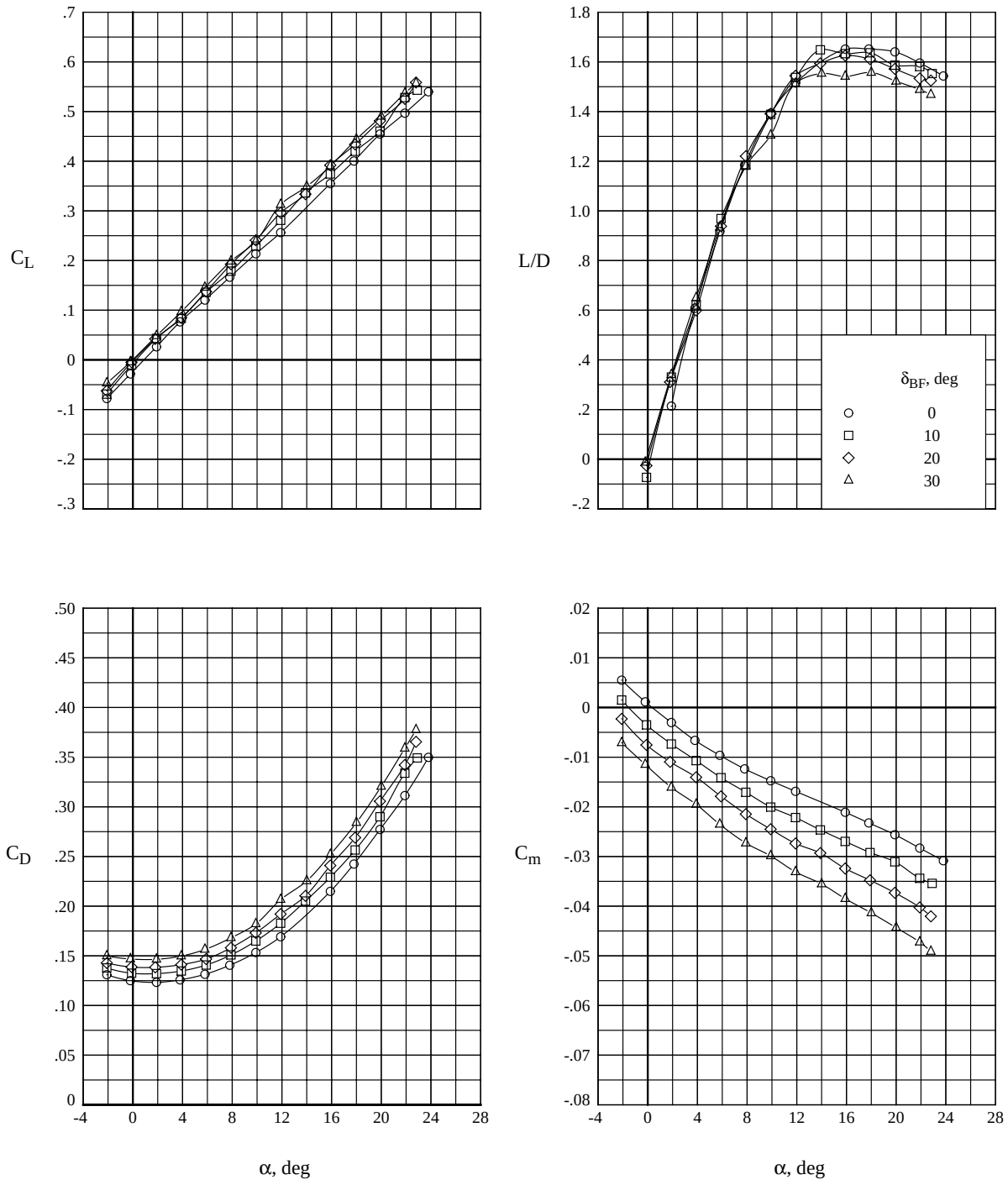

(c) $M = 2.5$.

Figure 9. Continued.

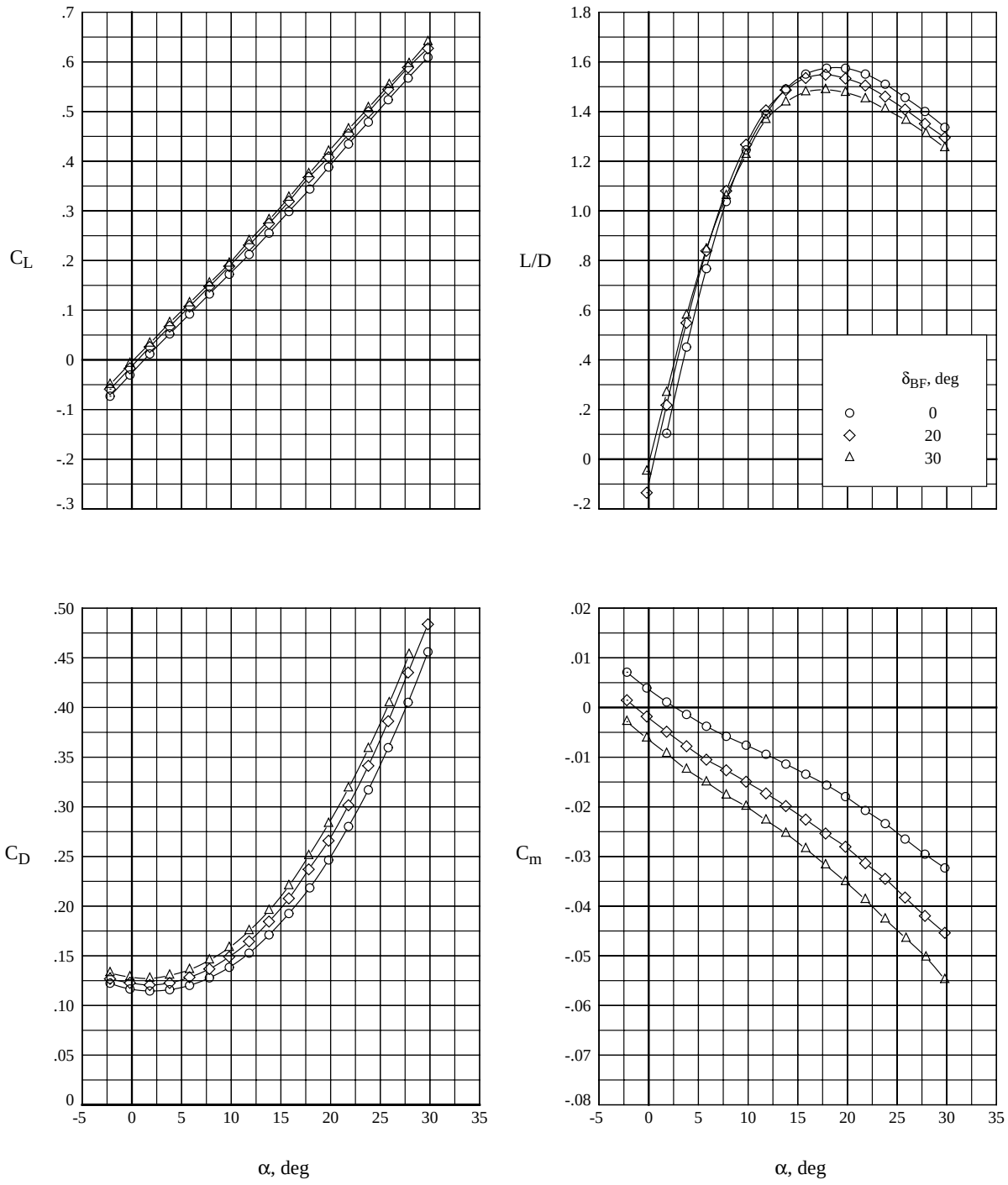

(d) $M = 3.0$.

Figure 9. Continued.

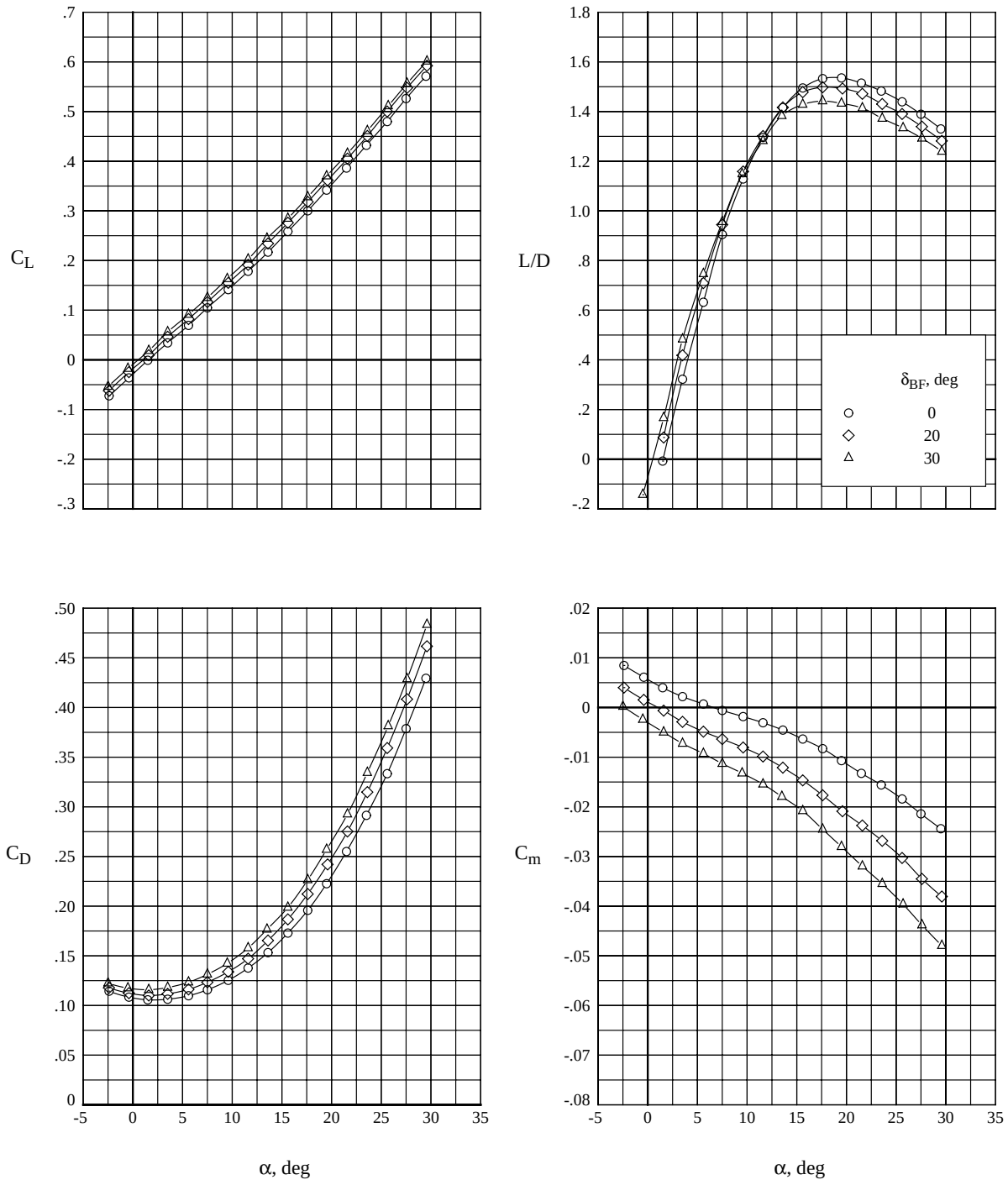

(e) $M = 3.5$.

Figure 9. Continued.

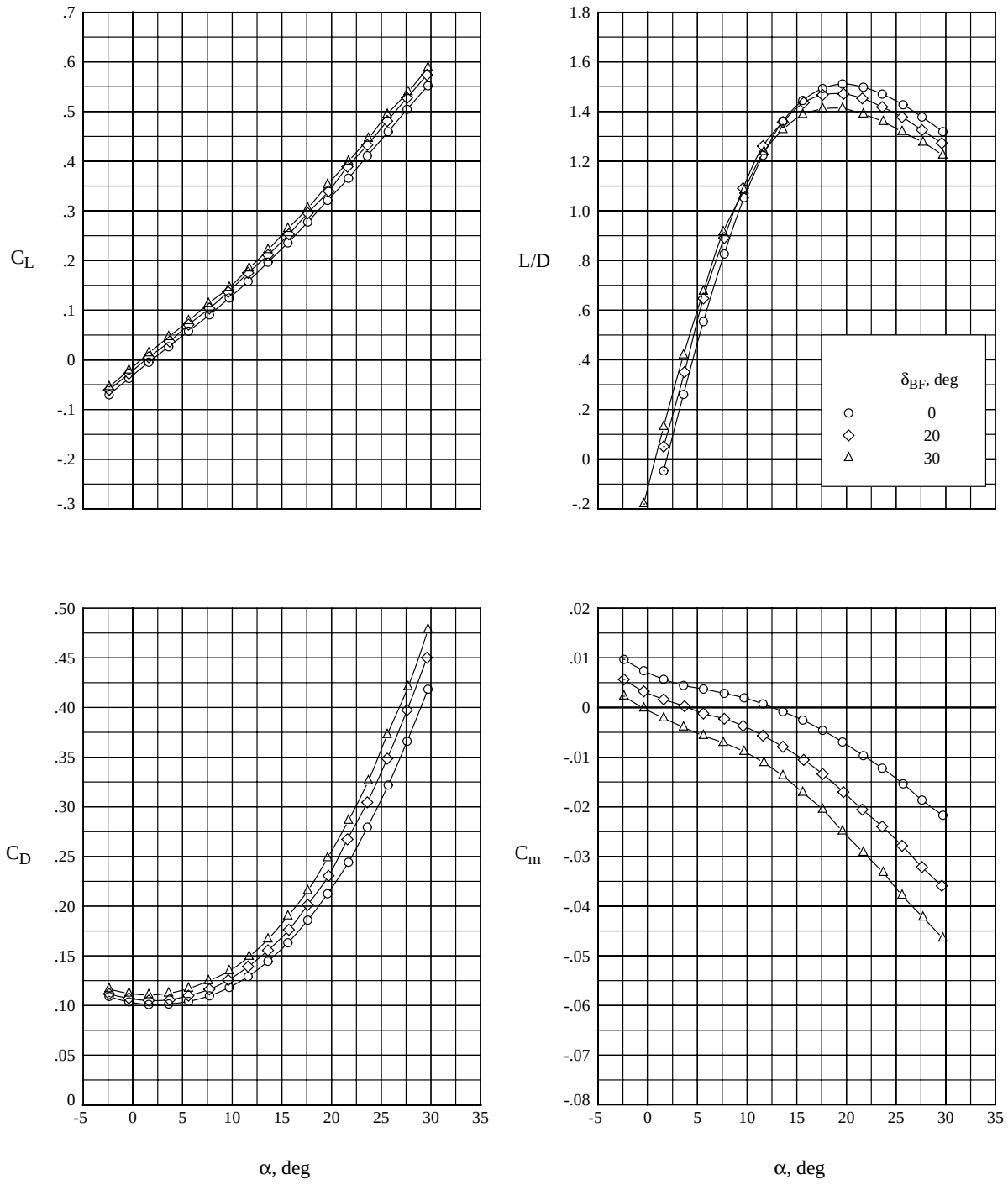

(f) $M = 4.0$.

Figure 9. Continued.

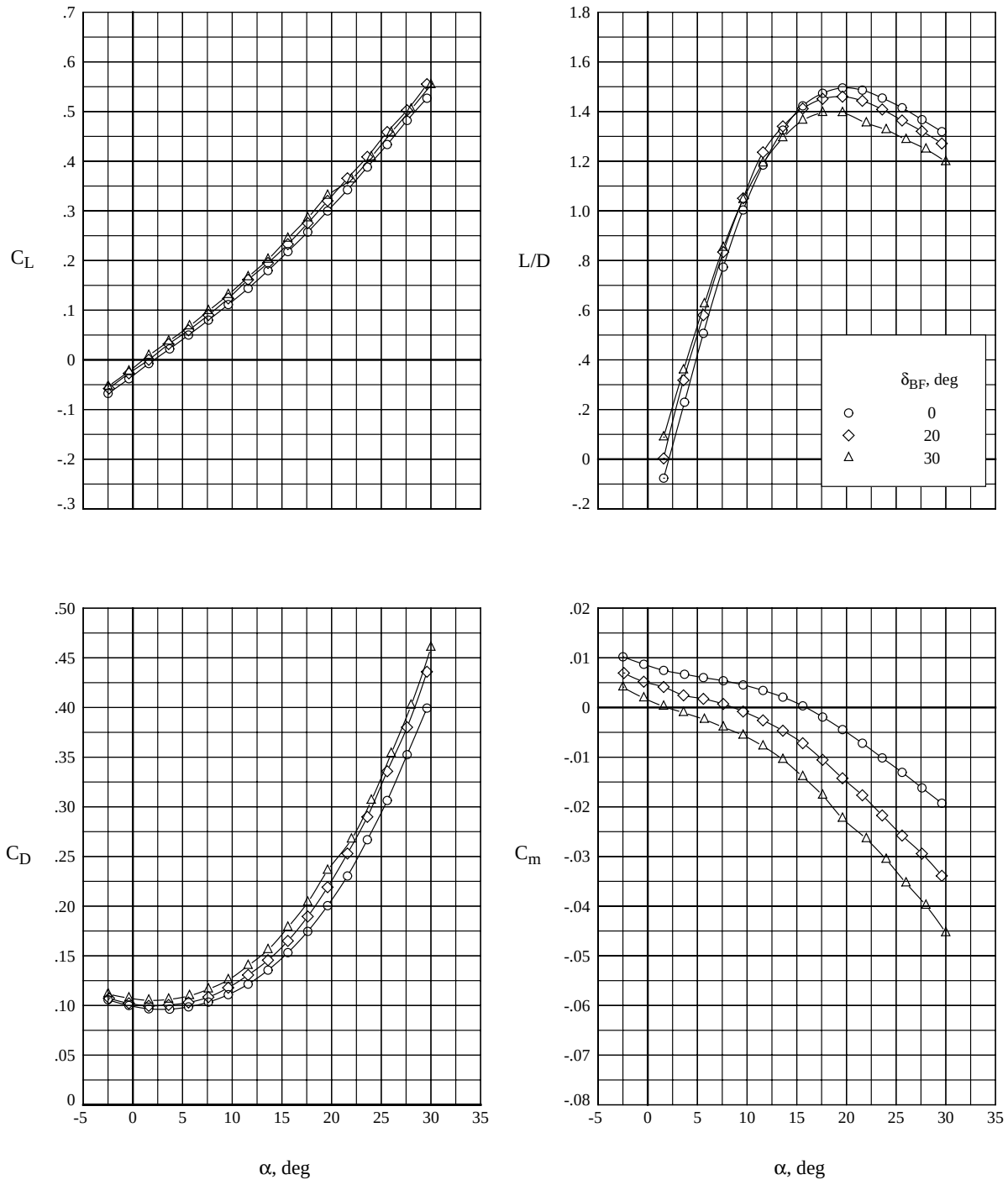

(g) M = 4.5.

Figure 9. Concluded.

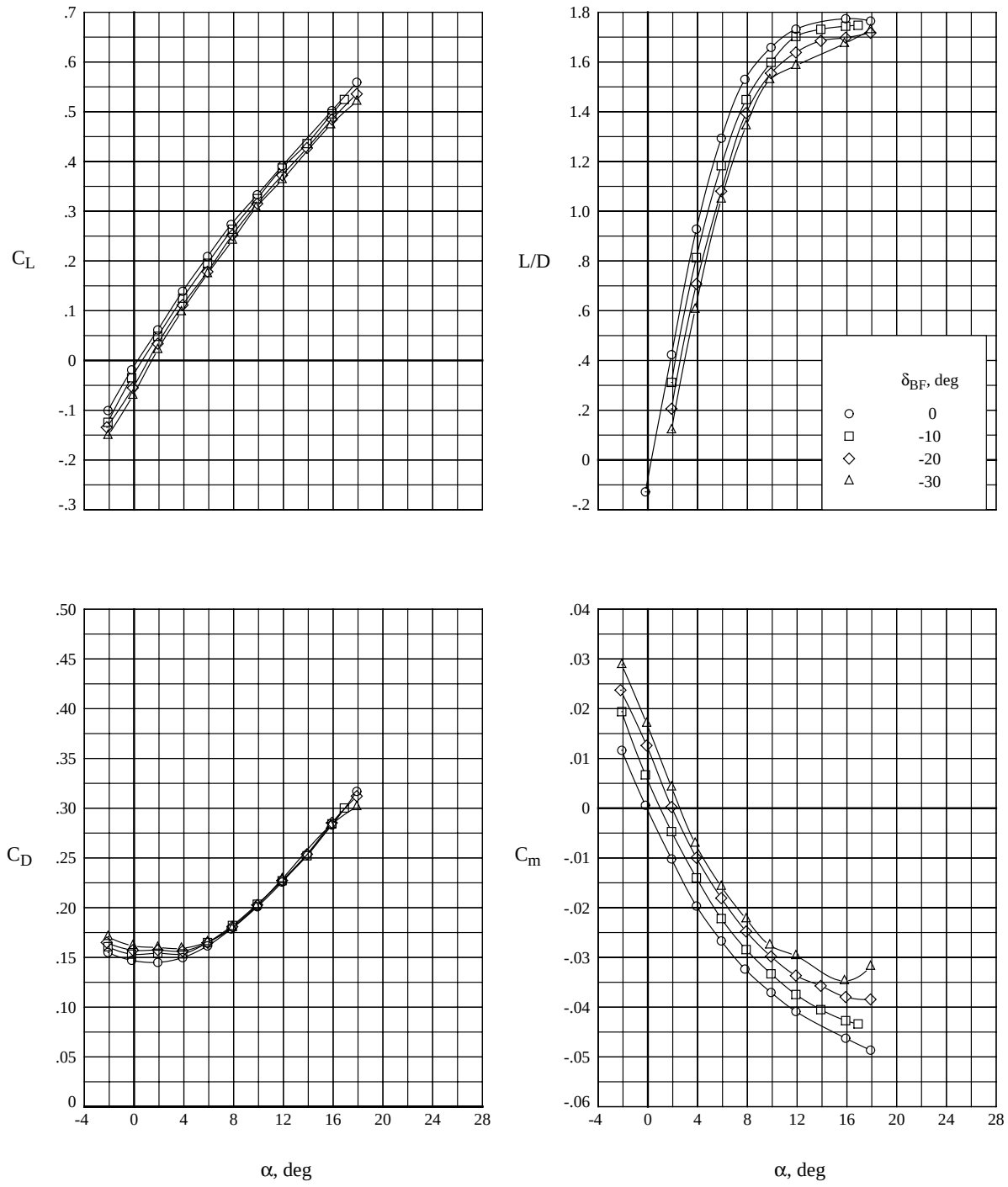

(a) $M = 1.6$.

Figure 10. Effect of negative body flap deflection on longitudinal aerodynamic characteristics.

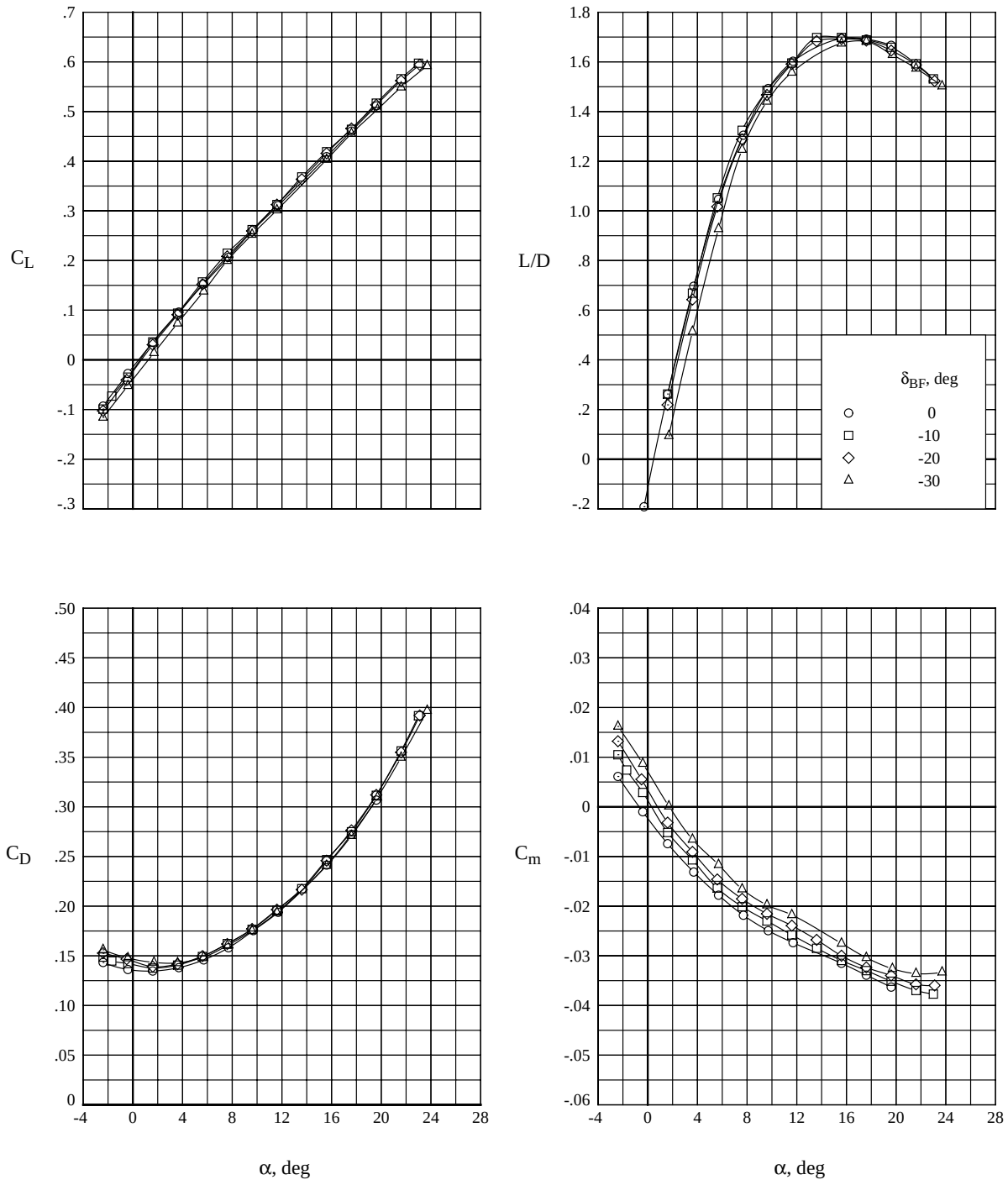

(b) $M = 2.0$.

Figure 10. Continued.

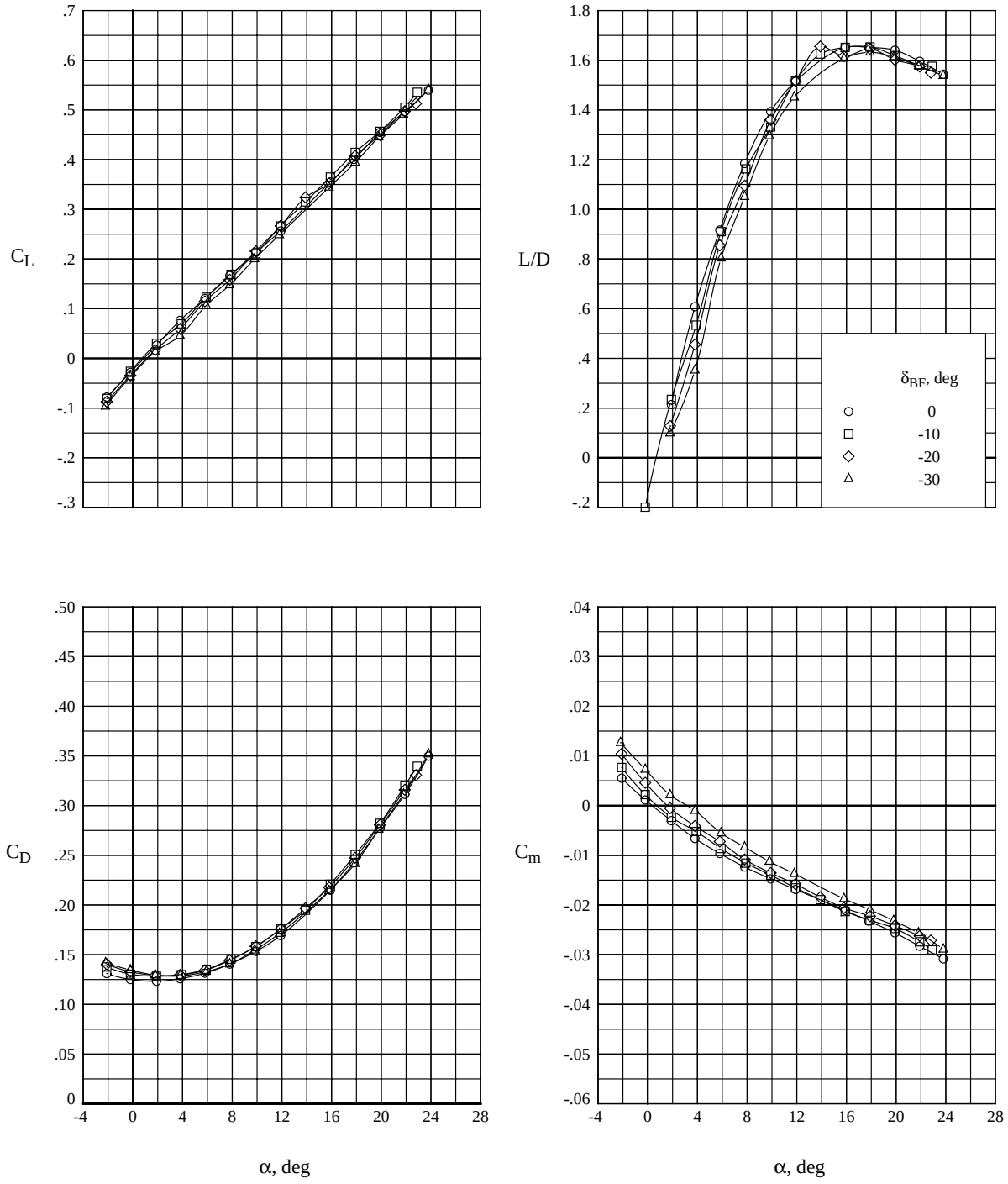

(c) $M = 2.5$.

Figure 10. Continued.

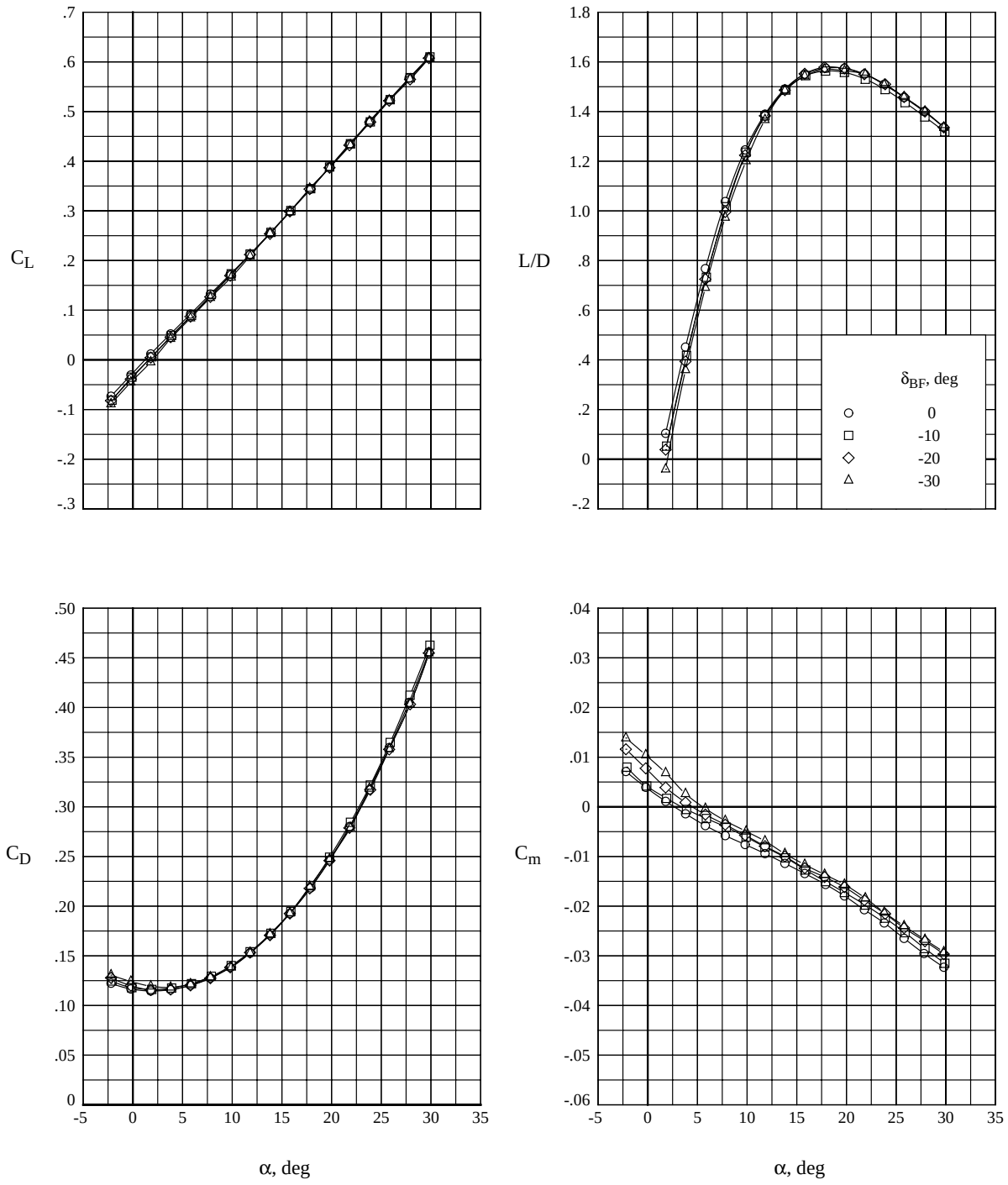

(d) $M = 3.0$.

Figure 10. Continued.

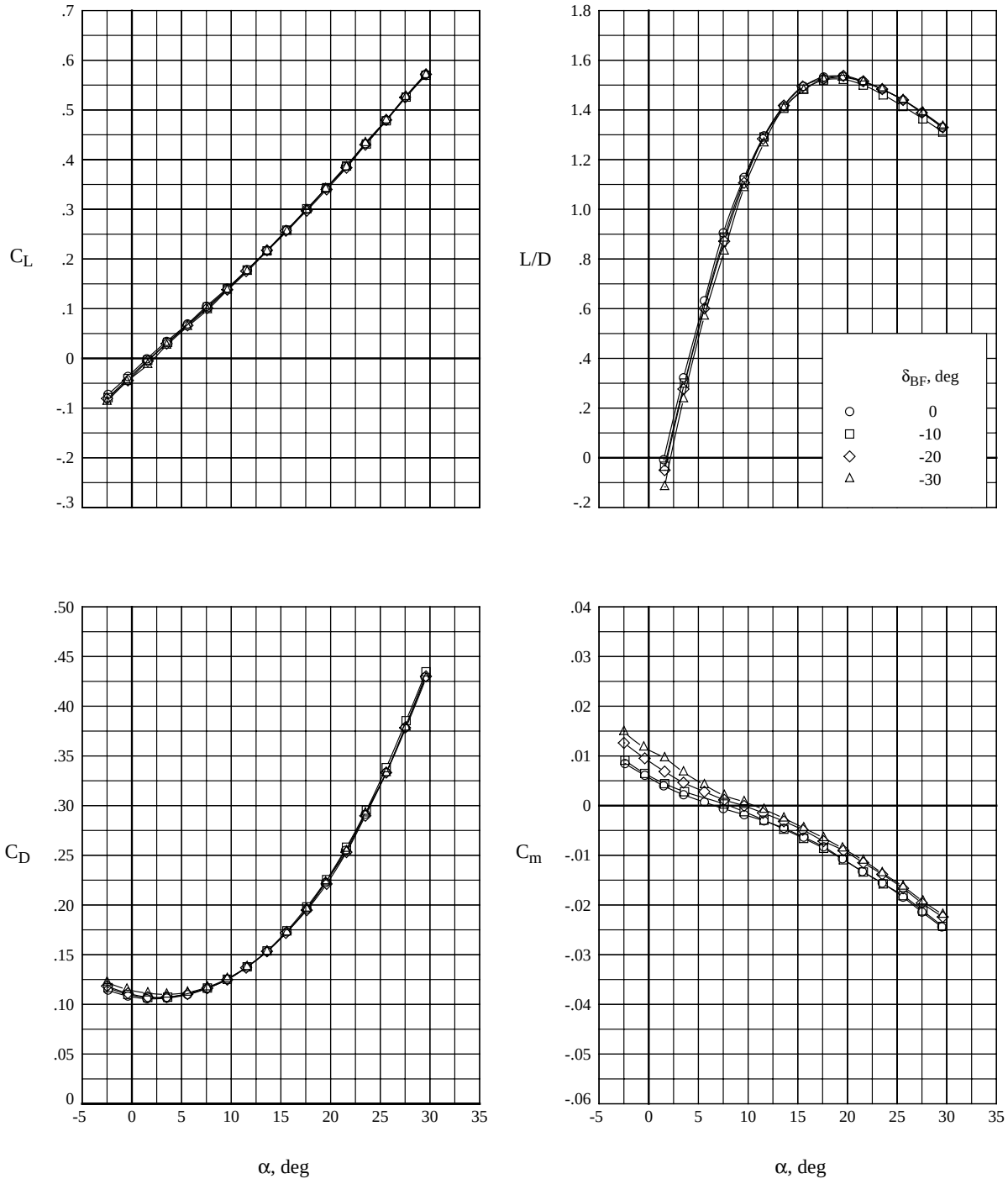

(e) M = 3.5.

Figure 10. Continued.

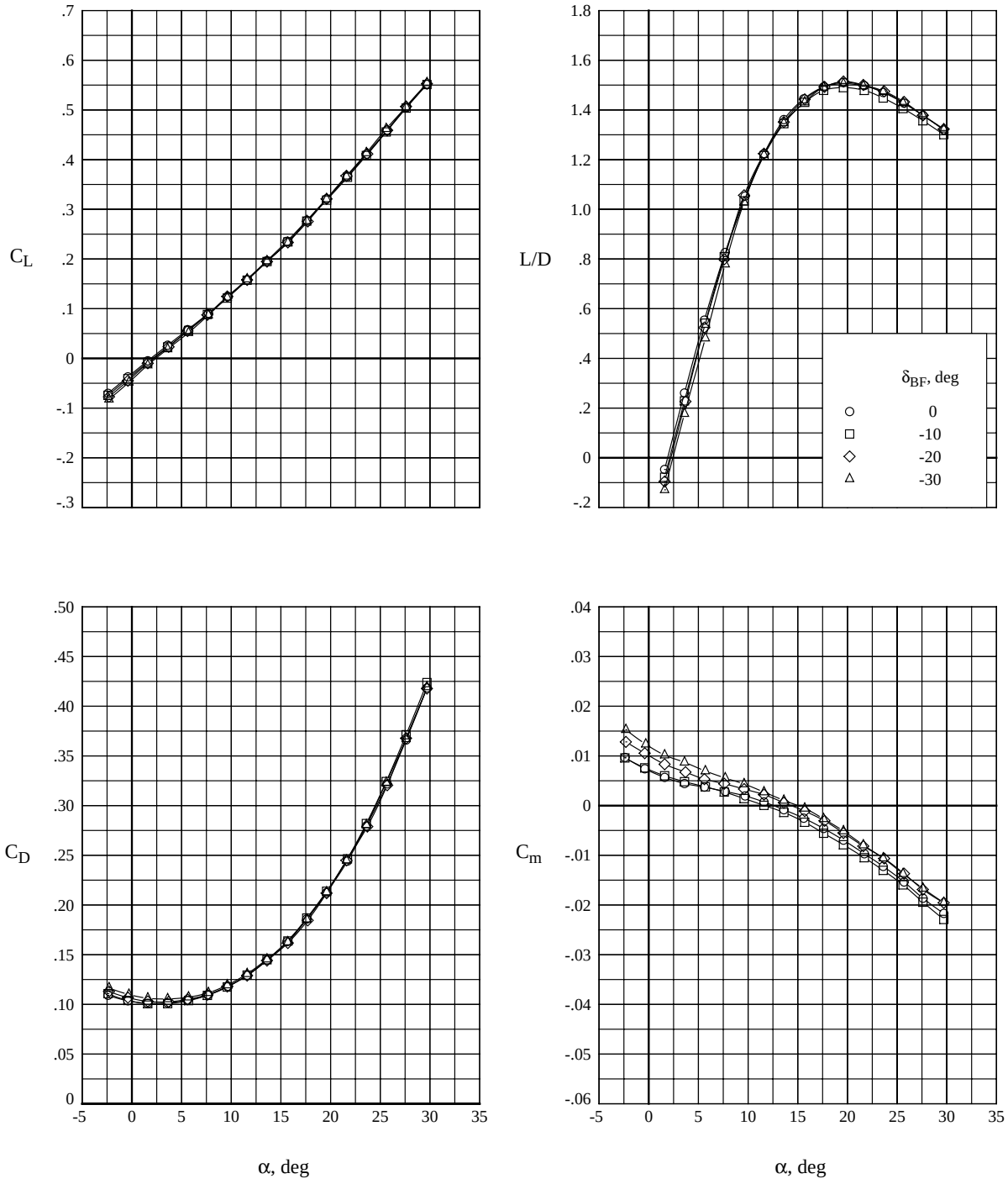

(f) $M = 4.0$.

Figure 10. Continued.

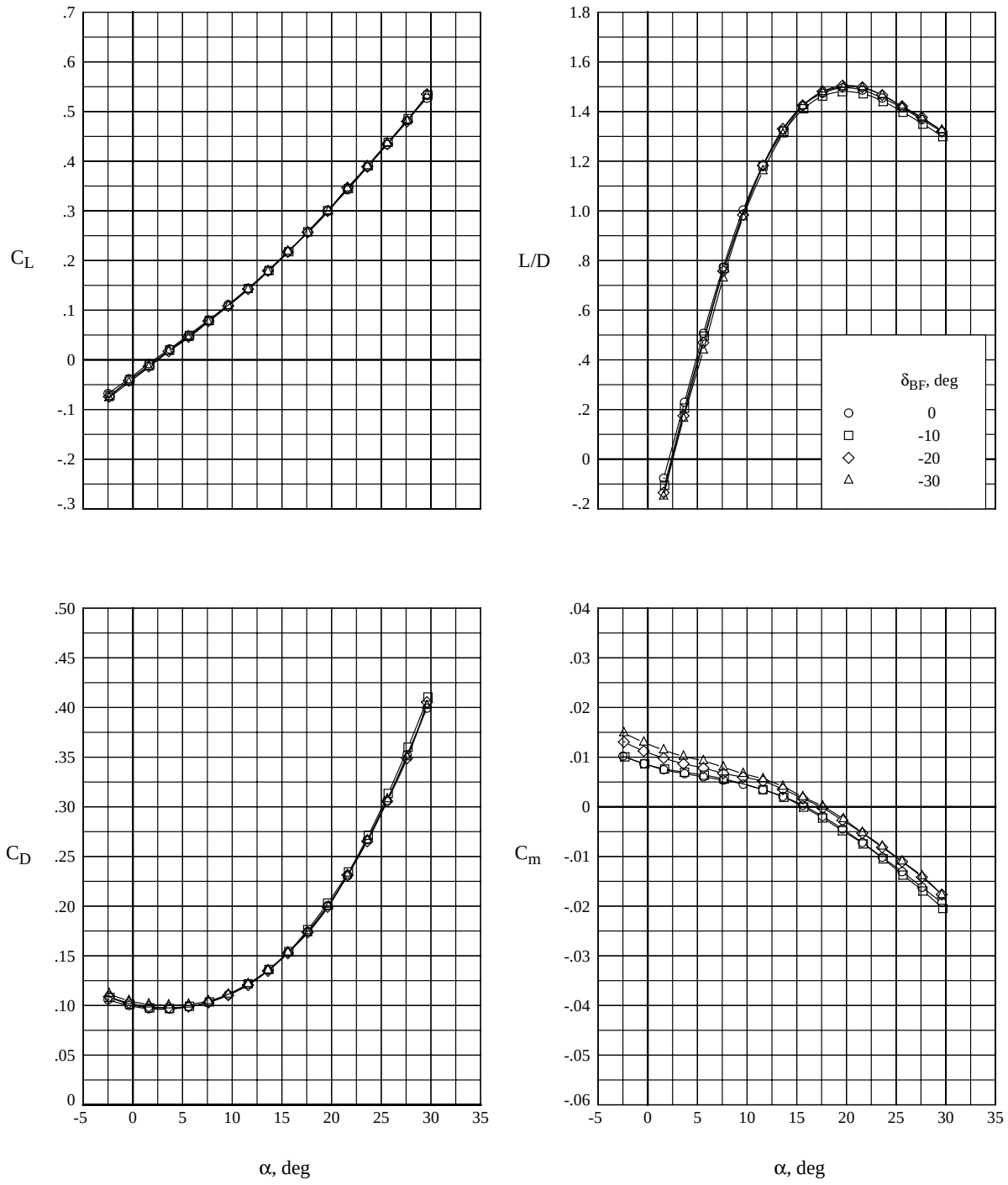

(g) $M = 4.5$.

Figure 10. Concluded.

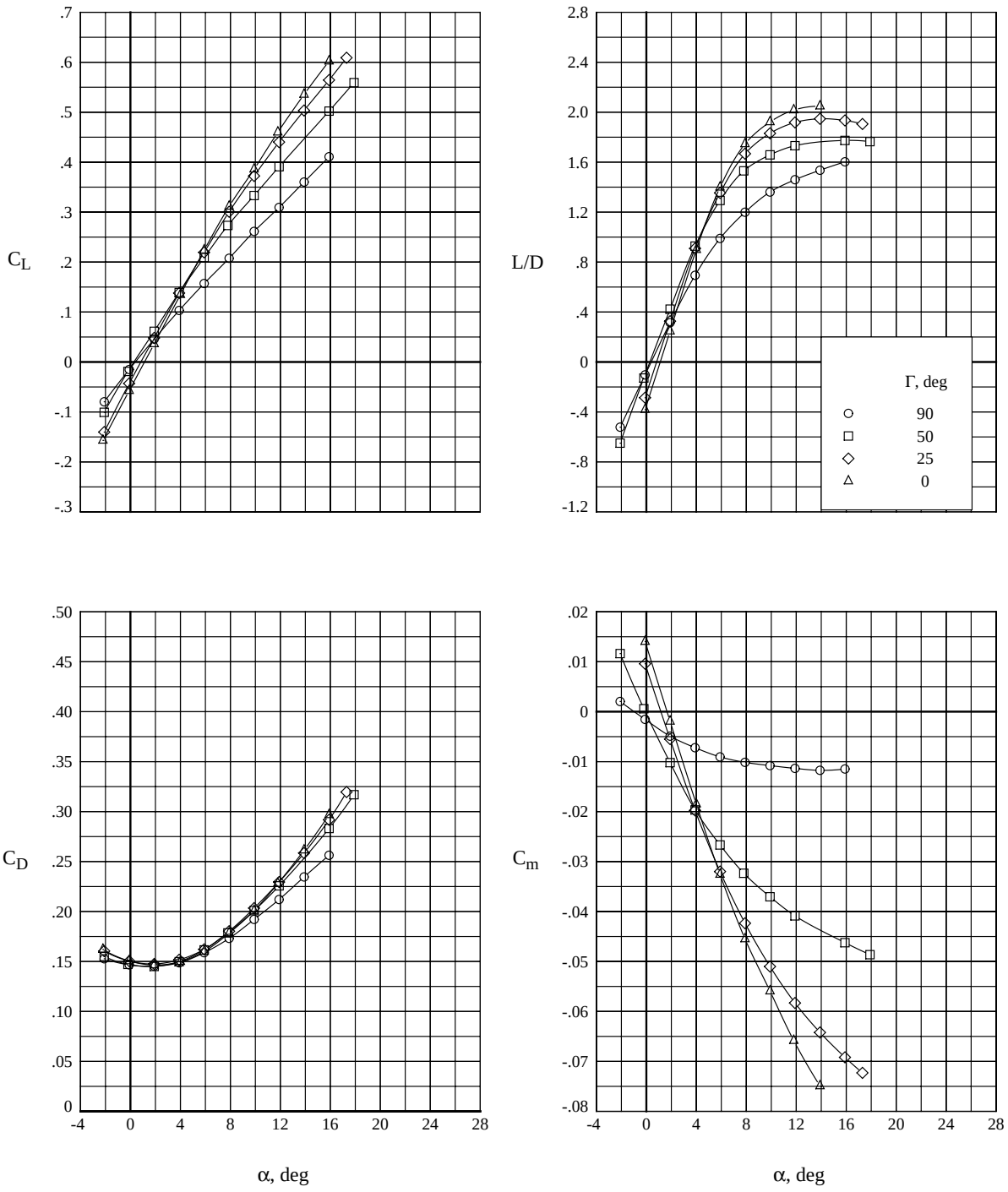

(a) M = 1.6.

Figure 11. Effect of tip-fin dihedral on longitudinal aerodynamic characteristics.

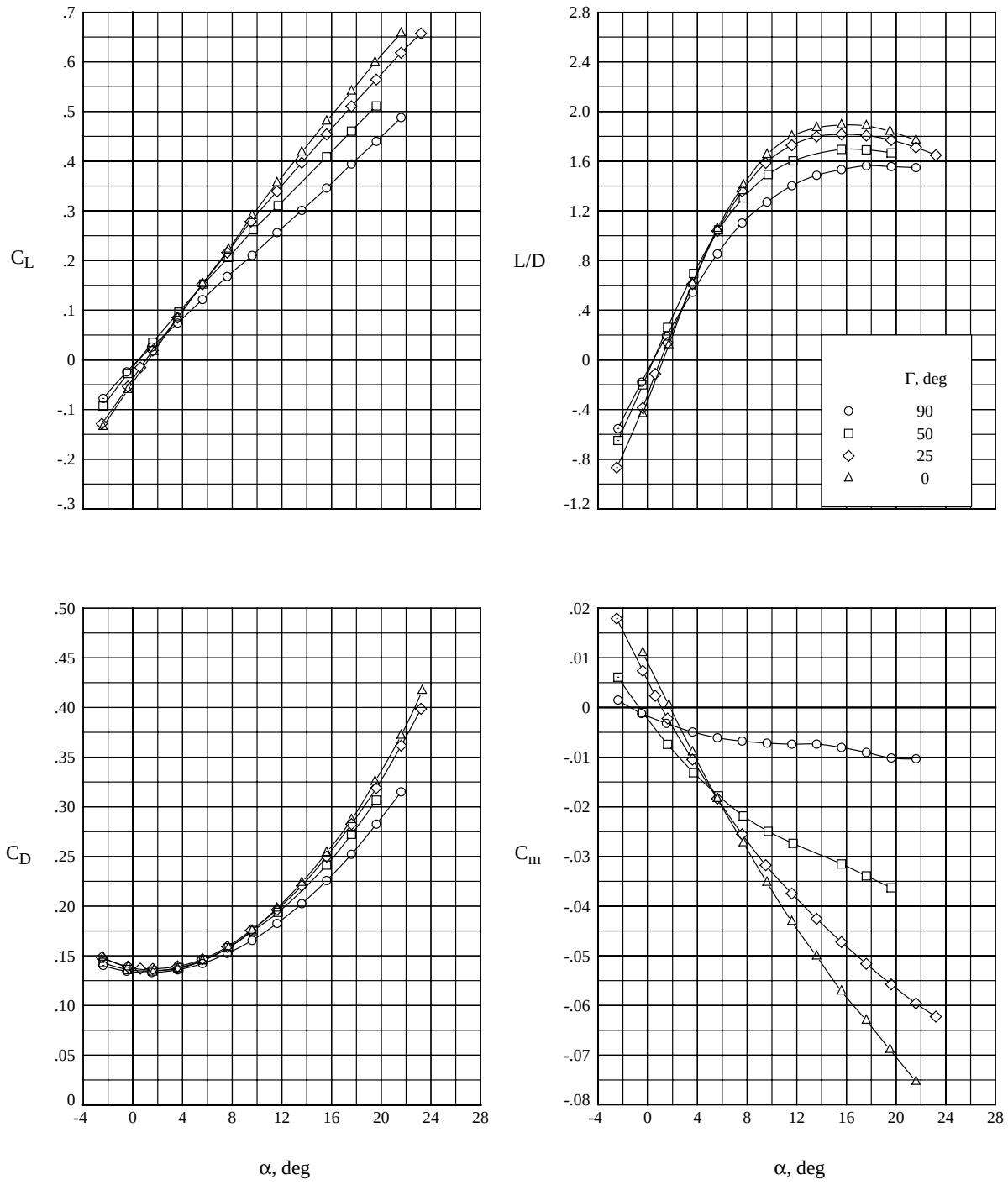

(b) $M = 2.0$.

Figure 11. Continued.

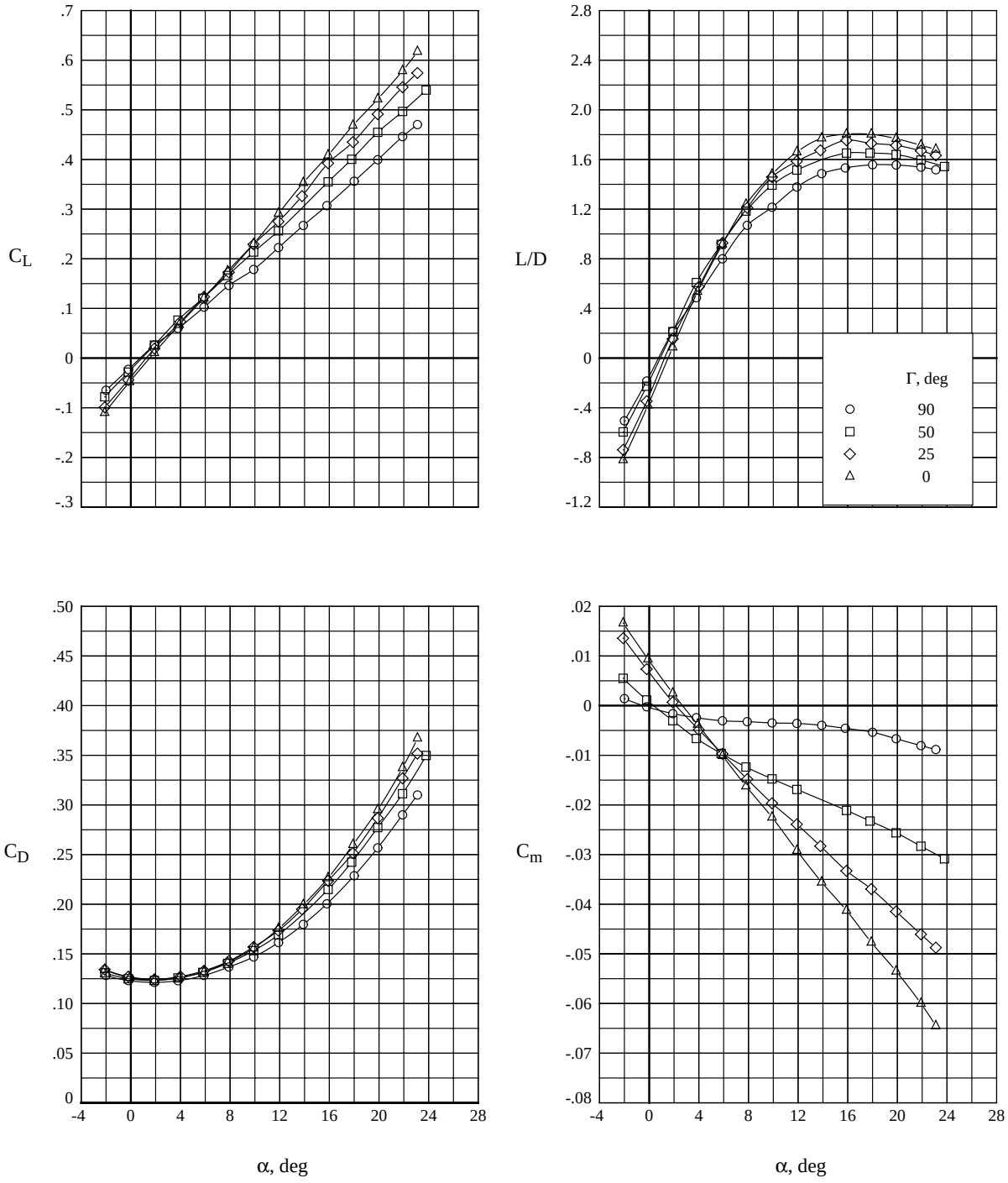

(c) $M = 2.5$.

Figure 11. Continued.

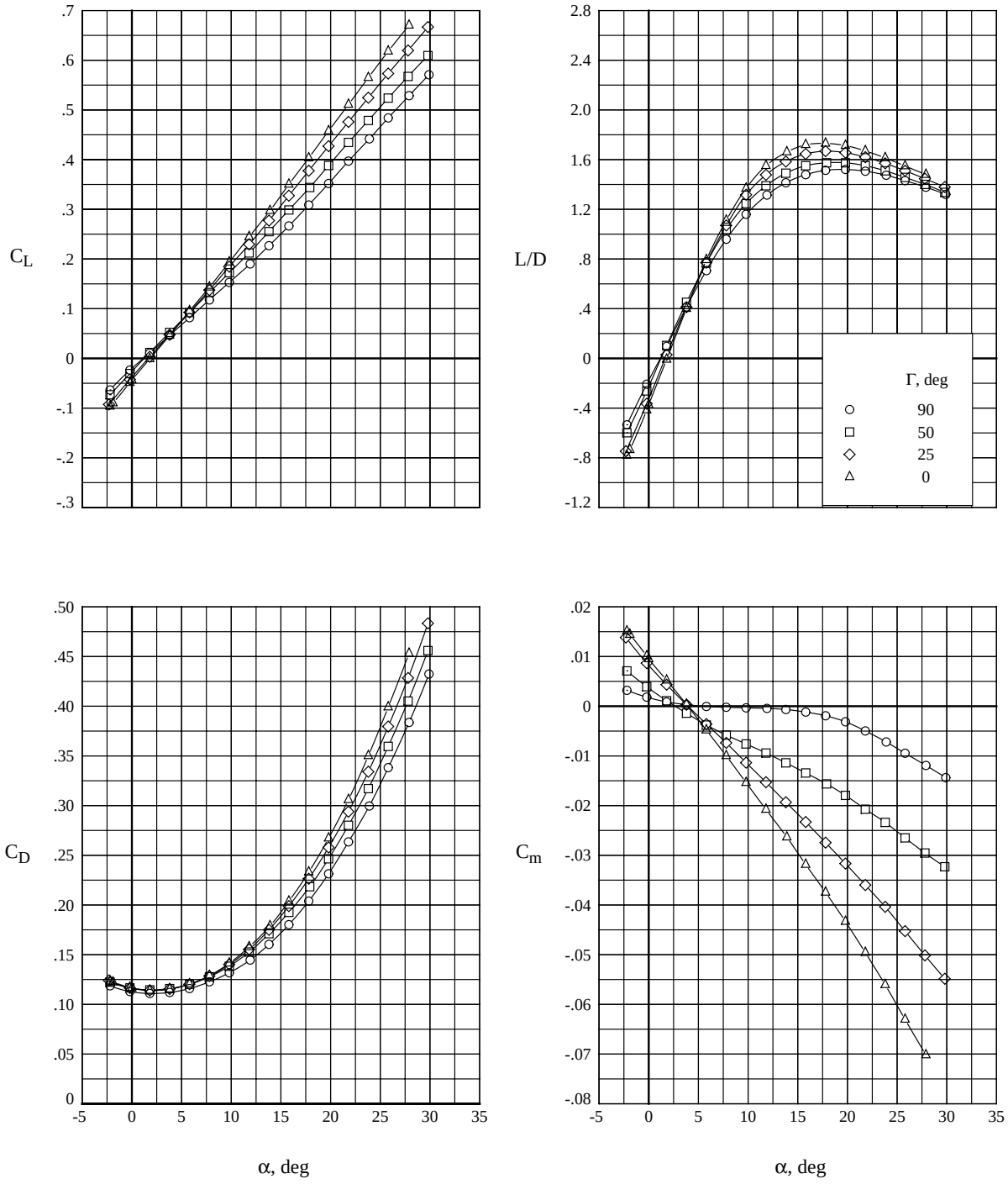

(d) $M = 3.0$.

Figure 11. Continued.

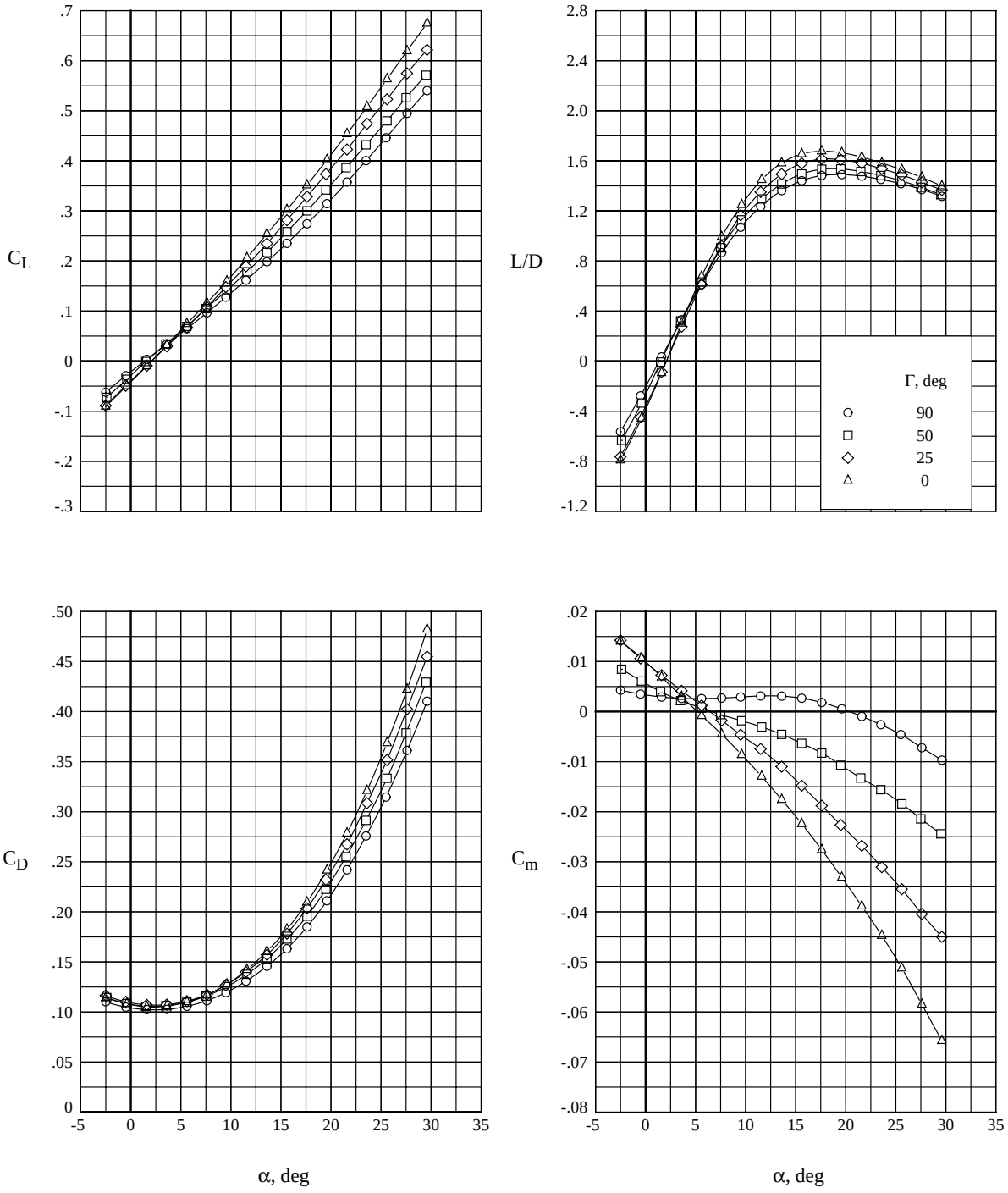

(e) $M = 3.5$.

Figure 11. Continued.

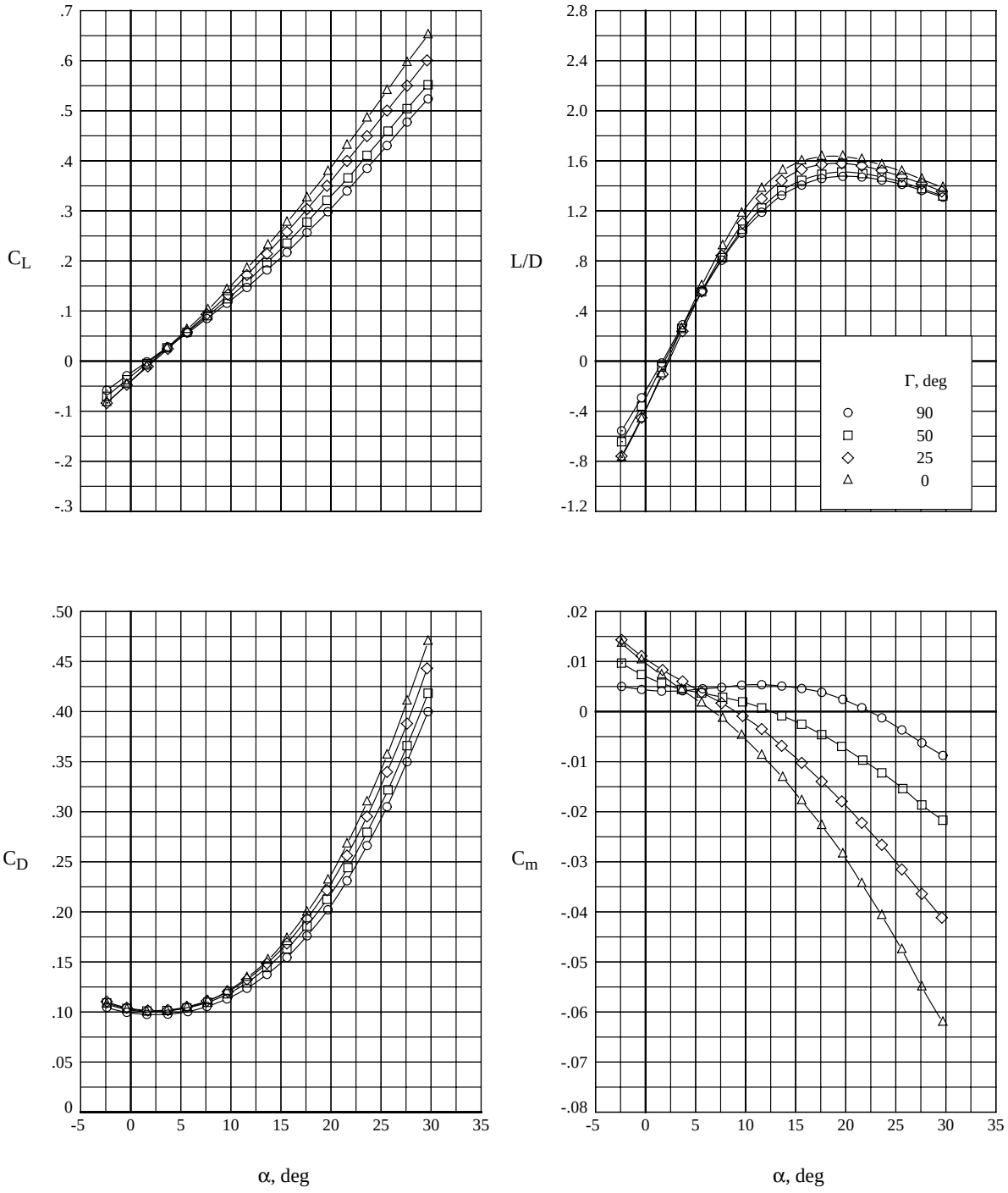

(f) $M = 4.0$.

Figure 11. Continued.

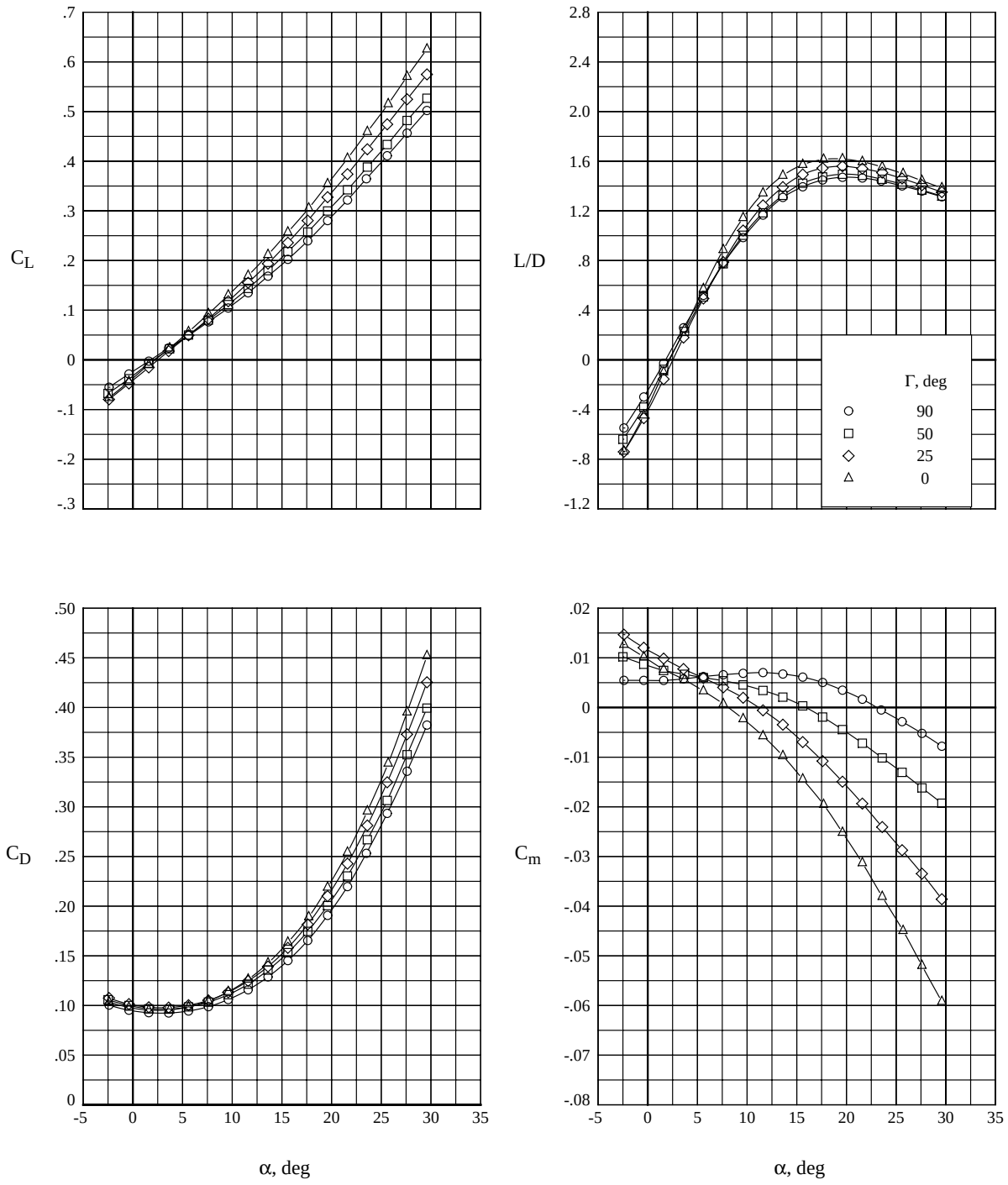

(g) M = 4.5.

Figure 11. Concluded.

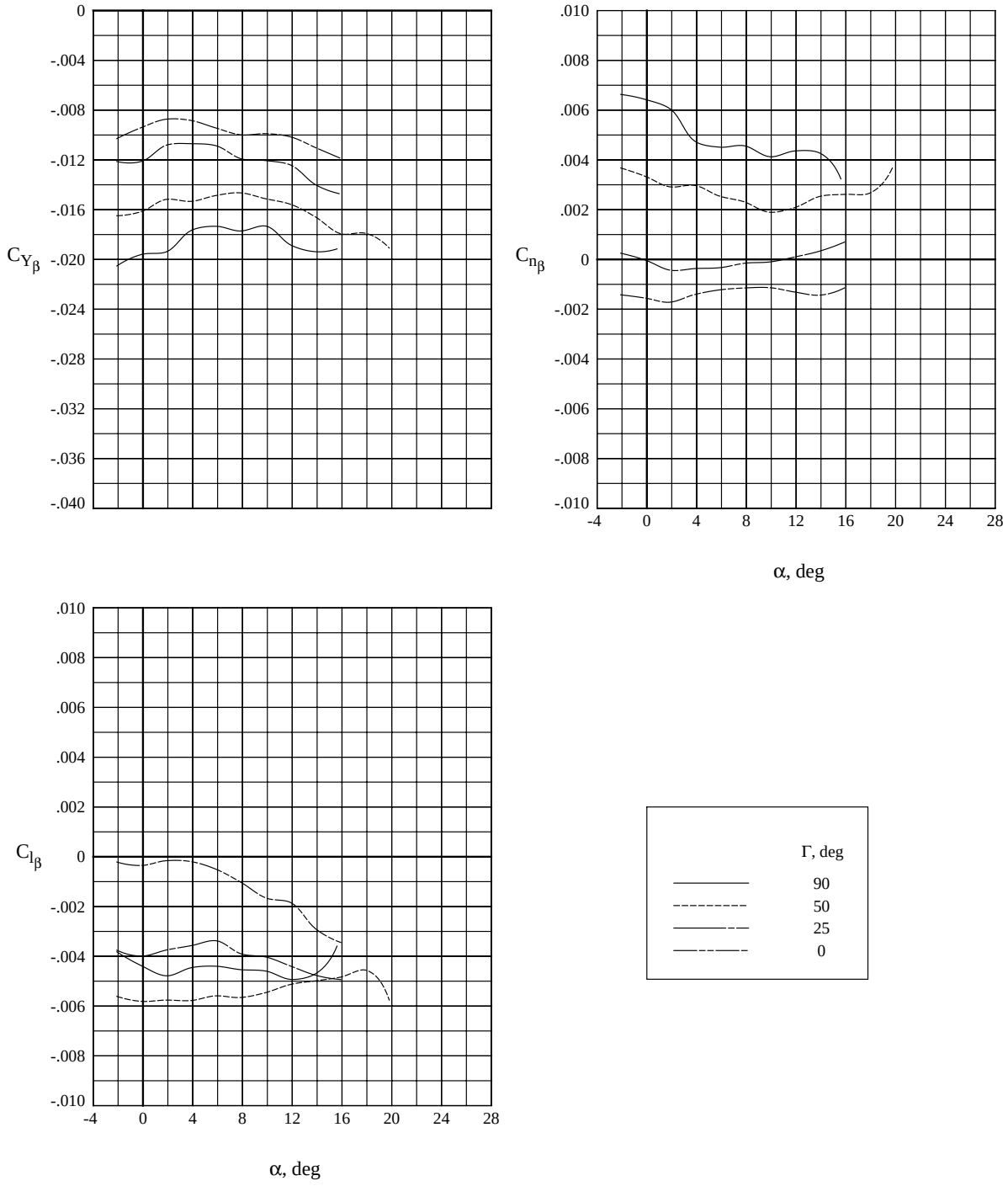

(a) $M = 1.6$.

Figure 12. Effect of tip-fin dihedral on lateral-directional stability characteristics.

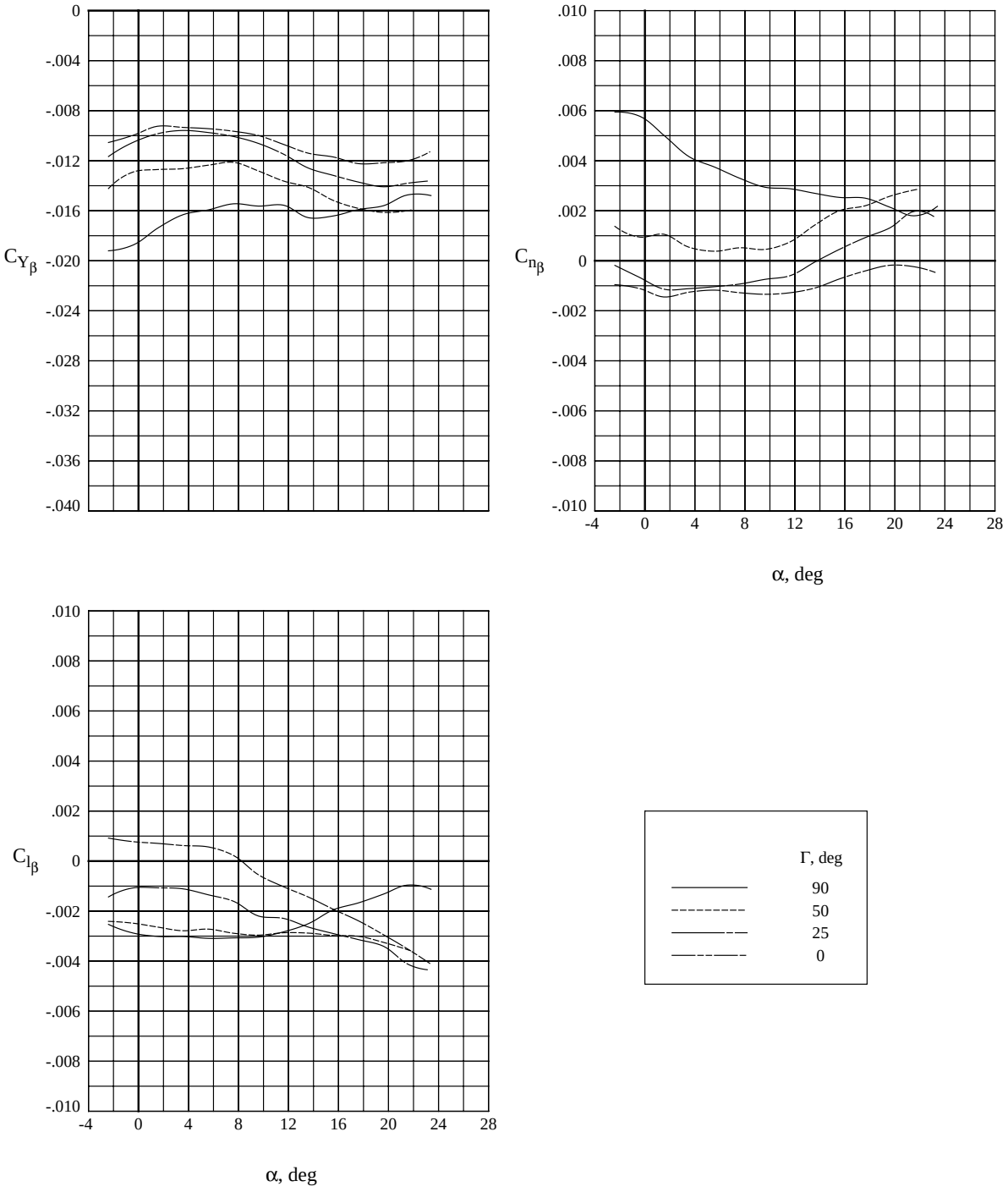

(b) $M = 2.0$.

Figure 12. Continued.

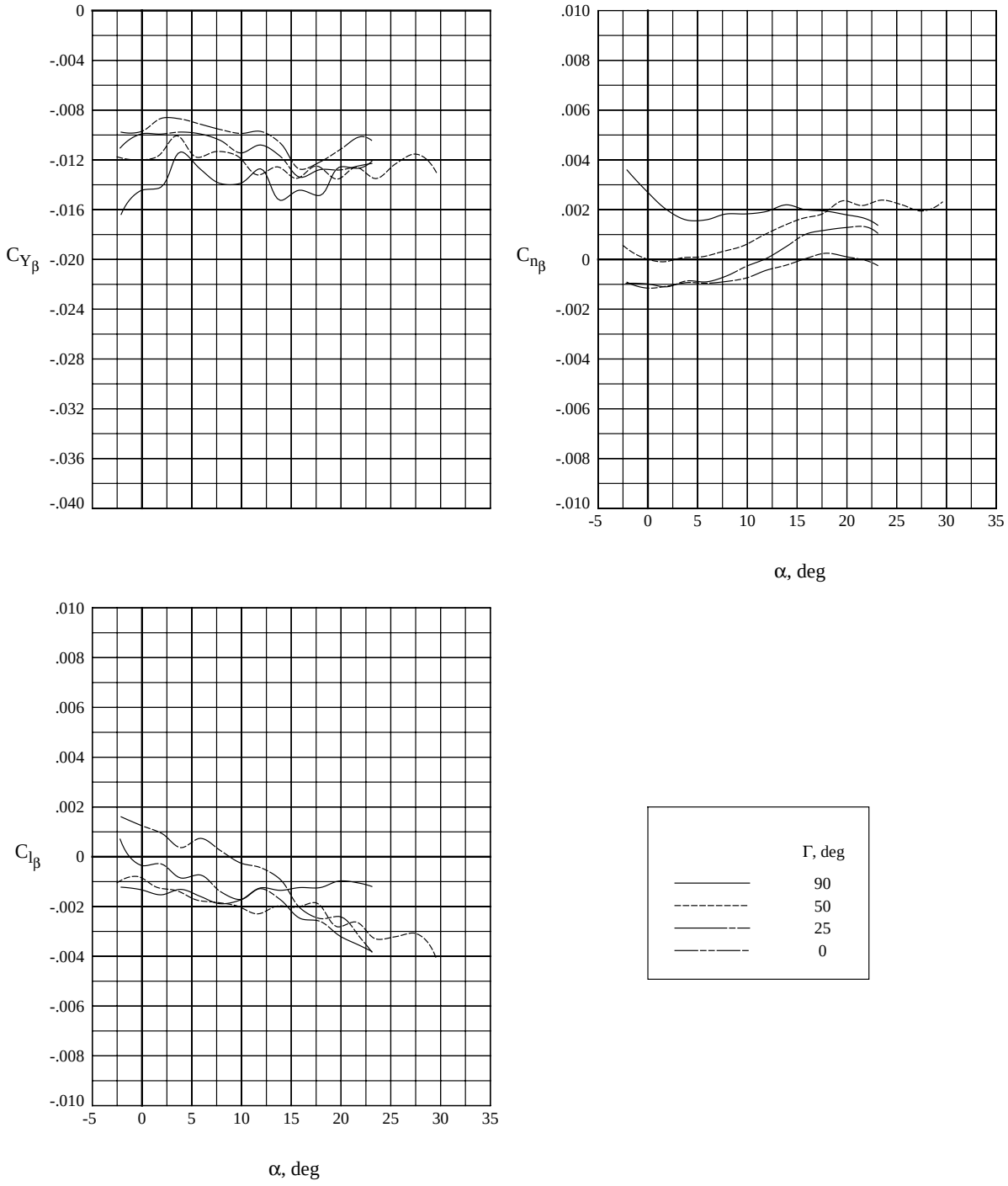

(c) $M = 2.5$.

Figure 12. Continued.

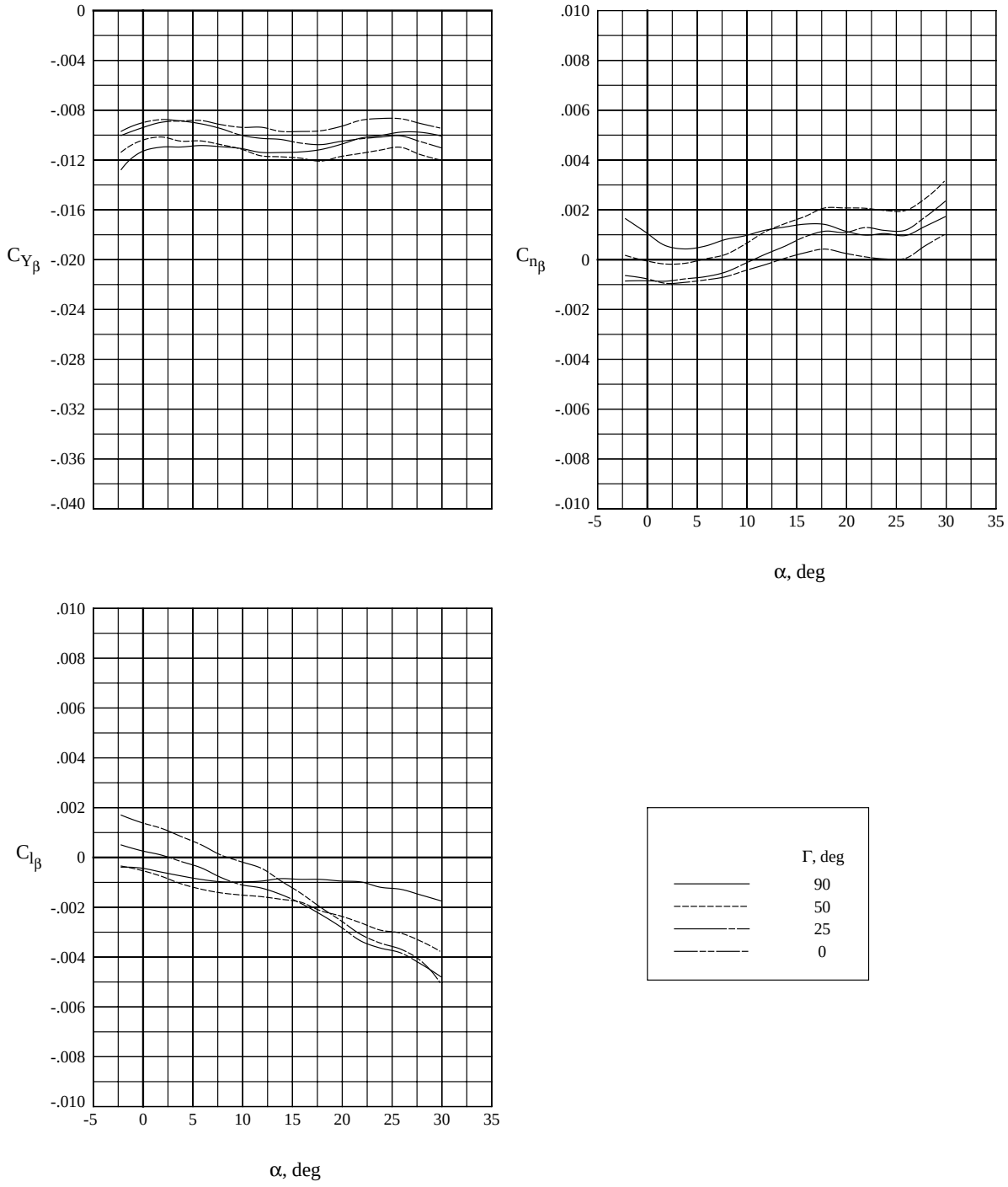

(d) $M = 3.0$.

Figure 12. Continued.

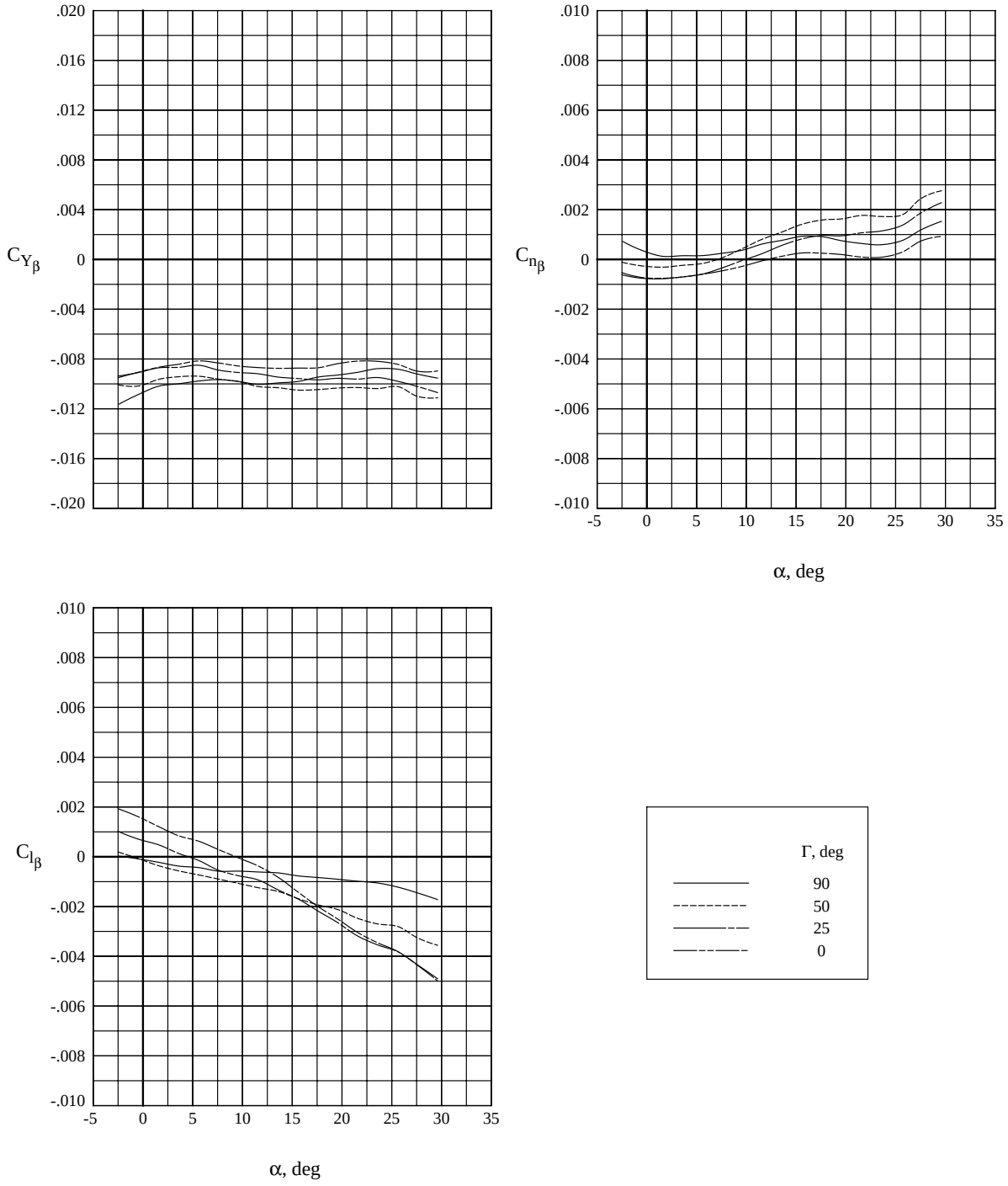

(e) $M = 3.5$.

Figure 12. Continued.

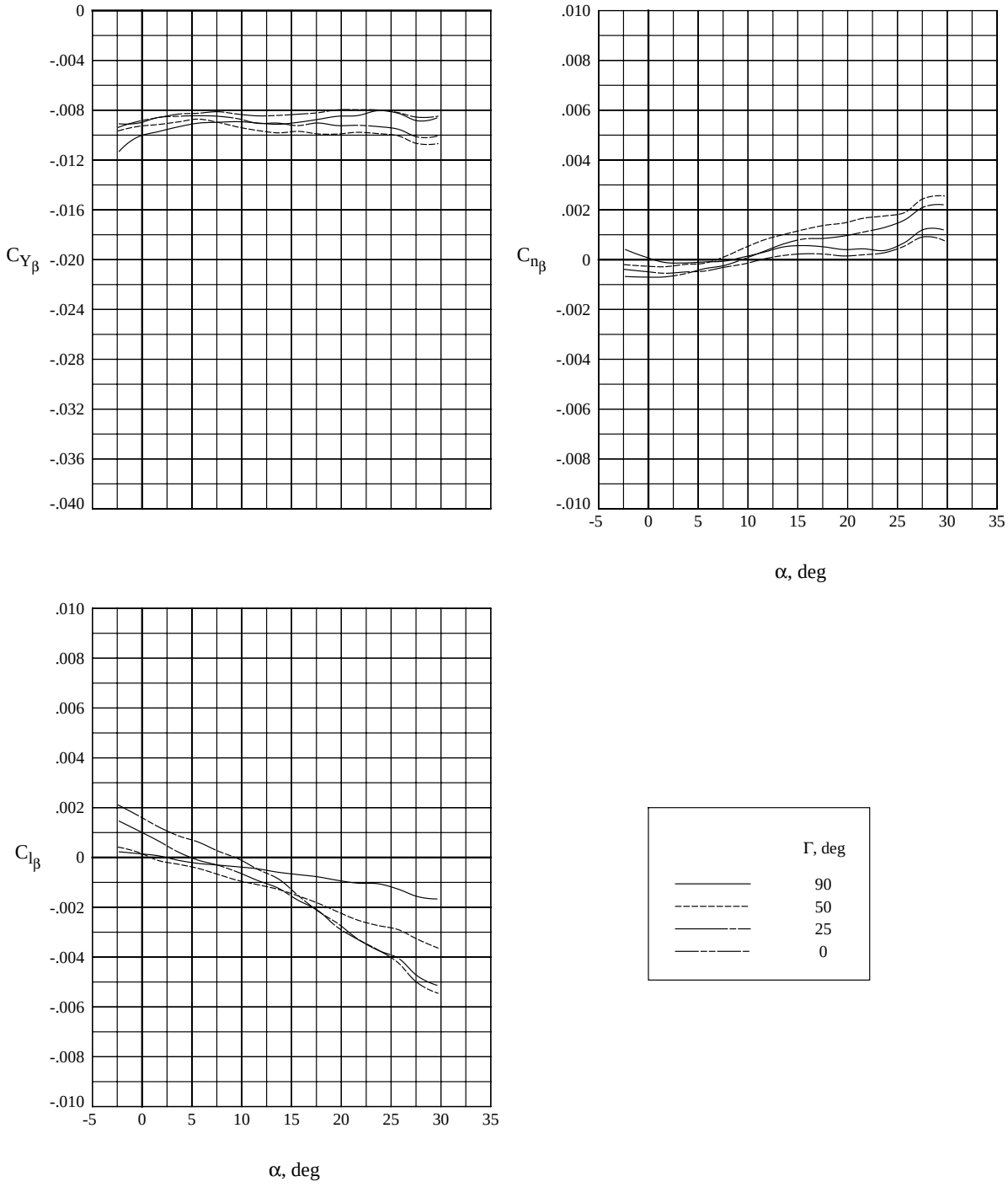

(f) $M = 4.0$.

Figure 12. Continued.

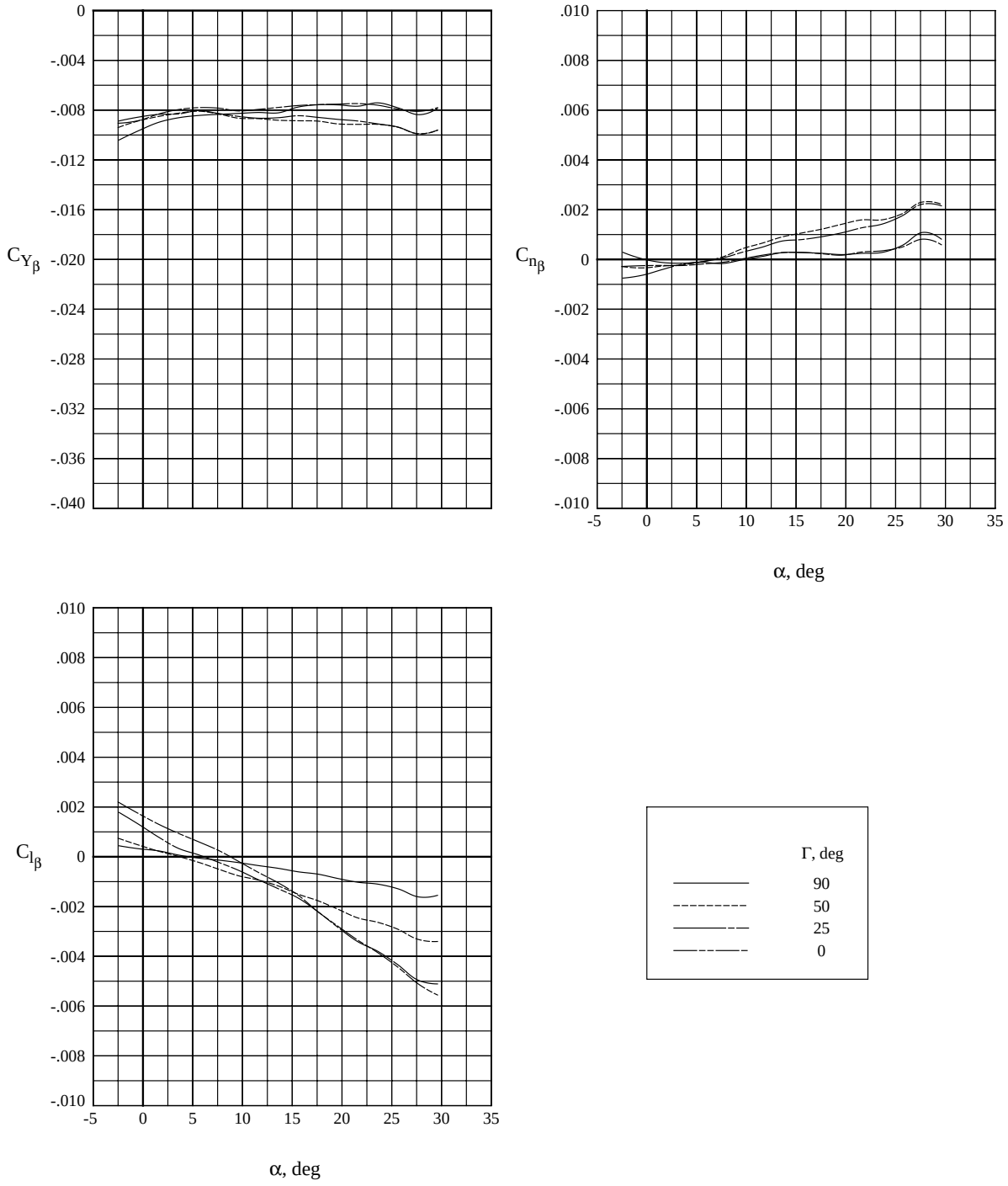

(g) $M = 4.5$.

Figure 12. Concluded.

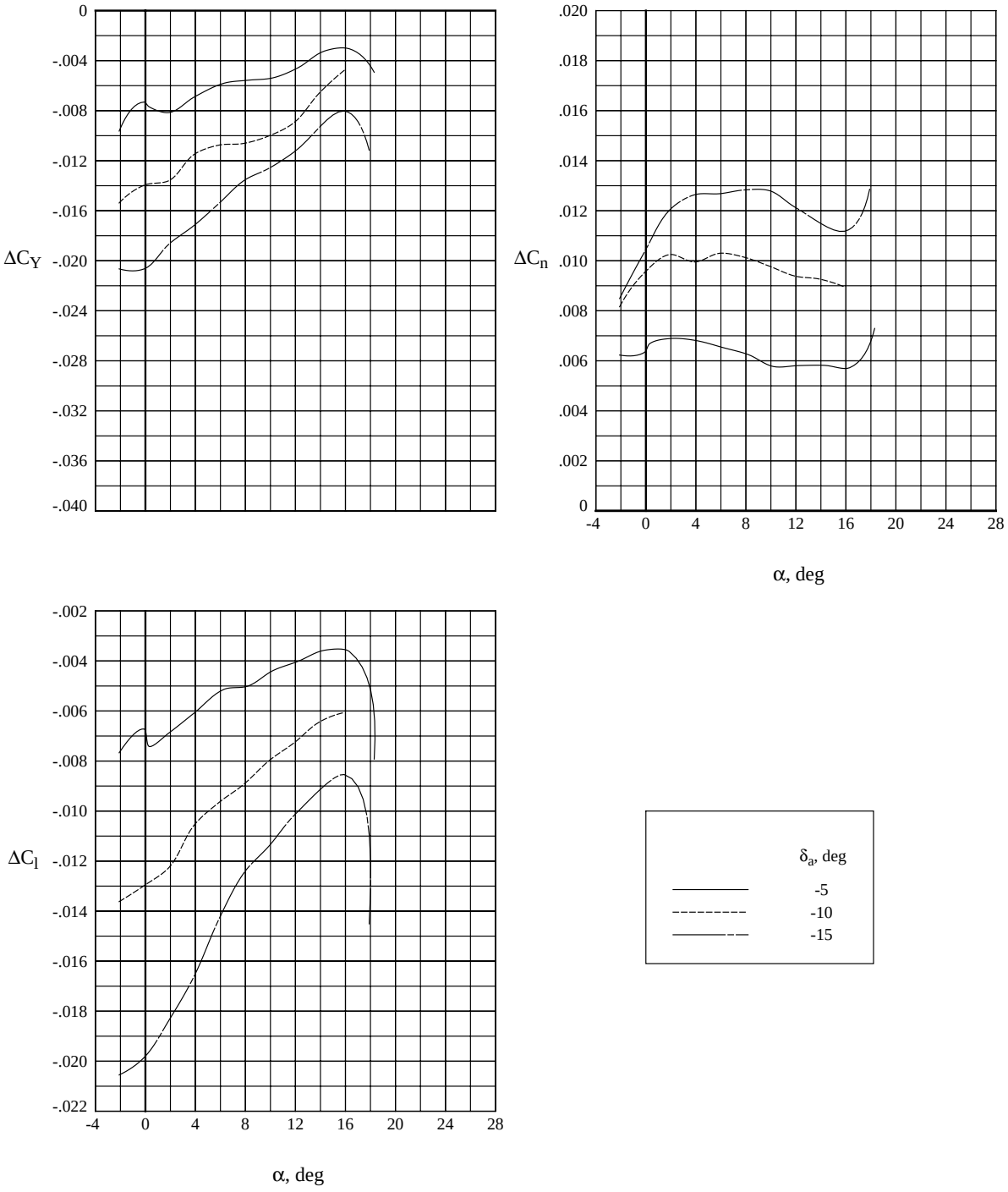

(a) $M = 1.6$.

Figure 13. Roll control effectiveness of elevons.

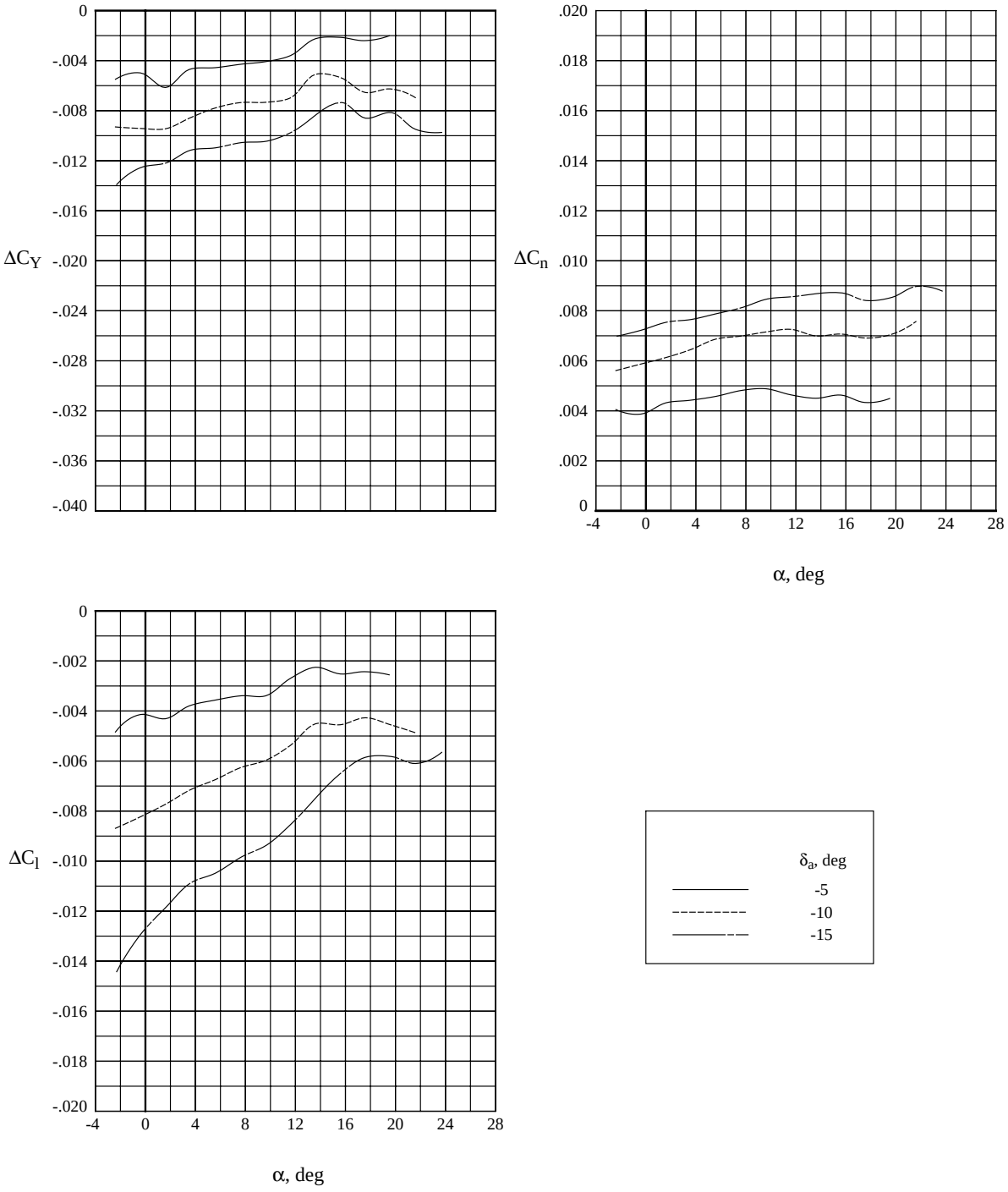

(b) $M = 2.0$.

Figure 13. Continued.

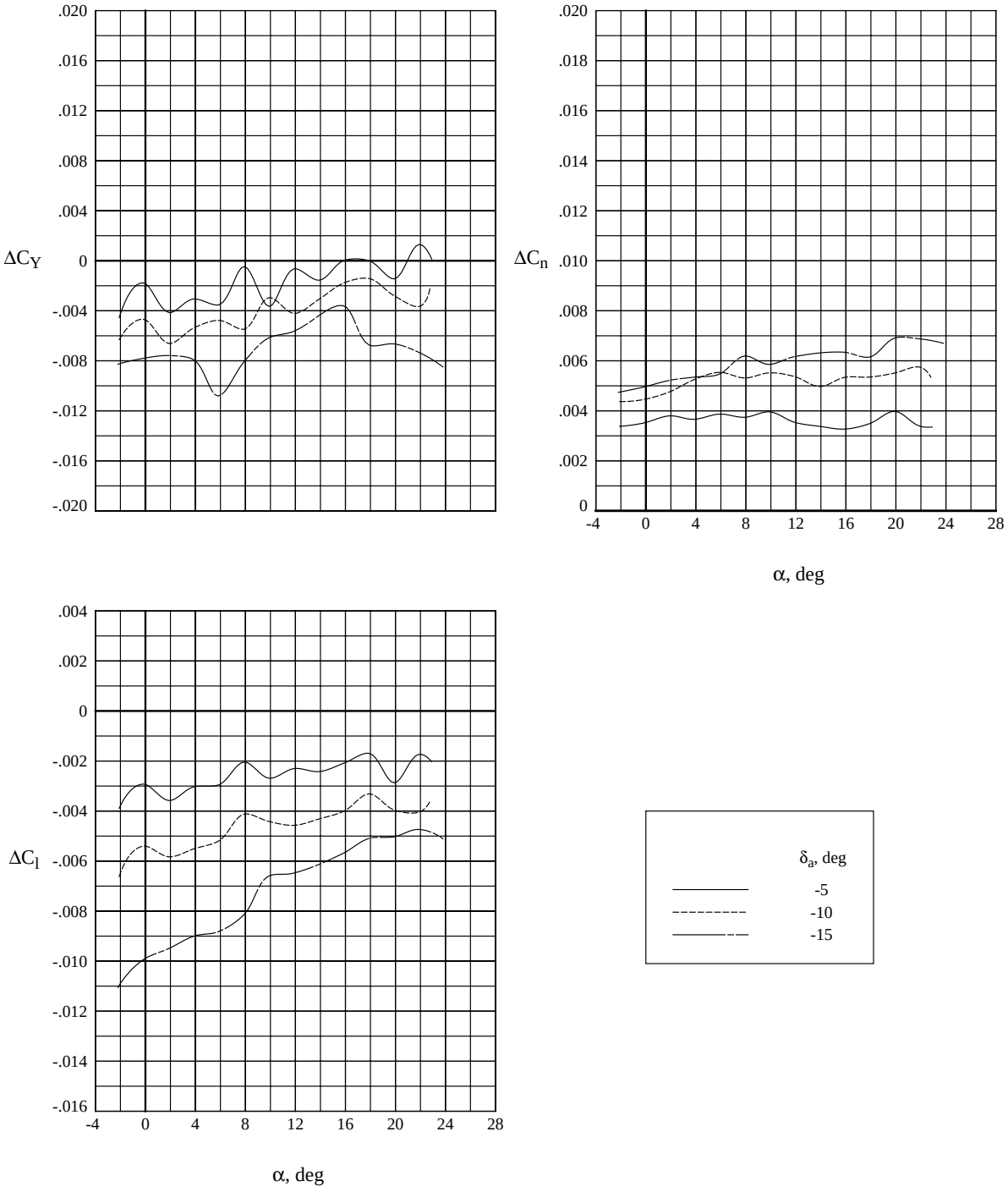

(c) $M = 2.5$.

Figure 13. Continued.

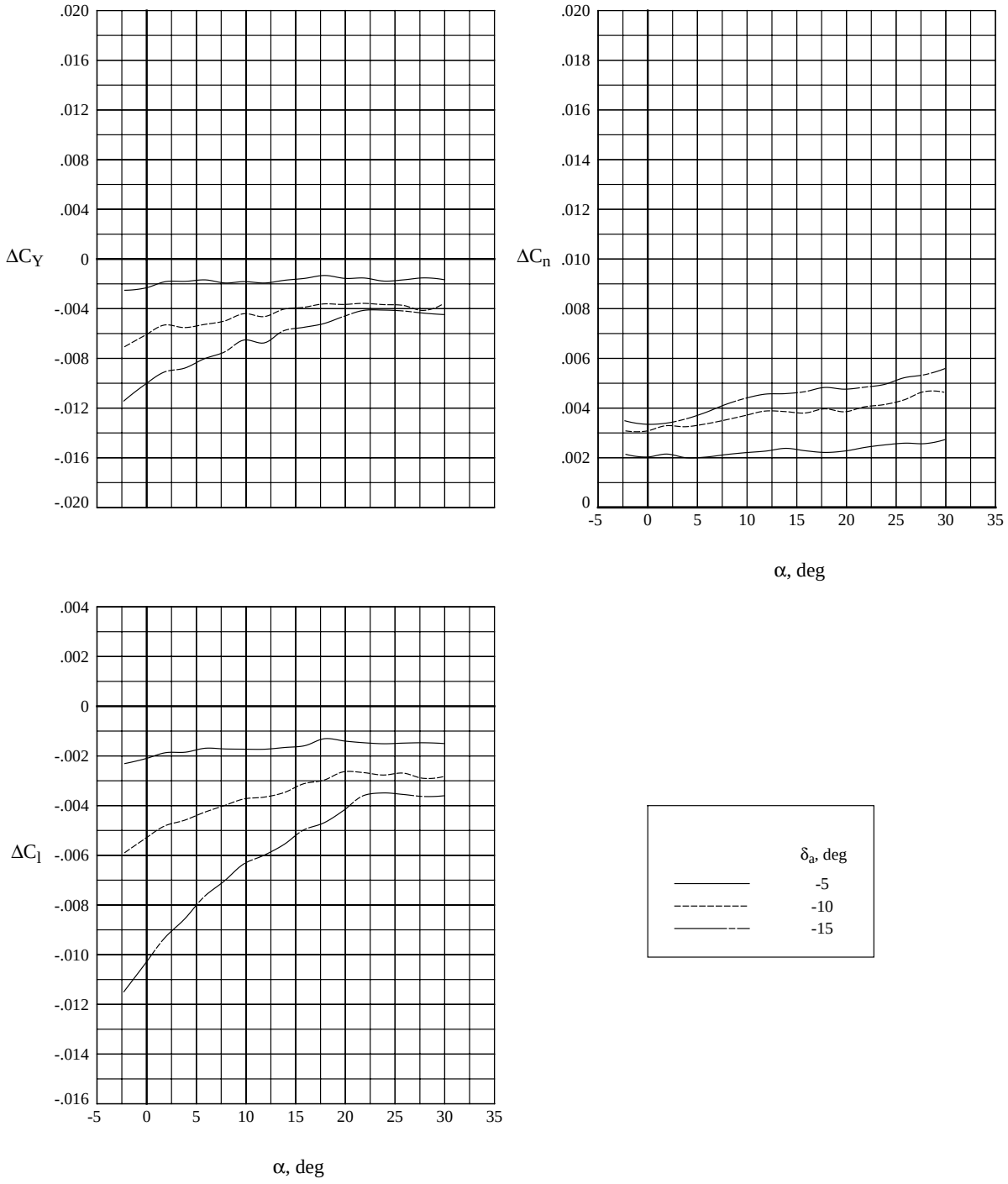

(d) $M = 3.0$.

Figure 13. Continued.

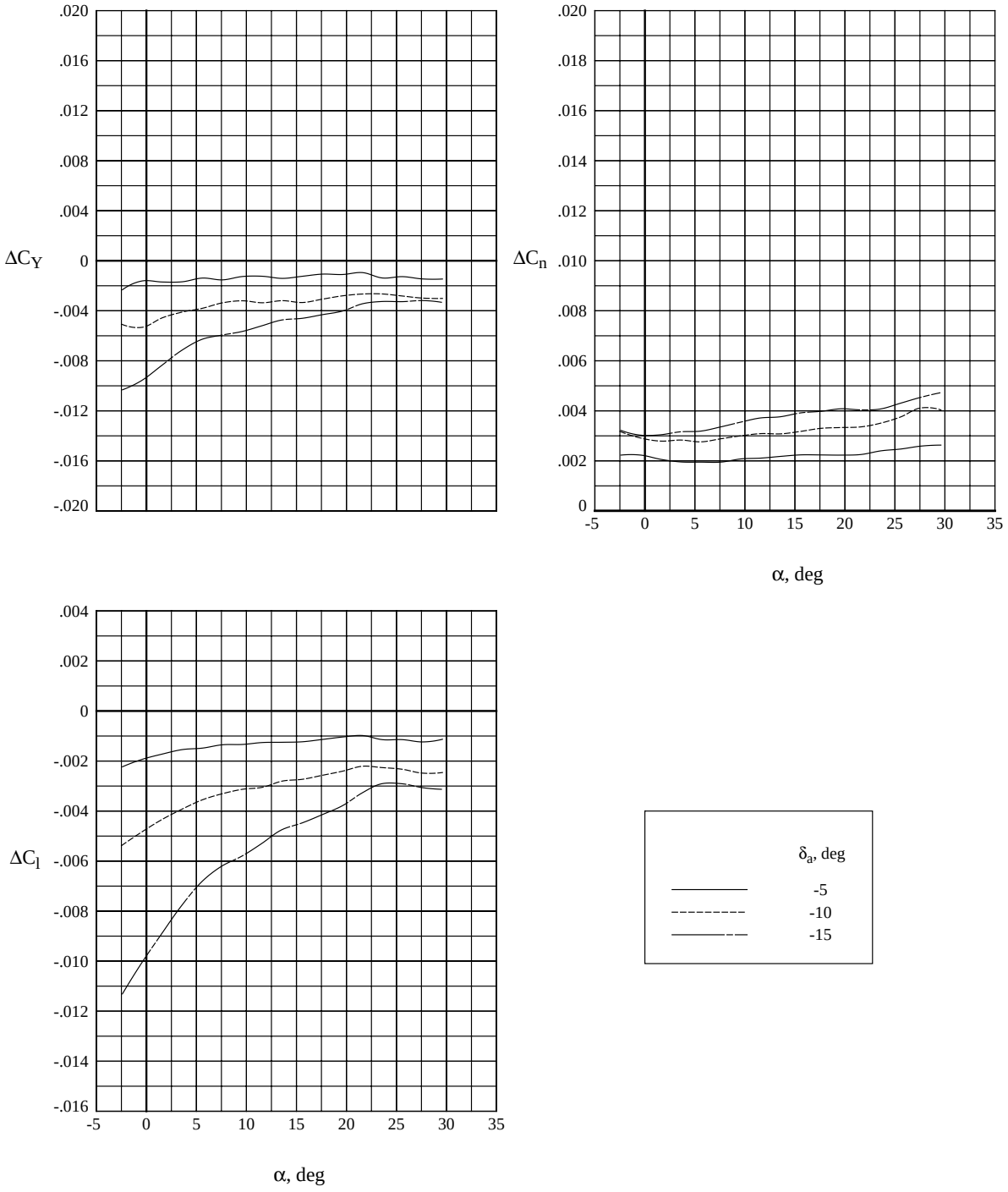

(e) $M = 3.5$.

Figure 13. Continued.

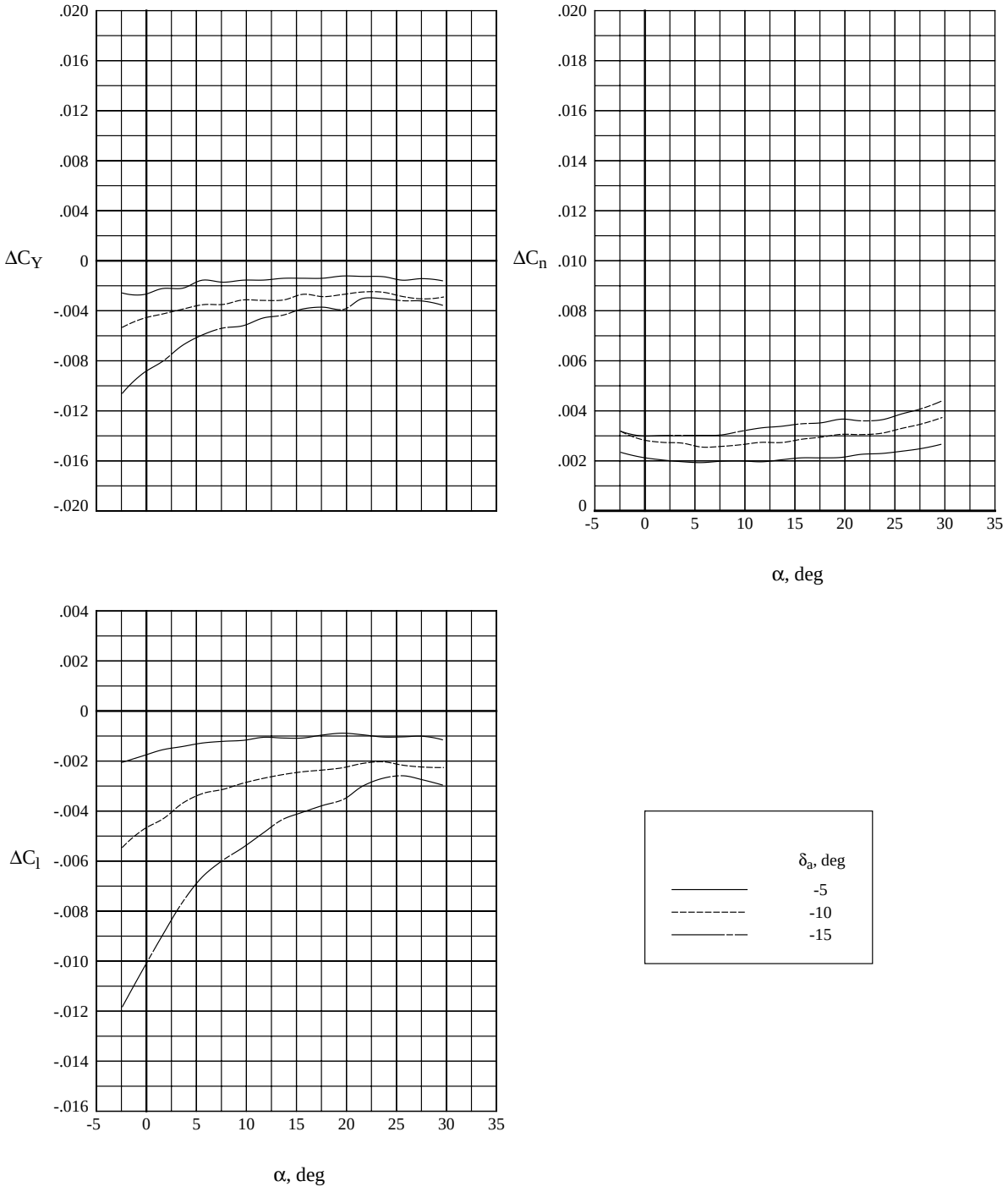

(f) $M = 4.0$.

Figure 13. Continued.

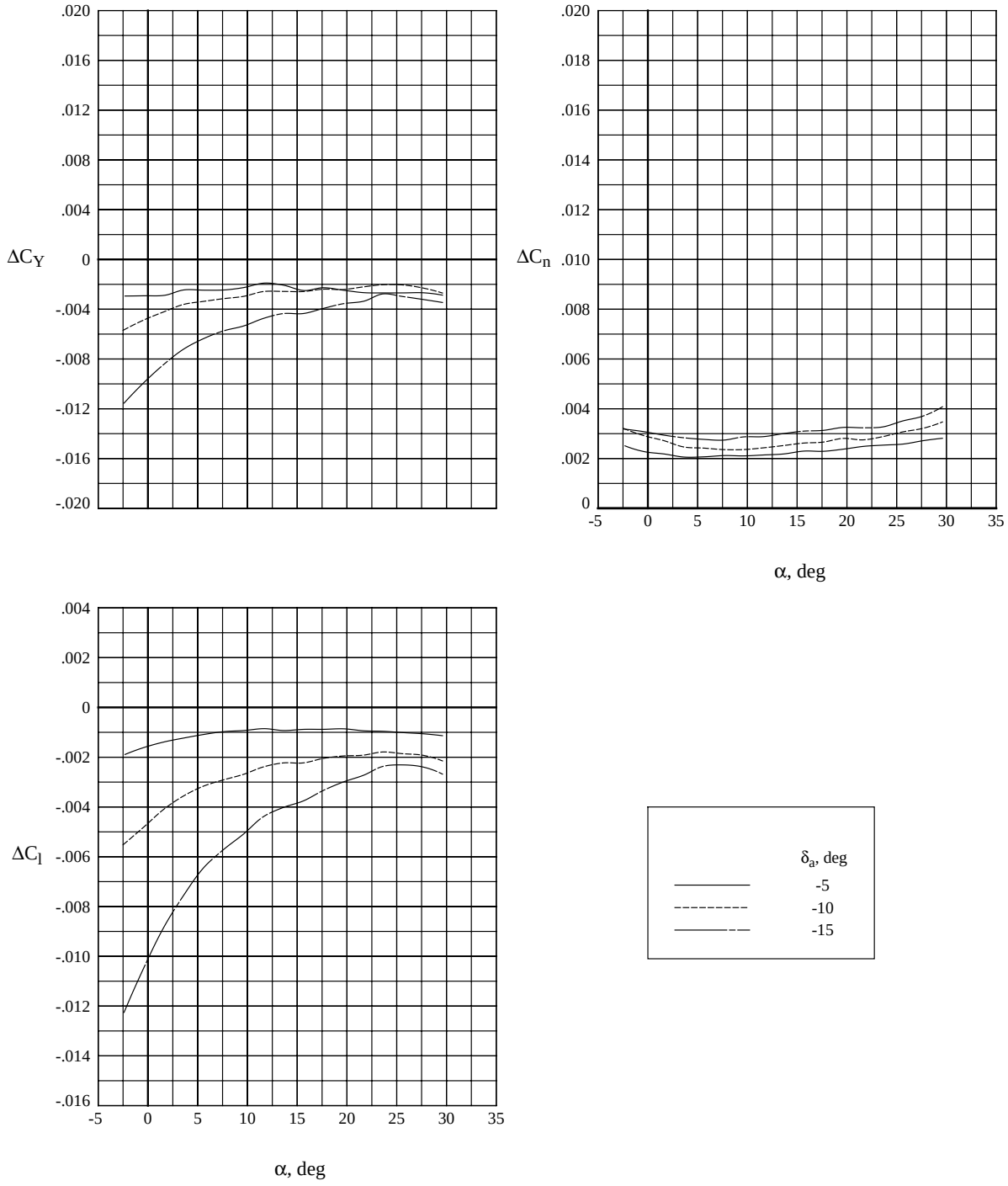

(g) $M = 4.5$.

Figure 13. Concluded.

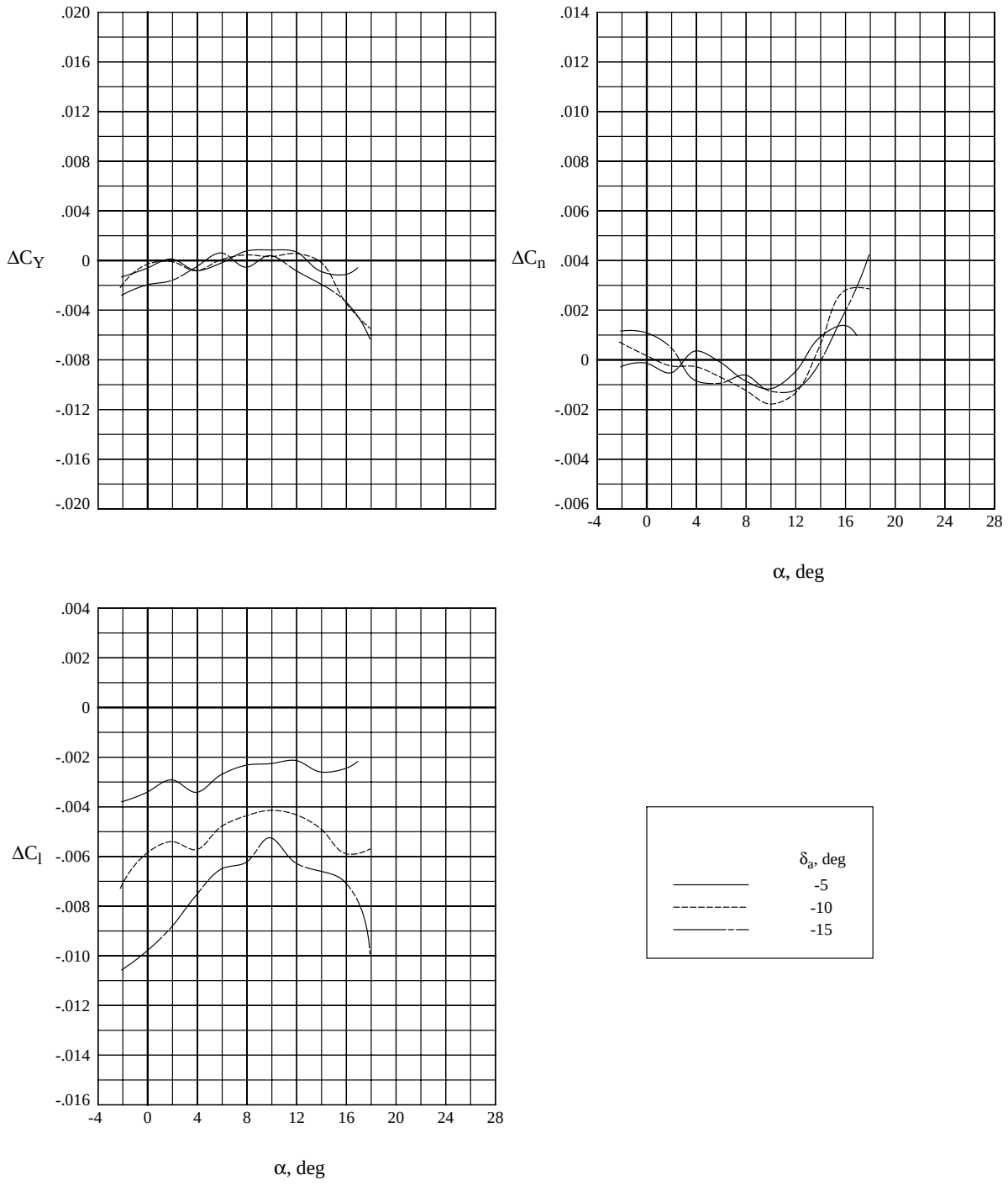

(a) $M = 1.6$.

Figure 14. Roll control effectiveness of body flaps.

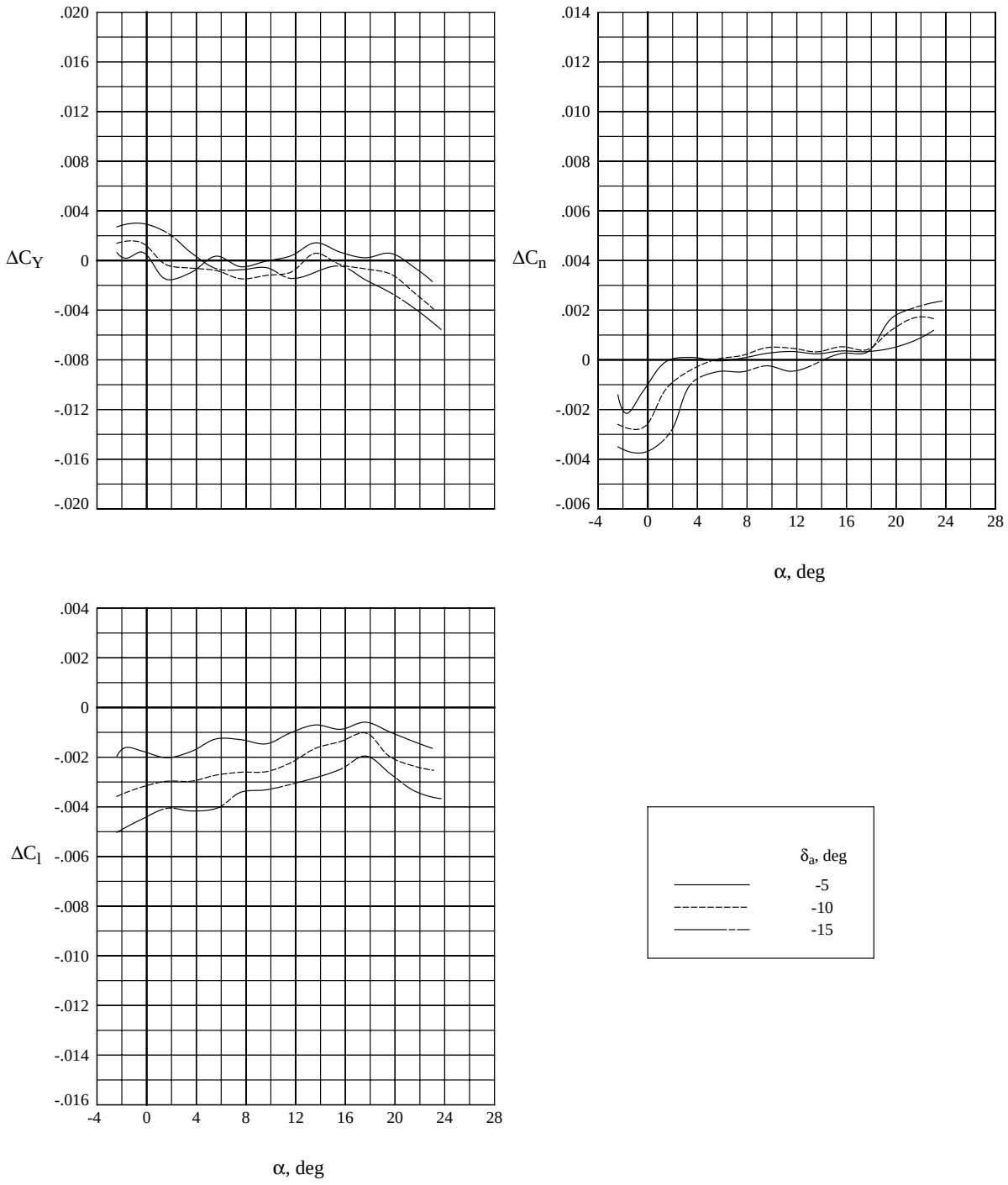

(b) $M = 2.0$.

Figure 14. Continued.

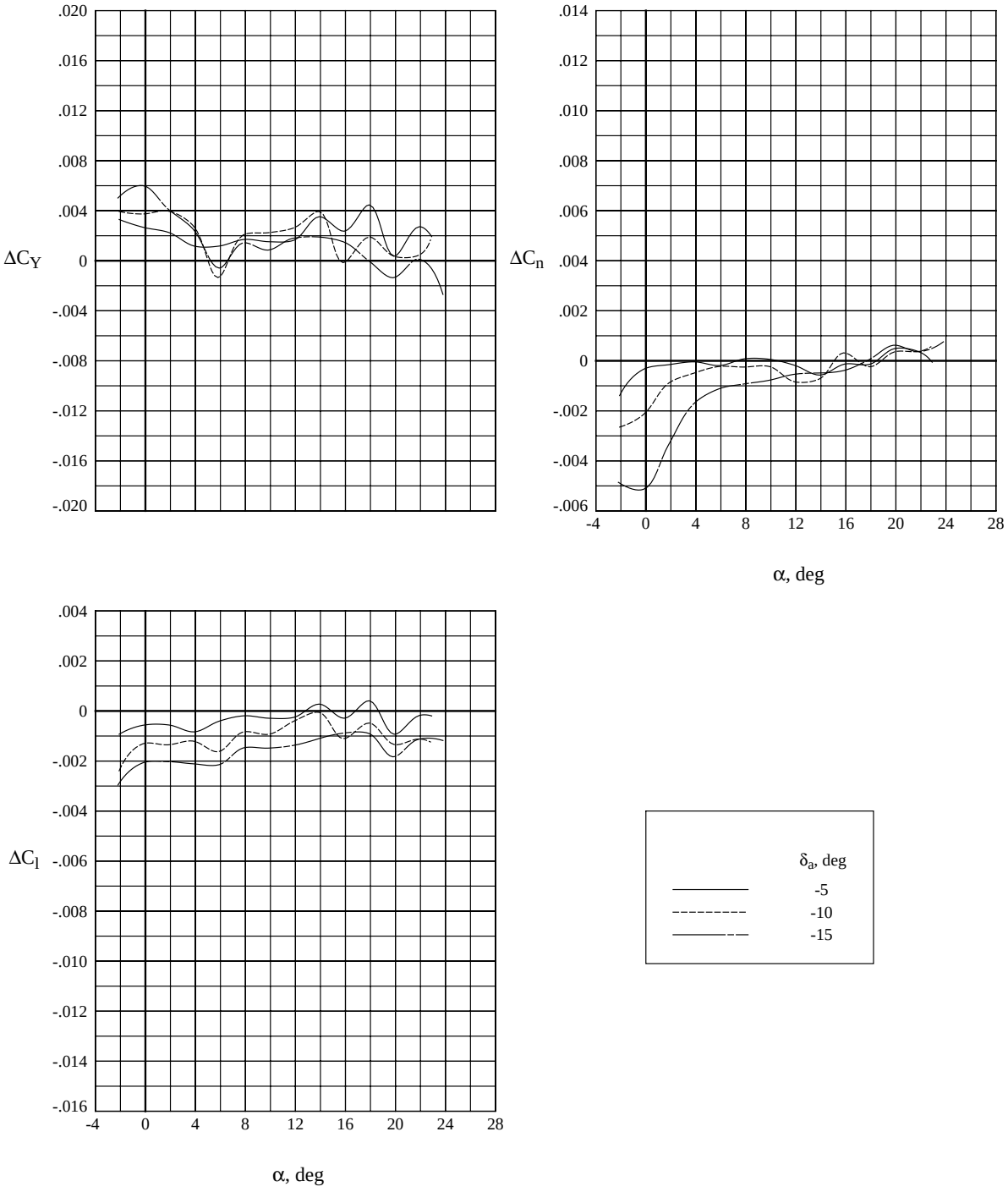

(c) $M = 2.5$.

Figure 14. Continued.

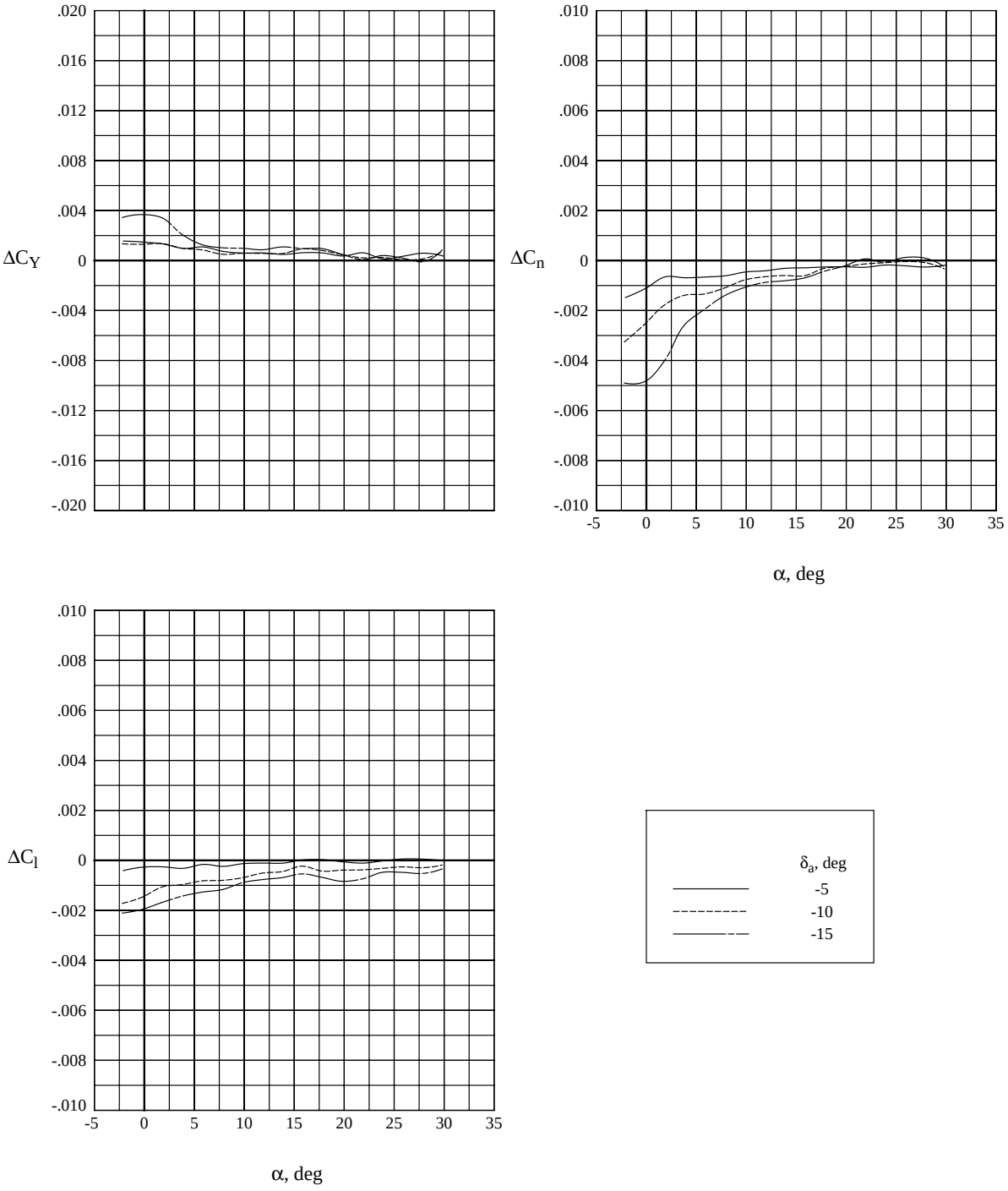

(d) $M = 3.0$.

Figure 14. Continued.

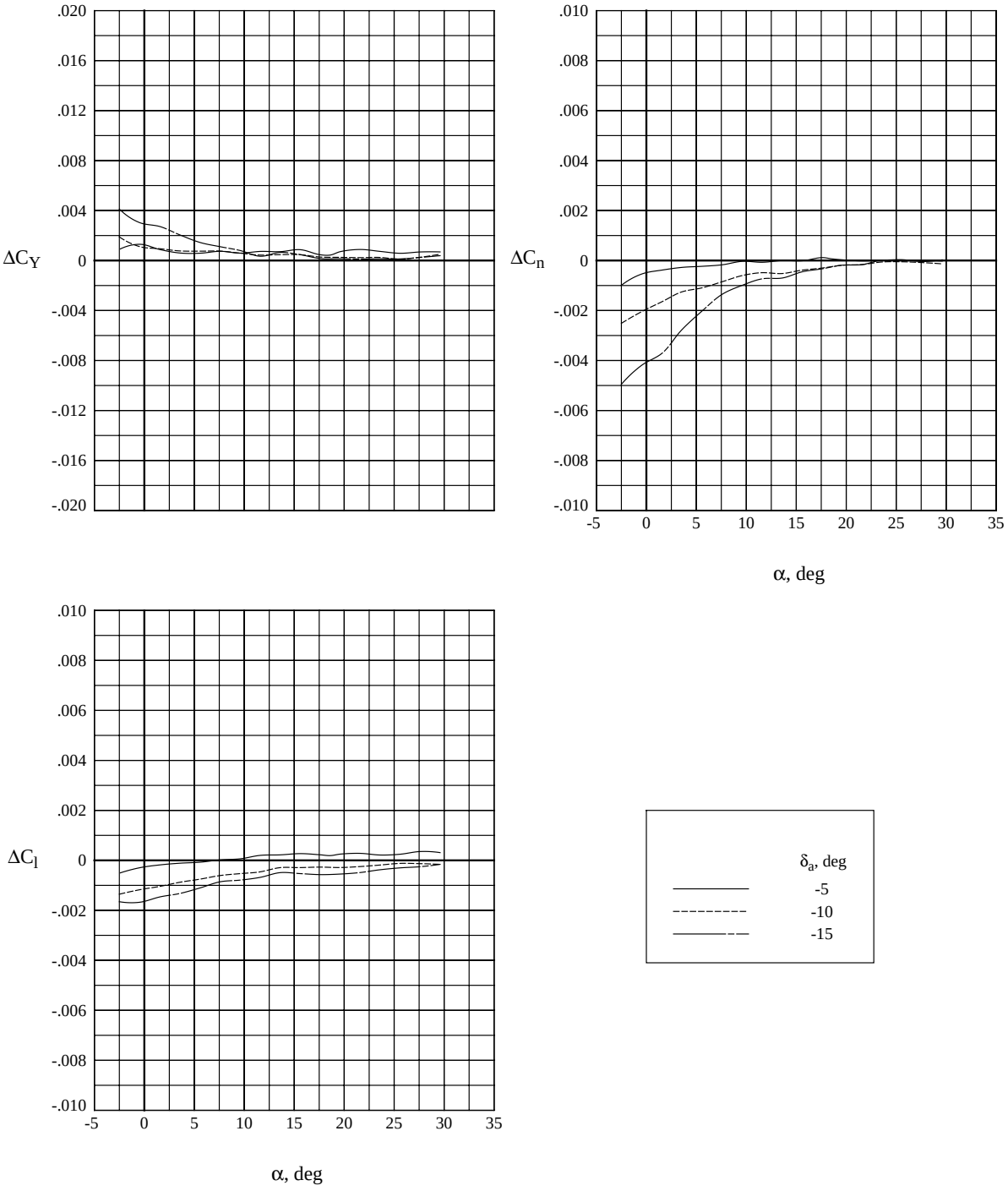

(e) $M = 3.5$.

Figure 14. Continued.

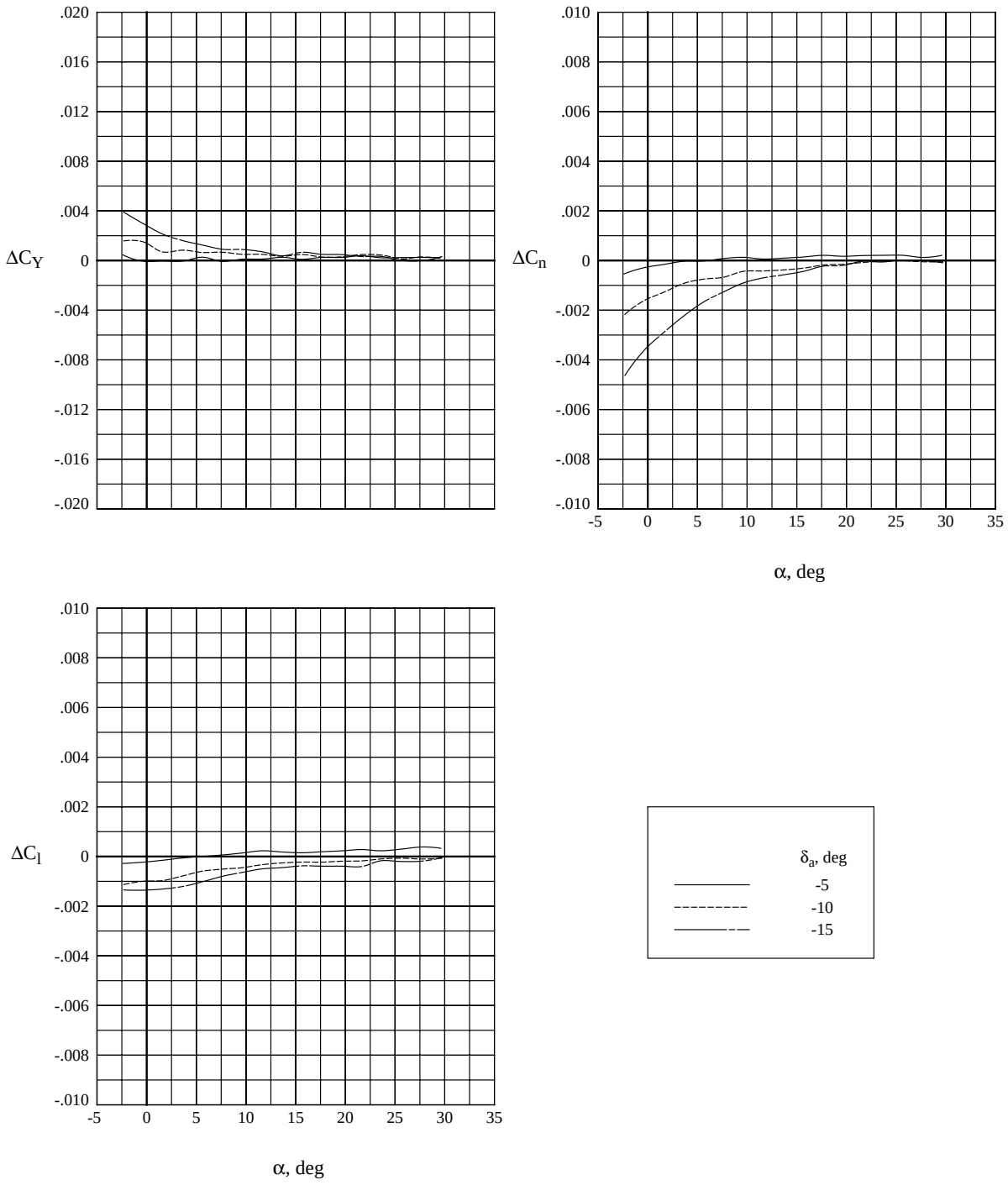

(f) $M = 4.0$.

Figure 14. Continued.

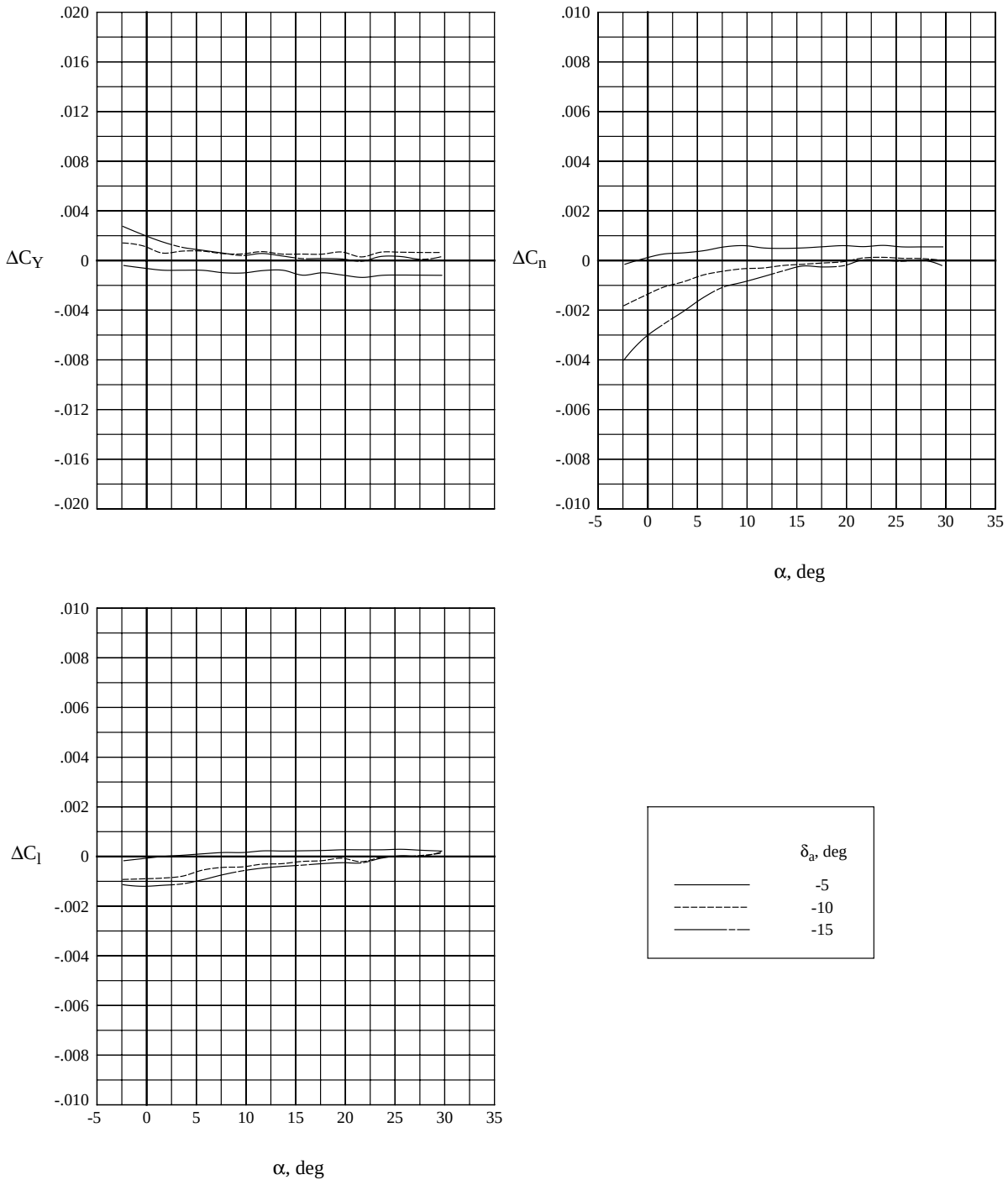

(g) $M = 4.5$.

Figure 14. Concluded.

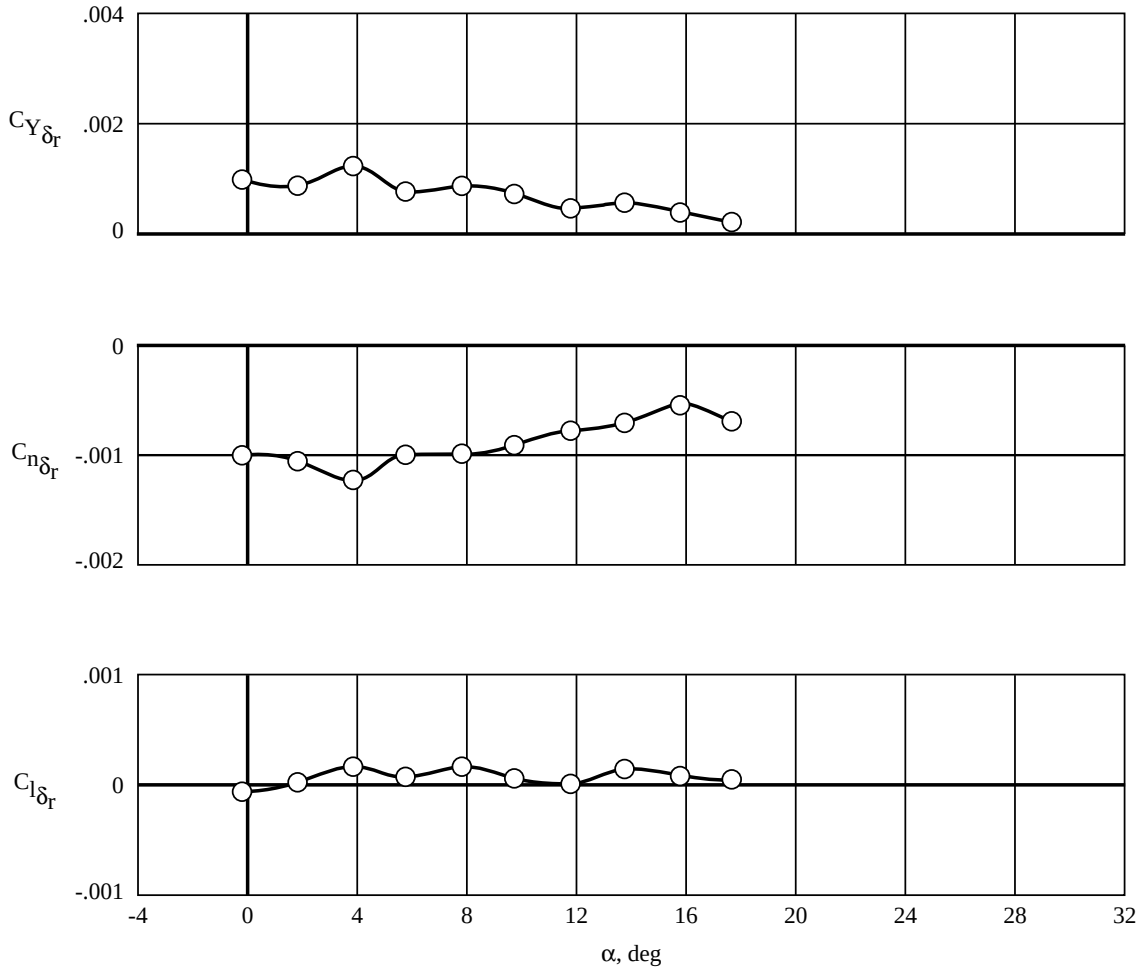

(a) $M = 1.6$.

Figure 15. Yaw control effectiveness of all movable center fin (ref. 9).

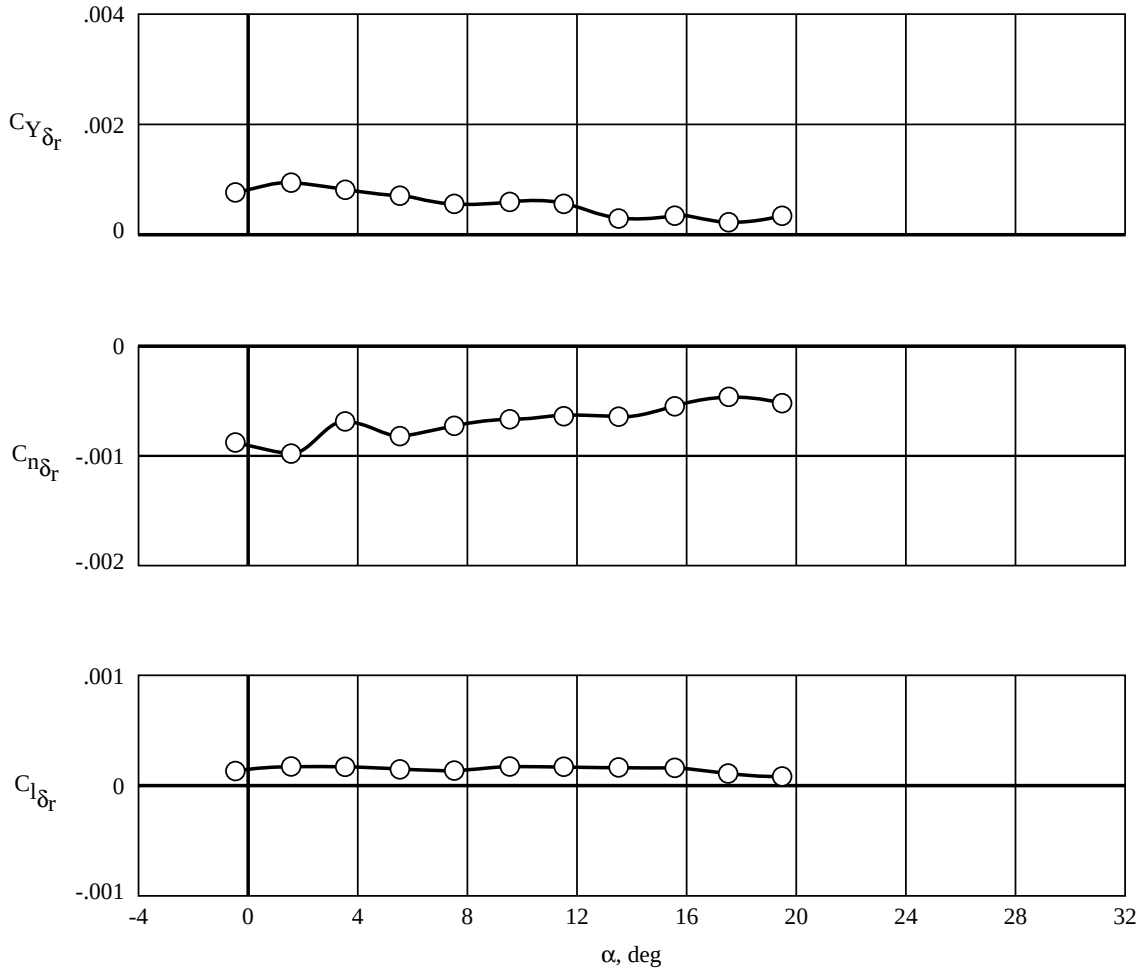

(b) $M = 2.0$.

Figure 15. Continued.

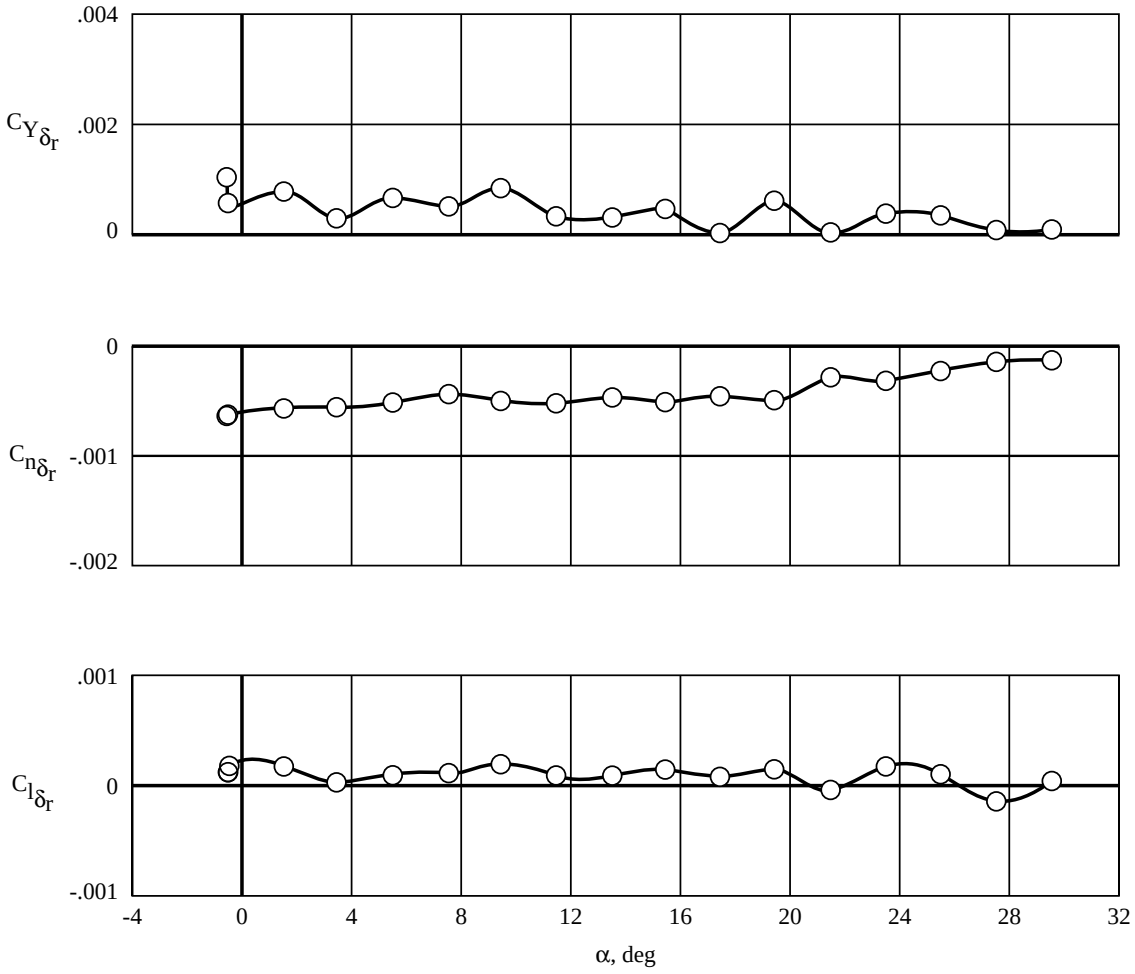

(c) $M = 2.5$.

Figure 15. Continued.

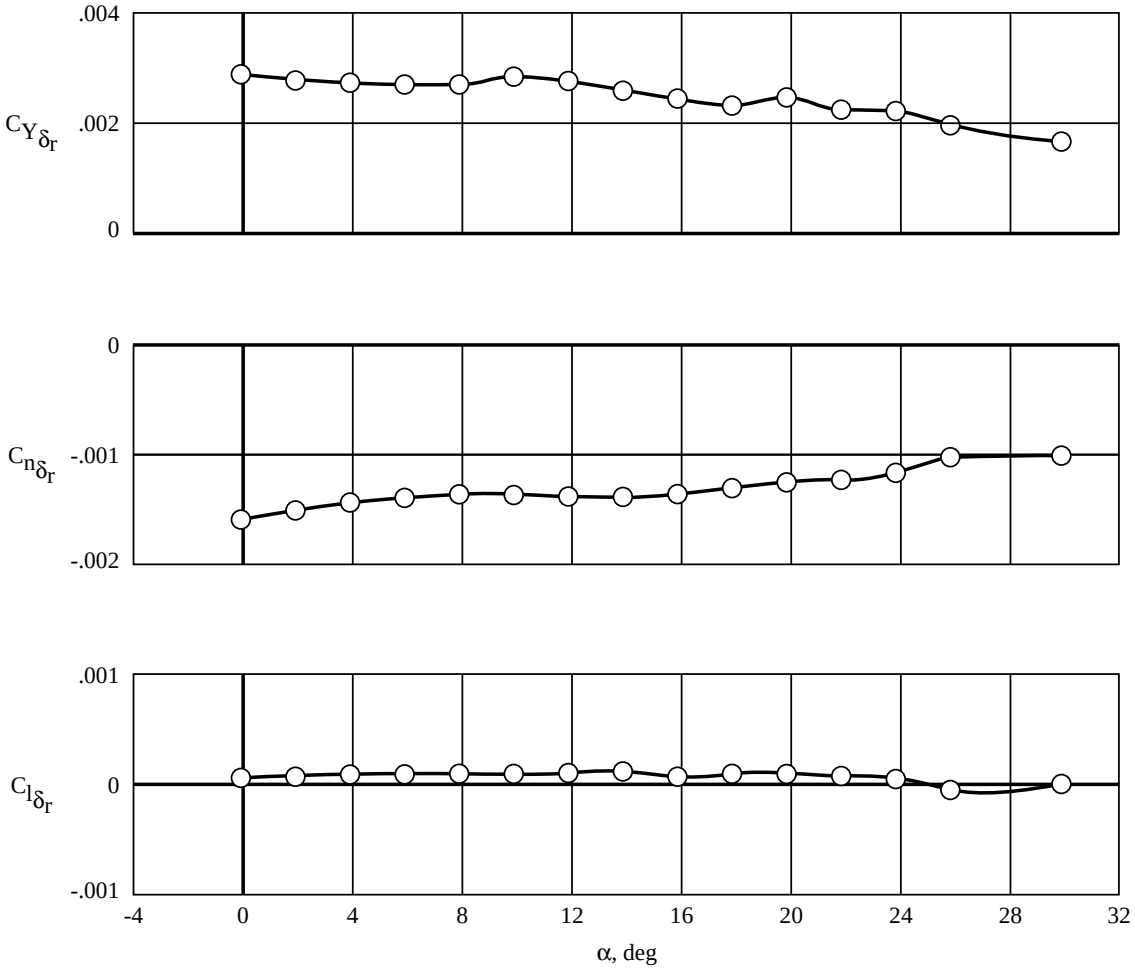

(d) $M = 3.0$.

Figure 15. Continued.

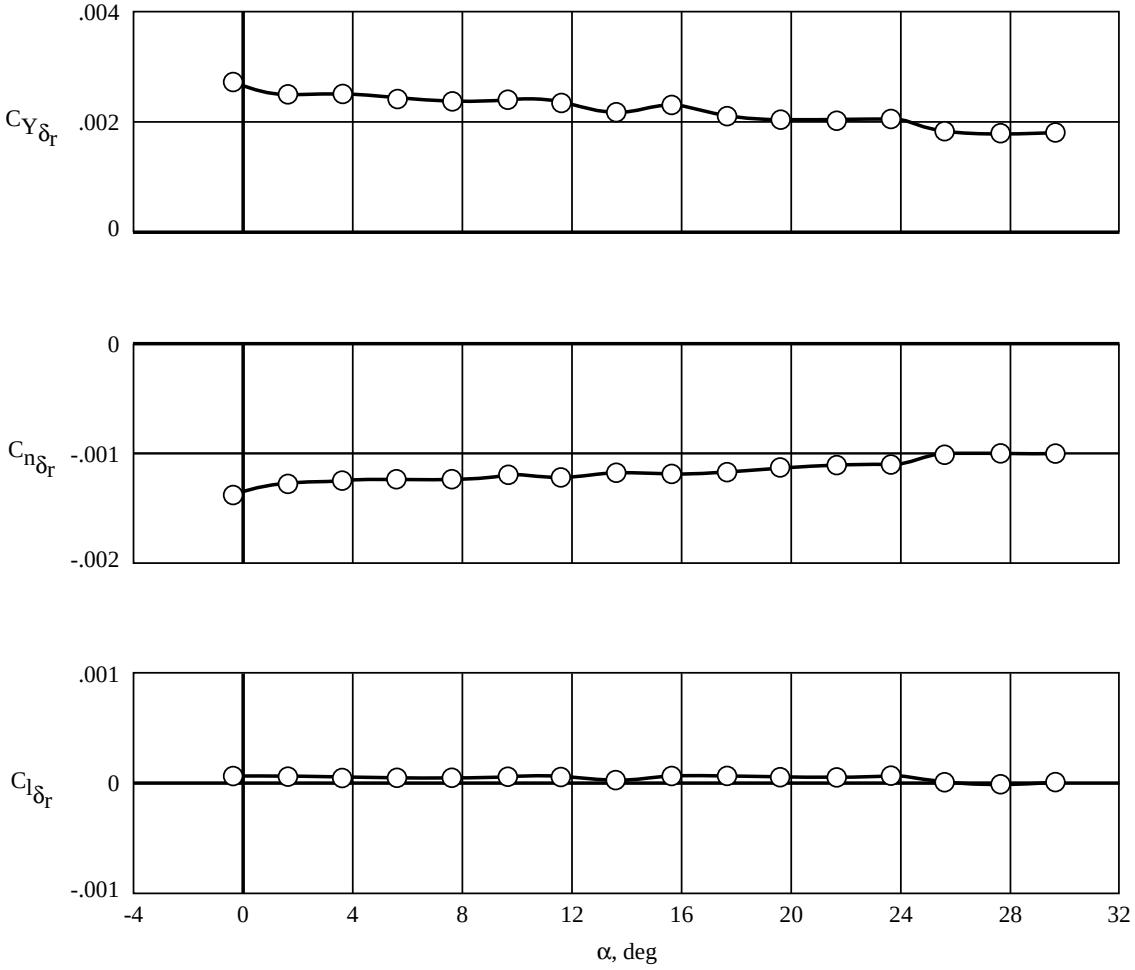

(e) $M = 3.5$.

Figure 15. Continued.

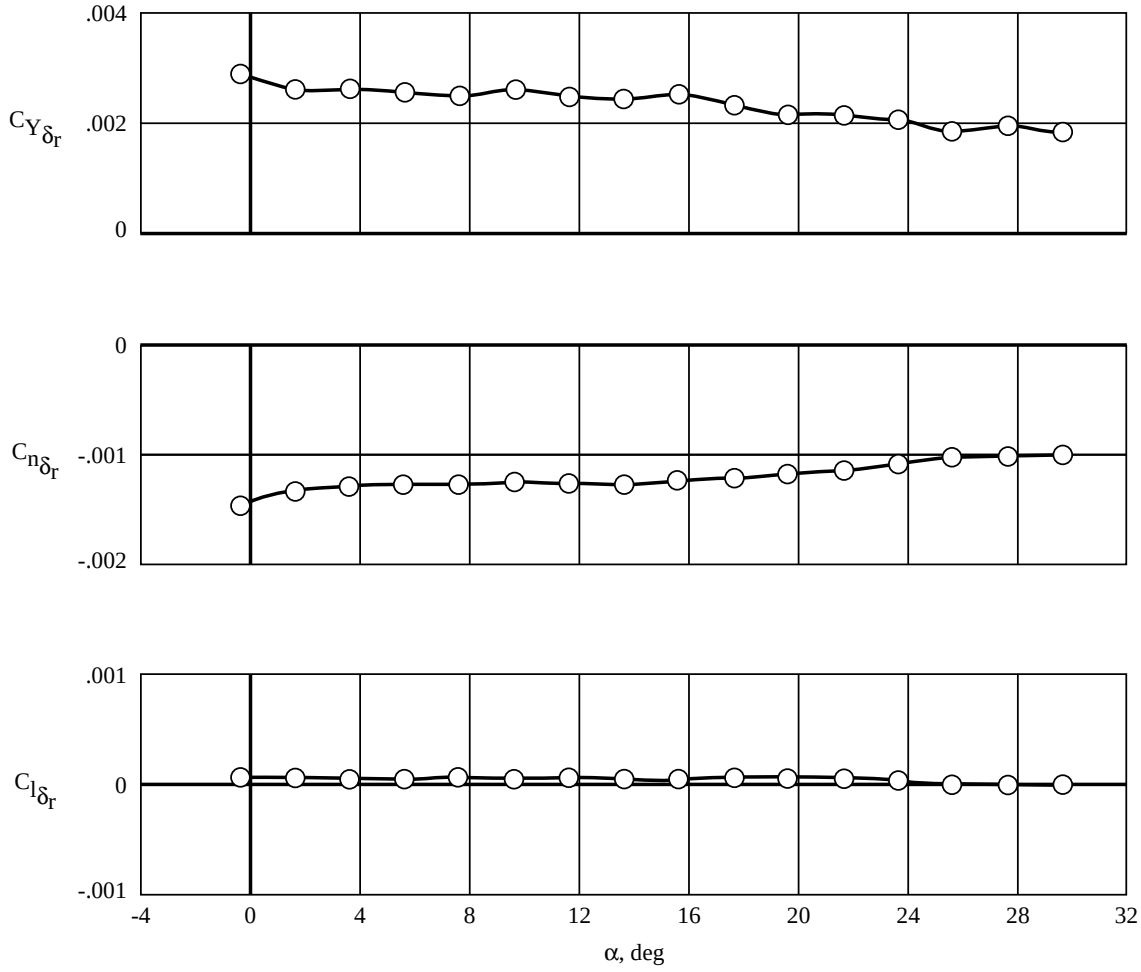

(f) M = 4.0.

Figure 15. Continued.

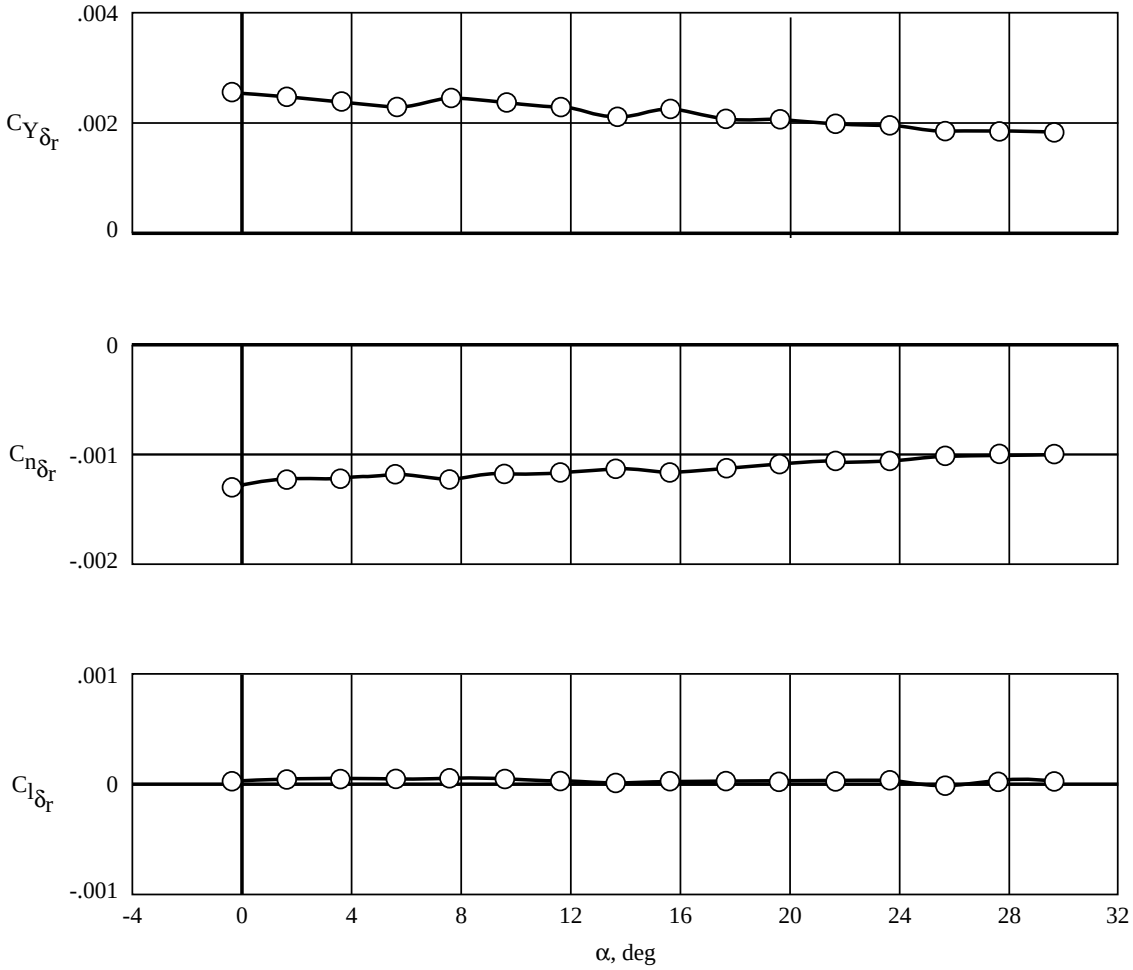

(g) M = 4.5.

Figure 15. Concluded.

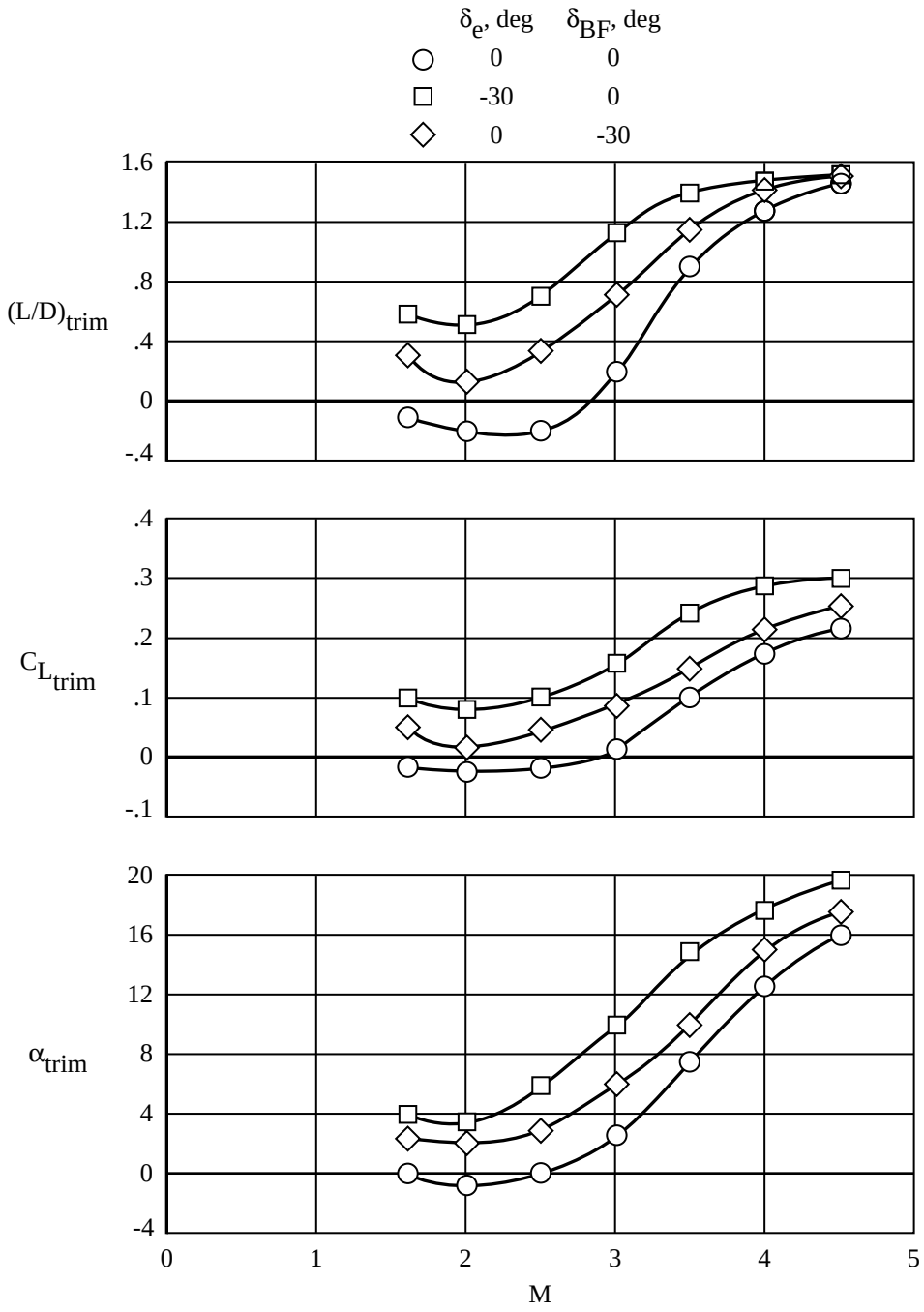

Figure 16. Longitudinal trim characteristics of HL-20 model.

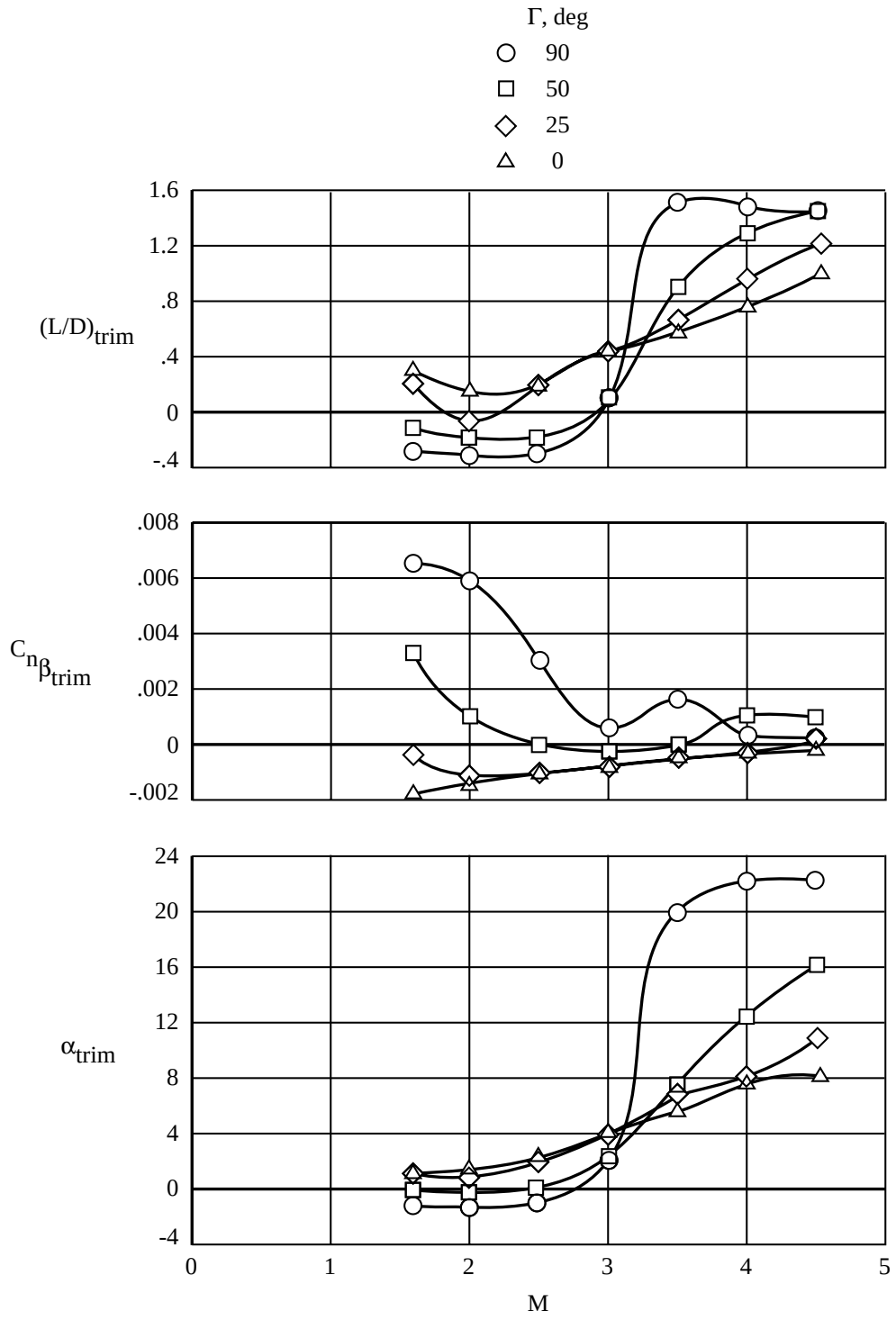

Figure 17. Effect of tip-fin dihedral angle on longitudinal trim characteristics of HL-20 model.

REPORT DOCUMENTATION PAGE

Form Approved
OMB No. 0704-0188

1. AGENCY USE ONLY *(Leave blank)*	2. REPORT DATE	3. REPORT TYPE AND DATES COVERED
	December 1995	Technical Memorandum

4. TITLE AND SUBTITLE
Control Effectiveness and Tip-Fin Dihedral Effects for the HL-20 Lifting-Body Configuration at Mach Numbers From 1.6 to 4.5

5. FUNDING NUMBERS
WU 506-40-61-01

6. AUTHOR(S)
Christopher I. Cruz and George M. Ware

7. PERFORMING ORGANIZATION NAME(S) AND ADDRESS(ES)
NASA Langley Research Center
Hampton, VA 23681-0001

8. PERFORMING ORGANIZATION REPORT NUMBER
L-17183

9. SPONSORING/MONITORING AGENCY NAME(S) AND ADDRESS(ES)
National Aeronautics and Space Administration
Washington, DC 20546-0001

10. SPONSORING/MONITORING AGENCY REPORT NUMBER
NASA TM-4697

11. SUPPLEMENTARY NOTES

12a. DISTRIBUTION/AVAILABILITY STATEMENT
Unclassified–Unlimited
Subject Categories 02, 15
Availability: NASA CASI (301) 621-0390

12b. DISTRIBUTION CODE

13. ABSTRACT *(Maximum 200 words)*
Wind tunnel tests were made with a scale model of the HL-20 in the Langley Unitary Plan Wind Tunnel. Pitch control was investigated by deflecting the elevon surfaces on the outboard fins and body flaps on the fuselage. Yaw control tests were made with the all movable center fin deflected 5°. Almost full negative body flap deflection (−30°) was required to trim the HL-20 (moment reference center at 0.54-percent body length from nose) to positive values of lift in the Mach number range from 1.6 to 2.5. Elevons were twice as effective as body flaps as a longitudinal trim device. The elevons were effective as a roll control, but because of tip-fin dihedral angle, produced about as much adverse yawing moment as rolling moment. The body flaps were less effective in producing rolling moment, but produced little adverse yawing moment. The yaw effectiveness of the all movable center fin was essentially constant over the angle-of-attack range at each Mach number. The value of yawing moment, however, was small. Center-fin deflection produced almost no rolling moments. The model was directionally unstable over most of the Mach number range with tip-fin dihedral angles less than the baseline value of 50°.

14. SUBJECT TERMS
Lifting body; Spacecraft; Aerodynamics

15. NUMBER OF PAGES
89

16. PRICE CODE
A05

17. SECURITY CLASSIFICATION OF REPORT	18. SECURITY CLASSIFICATION OF THIS PAGE	19. SECURITY CLASSIFICATION OF ABSTRACT	20. LIMITATION OF ABSTRACT
Unclassified	Unclassified	Unclassified	